MULTIDISCIPLINARY ENVIRONMENTAL STUDIES

SOLAR WATER PUMP FOR IRRIGATION

FINAL REPORT

1 9 8 2

NATIONAL RESEARCH CENTRE - A.R.E.

ENVIRONMENTAL PROTECTION AGENCY — U.S.A.

MULTIDISCIPLINARY ENVIRONMENTAL STUDIES

SOLAR WATER PUMP FOR IRRIGATION

FINAL REPORT

July, 1982

SPONSOR : Environmental Protection Agency, WASHINGTON, USA

CONTRACT: PR3 - 541 - 3

EXECUTOR: National Research Center, CAIRO, EGYPT

PRINCIPAL INVISTIGATORS :

1. Prof. Dr G.H. Talat (Aug. 1979 - Aug. 1981)
2. Dr M. Adel Riad (Sept.1981 - July 1982)

NATIONAL RESEARCH
CENTER (NRC)
DOKKI, CAIRO, EGYPT

ENVIRONMENTAL PROTECTION
AGENCY (EPA)
WASHINGTON, DC, 20460, USA

MULTIDISCIPLINARY ENVIRONMENTAL STUDIES

SOLAR WATER PUMP FOR IRRIGATION

Final Report

(July 1982)

LIST OF RESEARCH CONTRIBUTORS

Principal Investigators :

1.	Prof. Dr G.H. Talat	(Aug. 1979 - Aug. 1981)
2.	Dr M.A. Riad	(Sept. 1981 - July 1982)

Contributors :

1.	Dr M.F. EL-Akkad	Ph.D.
2.	Dr M.M. EL-Nahas	Ph.D.
3.	Dr F. Terra	Ph.D.
4.	Dr B. Mansour	Ph.D.
5.	Ms I.A. Kamal	Research Assistant
6.	Ms A.M. Farid	Research Assistant
7.	Dr A.M. Samuel	Ph.D.

ABSTRACT

A quantitative analysis of the factors influencing CdS / Cu_2S solar cell efficiency has been conducted. The studies encompassed investigation of the structural and physical properties of CdS and Cu_2S layers prepared in thin film and ceramic forms, and obtained by various techniques. The properties investigated covered the optical, electrical and photoconductive properties. The dependence of these properties on the preparation procedure and / or parameters was also studied.

Different forms of CdS/Cu_2S solar cells have been fabricated and tested. For single crystal CdS/Cu_2S cell, the short circuit current and open circuit voltage were found to be 3.75 mA and 0.405 volts, respectively, and the efficiency was 2.34% . For thin film CdS/Cu_2S cell, the respective values were 0.069 mA, 0.192 volt and 0.66%. Further development of these cells is expected to improve their energy conversion efficiencies.

CONTENTS

000o000

0

LIST OF FIGURES

FIGURES (continued)

FIGURES (continued)

FIGURES (continued)

LIST OF PHOTOS

LIST OF TABLES

ACKNOWLEDGMENTS

The financial support of the project by the American Environmental Protection Agency, EPA, is gratefully acknowledged.

A great deal of cooperation has been received during the conduct of this study from the following laboratories:

The Central Services Laboratories, National Research Center, CAIRO.

- X-ray Lab.
- Scanning electron microscopy Lab.
- Spectroscopy Lab.

The Institute of Scientific Instrumentation, CAIRO.

- Optics Lab.
- Micromechanics Lab.
- Mechanics Workshop.

Optics Laboratory, Faculty of Education, Ein Shams University, CAIRO.

The Bureau of Foreign Contracts, National Research Center, is duly acknowledged for administrative assistance.

SECTION 1

CONCLUSIONS

In the present investigations CdS and Cu_xS were studied in different structural forms, with the aim of characterizing the optimum type of the said materials for the fabrication of CdS/Cu_xS solar cell system to be ultimately used in driving solar energy water pumps.

The conclusions that were arrived at from the results obtained are given below under two main categories.

1.1. PHYSICAL AND STRUCTURAL CHARACTERIZATION.

The present investigations throw light on the dependence of the properties of the CdS and Cu_xS layers of the Cu_xS/CdS heterojunction, on the preparation parameters like substrate temperature, film deposition rate, annealing, etc. One therefore needs to carefully monitor these parameters in order to obtain optimum results.

1. The value of the energy gap for CdS films was determined as 2.42 eV and was found to be slightly affected by the preparation parameters.

2. The direct and indirect optical band gaps for Cu_2S were determined to be $E_{gd} = 1.7$ eV and $E_{gi} = 1.1$ eV.

3. From the spectral behaviour of the transmittance of CdS films in the transparent spectral region, it can be concluded that the observed features arise due to inhomogeneities in the films.

4. The dark electrical resistivity of CdS thin films are affected by the preparation parameters. The most important factor is the annealing temperature which results in a large decrease in the resistivity ($\rho = 10^2 \Omega.cm$ at $T_A = 400^\circ C$ from initial values of $10^4 \Omega.cm$ at annealing temperatures below $100^\circ C$).

The effect of all these parameters may be related to the degree of crystallinity and preferred orientation of the films along (002) direction. A high degree of both is obtained with increasing film thickness and a corresponding decrease in the resistivity is observed.

5. In the case of Cu_2S films, the dark resistivity is seen to be independent of film thickness in the range 0.044 - 0.254 μm, and has a value $\sim$ 870Ω.cm. This thickness range was investigated as it covers the optimum value required for a Cu_2S layer in a Cu_2S/CdS solar cell.

6. The degree of crystallinity and preferred orientation of CdS crystallites in the thin films depends upon the substrate temperature and the deposition rate. The grain size is found to increase with increasing substrate temperature and reaches a maximum at $200^\circ C$ ($\sim 1.6 \mu m$).

Both grain size and degree of preferred orientation increase with decreasing deposition rate ($\sim$ 1.7 μm at deposition rate of 0.06 μm/min). However, above a deposition rate of 0.5 μm/min, the change in grain size ($\sim$ 1.1 μm) is very slight.

7. The Cu_xS layers were prepared either by solid state reaction or by the dipping technique. The lattice parameters obtained from the former method are found to correspond to Cu_2S while the latter always produces a non-stoichiometric variant Cu_xS with x close to 2. Therefore, the dip reaction is preferable to the solid state reaction for obtaining a Cu_xS layer with $x \sim 2$, the optimum value being quoted as 1.995 for the formation of the heterojunction.

8. SEM analysis reveals definitely the formation of the Cu_2S layer by chemical reaction on the surface of the ceramic CdS samples. For Cu_2S thin film thickness less than one micron, the Cu_2S layer is not detectable by means of X-ray diffraction. From SEM micrographs, we observe the penetration of the Cu_2S layer into the CdS layer through cracks in the latter. This is one of the possible reasons for degradation of the heterojunction. The average grain size of the Cu_2S layer formed on CdS sintered base is $\sim$ 4-7 μm.

9. The observed photoconductivity for CdS single crystals showed the effect of surface treatment and Cu content upon their spectral distributions. It is thus necessary to control the doping level of Cu impurities, since these impurities

influence the photoconductivity of CdS. This, in turn, affects the I-V characteristics of the Cu_2S/CdS heterojunction. The Cu impurities can be obtained from the dissociation of Cu_2S.

1.2. SOLAR CELLS

1. The I-V curves measured in the light and dark are found to intersect. This cross-over of the curves may be attributed to the strong photoconduction in CdS.

2. The mean values of the open circuit voltage V_{oc} and short circuit current I_{sc} obtained for $CdS_{\text{single cryst.}}/Cu_2S_{\text{thin film}}$ solar cells was found to be 0.405 volt and 3.75 mA, respectively, and the efficiency η was 2.34%.

3. For $CdS_{\text{thin film}}/Cu_2S_{\text{thin film}}$ solar cells, however, V_{oc}, I_{sc} and η were only 0.192 volt , 0.069 mA, and 0.66% , respectively.

4. Rather high values for series resistance R_s and rather low values for shunt resistance R_{sh} were obtained for both the $CdS_{\text{single crystal \& thin film}}/Cu_2S_{\text{thin film}}$ solar cells compared to $R_s = 0$ and $R_{sh} = \infty$ for an ideal cell. This is understood in view of the low fill factors (0.385 & 0.314) and low efficiencies (2.34% & 0.66%) of the cells.

5. The effect of intensity of illumination was also investigated. For the single crystal CdS / Cu_2S thin film

cells, V_{oc} varied slightly between 0.345 to 0.370 volt , while I_{sc} varied rapidly over a range of 71.5 to 206 μA when the light intensity was changed from 6.2 to 18.1 mW/cm^2. For the thin film CdS / Cu_2S thin film cells, both V_{oc} and I_{sc} exhibited bigger changes, V_{oc} from 100 to 202 mV and I_{sc} from 27 to 180 μA for the same light intensity variation.

6. The dependence of V_{oc} on the wavelength λ indicated an intensive maximum at 0.49 μm and a less intensive peak at 0.655 μm. The former may be associated with the band edge of CdS, while the latter is correlated to the direct band gap of Cu_2S.

7. Ceramic CdS / Cu_2S thin film heterojunctions are found to be more easy to prepare than their thin film counterparts. In addition, they often exhibit reasonable I-V characteristics.

SECTION 2

REMARKS & RECOMMENDATIONS

The project was planned for 3 years according to our initial proposal and included setting-up of laboratory facilities for the physical characterization of materials, preparation of solar cells and improvement of cell efficiency, to be undertaken in the periods: Sept. '79 - Aug. '80, Sept. '80 - Aug.'81 and Sept. '81 - Aug. '82, respectively.

The choice of CdS/Cu_2S cell is a thoroughly justified one in view of the fact that it is one of the most promising low cost-high efficiency cells to have been developed so far besides the commercially available silicon solar cells. At the time of starting (1978) reported efficiencies were around 6 - 7% and the extensive literature since then on these cells have proved their esteem with recent efficiencies going as high as 9%.

Therefore, from both these points of view, viz., high efficiency and low cost, the study, fabrication and ultimate utilization of these cells in the manufacture of solar cell arrays for various application purposes will benefit many aspects of the national economy.

The budget initially alloted to this project was $30,000. Such a field of research as covered by the project is considered to be one of the most complicated research programs in solid state electronics and needs different profiles of specialization as it starts from studying the basic physical properties of materials, then goes on to the preparation of a complicated electronic device like the solar cell & optimizing its parameters to achieve economically feasible/assessable low cost solar cells. Finally these cells are used to fabricate array systems from them.

During the course of the study we had to use some additional equipment e.g. solar simulator, C-V bridge among others, but the budget of the project did not enable us to purchase any of these items. For example, the cost of the solar simulator and the C-V bridge ($24,000) itself is nearly 80% of the total budget of our sub-project. For the same reasons we had to conduct some essential experiments outside the Lab. (SEM and some optical measurements).

We regret to say that the budget was cut (for the third year) at a critical point of our research since the nearly completed Lab. setup combined with the invaluable experience gained and reasonable results obtained in the previous 2-year period had made us all set to carry out further and more specialized work in this field with all potential for bringing the project to fruitful completion.

In the first-year period, there was an initial delay in receiving important consignment like the coating unit and other items. Almost two-thirds of the year were spent in procuring these items before which, therefore, no research work could be started. In addition, very specific parts, raw material and material of great importance (e.g. masks, epoxy resin, CdS powder, etc.) were received in late time.

In spite of the above-mentioned difficulties and lack of some essential equipment, time and funds, we have obtained results and the conclusions of the work are reasonable. The efficiencies for the single crystal and thin film solar cells obtained were 2.42% and 0.7% , respectively, which are rather low compared with existing values. These low values may be attributed to the fact that the CdS films used in our experiments were only about 4 μm thick with corresponding resistivities of the order of $10^2 \Omega$.cm or more. Moreover, the grid used for making the top contact was fabricated in a very primitive way. Only recently, have we been able to procure sophisticated masks for evaporating grids constituting a very fine mesh and which are recommended for such cells.

Another fact resulting in the low efficiencies observed is that no encapsulation was used to cover the cells.

All these points combined to degrade the efficiency of the cell. We hope to make improvements on the present efficiencies by incorporating all these factors and using our recently

constructed graphite boat to obtain CdS layers of optimum thicknesses ($\sim$ 20 μm). Such thick layers should give resulting resistivities lying in the 1 - 10 Ω.cm range when combined with the proper doping / annealing procedures. Encapsulation of the cell, in addition, should definitely yield better results.

Among the achievements of this project have been i) the organization of our research group in the field of photovoltaics, able to contribute in solving the problem of energy by photovoltaic conversion, and ii) the integration of a multi-disciplinary group working in the field of environmental pollution.

Based on our experience and observations, we propose that future research programs in this field and on the same subject of CdS/Cu_2S solar cell fabrication, should be continued taking the following points into consideration:

i. Preparation of CdS films using a specially designed graphite boat to obtain thick layers ($>$ 10 μm). This will require a more powerful coating system to supply high currents $>$ 150 A.

ii. Development of the ceramic technique.

iii. Addition of ZnS to CdS for the development of $Cd_{1-x}Zn_xS$ / Cu_2S cell which proves to be a promising cell.

iv. Application of new techniques to obtain CdS layer, e.g. the chemical spray deposition technique of CdS on glass

substrate, to decrease the cost of production.

v. Study the degradation and other problems relating to such cells.

Such intensive research, if carried out in future, should lead to the fulfilment of the goal of solving the crisis of non-renewable energy sources by replacing them with renewable sources via photovoltaic conversion. The use of solar cells for electric power generation to drive water pumps will indirectly help the environmental pollution problems. Simultaneously, we will then be solving both the energy and pollution problems to the interest of the nation's economy.

SECTION 3

INTRODUCTION

3.1. WATER AND AIR POLLUTION

The problem of water and air pollution is now receiving great attention from scientific, health and social establishments as well as from many governments. This situation is motivated by the great impact of such a problem on human life.

Polluted water has serious consequences on the health of people which leads, at the end, to serious effects on the national economy.

The system of water irrigation in Egypt does not depend on rains except in some places located north near the Mediterranean Sea. Usually, farms are irrigated from a Nile network canal system by raising the water via an animated system. This system demands the exposure of a great portion of population to highly polluted canals and drain water.

Skin penetrating parasites, like the circarias of bilharzia disease mainly infect the farmers because of such irrigation techniques. Bilharzia is the most prevalent disease among farmers and their children as it attacks not less than 80% of them. Water lifting from canals by electric pumps (where electricity is available) or by diesel driven pumps are also

common. Besides consuming energy, the latter type of pumps cause air pollution via their exhaust.

In order to solve the above mentioned problems which are directly related to water and air pollution, the idea of the utilization of water pumps on the basis of photovoltaic conversion of solar energy is receiving a great attention in many countries. Such kind of water pumps are now developed and proved to be efficient for many purposes. This clean source of energy is successfully gaining access in many countries since it helps to prevent, indirectly, the pollution of water and air by using new techniques of irrigation (spray or dropping).

3.2. CLEAN SOURCE OF ENERGY

Photovoltaic conversion of solar energy and the use of photovoltaic cells for direct energy conversion has been mainly confined to space applications since 1956. However, the increasing need for alternate terrestrial energy sources has made solar energy the principal renewable energy source and photovoltaic conversion an active area of research and development. For terrestrial applications, the cells must be inexpensive to compete with conventional energy costs.

The Solar Cell

The direct conversion of sunlight into electric power is achieved by means of solar cells by a process which is called

the photovoltaic effect. This effect gives rise to an e.m.f. when the radiation from the sun strikes on a semiconductor near a built-in potential barrier. The barrier can be formed in a semiconductor by several means, for example, with a metal-semiconductor contact or with p-n junctions.

If this barrier is illuminated, the excess electric charges created by light will be separated by the barrier yielding a positively charged region on one side and a negatively charged region on the other side of the junction. Therefore an illumination current appears with a certain photovoltage and hence a certain amount of power is developed if the cell is connected to an external load. This photovoltaic effect can be achieved in all semiconductors. Insulators and metals are generally unsuitable: insulators because of their low conductivity, and metals because of their high electron concentration in the dark.

Silicon (Si) solar cell. Silcon is the most important semiconductor material for photovoltaic solar energy conversion. Such cells are made from silicon single crystals and this is the reason for their high price. At present, these are commercially the only available cells, except for some recent production of CdS / Cu_2S cells by the Solar Energy System Corporation. A considerable research and development effort is, however, taking place on other structures, e.g., Si: polycrystalline and amorphous, with the object of exploring new solutions for low cost Si solar cells. Silicon solar

cells are characterised by their stable performance over a long life time (about 20 years). The maximum theoretical conversion efficiency for silicon solar cells under maximum illumination with solar light on ground is about 23%. The efficiencies achieved with commercial silicon solar cells lies between 12 and 18%. Silicon cells made of ribbons are now under intensive development.

Gallium Arsenide (GaAs) solar cell. Single crystal and thin film cells based on GaAs are the most efficient solar cells. Efficiencies of 13 - 19% have been obtained. On the other hand, such cells are very expensive.

Cadmium Sulfide (CdS) solar cell. A number of CdS-based heterojunction cells having efficiencies in excess of 9% have already been reported in the literature. Table 1 gives a summary for the different types of solar cells with the corresponding efficiencies.

Since its discovery in 1954 by Reynolds et al, the copper sulfide/cadmium sulfide (Cu_xS / CdS) heterojunction photovoltaic solar cell has had more research effort expended on it than has been spent on any other solar cell except the silicon single crystal cell. The interest in this cell derives from the expectation that it will be possible to fabricate thin film Cu_xS/CdS cells having reasonable solar energy conversion efficiencies at a substantially lower cost than the minimum cost of a comparable silicon single crystal cell. This Cu_xS/CdS thin film solar cell exhibits one of the

Table 1

Experimentally achieved efficiencies for various solar cells.

Cell Material	Maximum Exptal. η	Reference
Single crystal solar cells		
Silicon (czochralski)	17 %	Hunt et al, 1976
p-GaAs/n-GaAs	17 %	Fan et al, 1978
p-$Ga_xAl_{1-x}As$/n-GaAs	21.8%	Hovel and Woodall, 1973
p-CdTe/n-CdS	8 %	Yamaguchi et al, 1976
p-InP/n-CdS	17 %	Shay et al, 1976; 1977
p- $CuInSe_2$/n-CdS	12 %	Shay et al, 1975
Thin film solar cells		
p-Cu_2S/n-CdS	9 %	Meakin, 1979
p-Cu_2Te/n-CdS	6 %	Cusano, 1966
Thin film amorphous silicon	6 %	Carlson and Wronski, 1976
p-$CuInSe_2$/n-CdS	6 %	Kazmerski et al, 1976
Thin film GaAs	6 %	Chu et al, 1978

highest efficiencies observed in a thin film cell, namely about 9% for natural sunlight illumination (Rothwarf and Böer, 1975; Rothwarf, 1976; Hovel, 1977; Rothwarf et al, 1978; Bragagnolo, 1978; Meakin, 1979).

Besides the USA, which appears to be leading in these R&D Programs, studies of Cu_xS/CdS solar cells are also being carried out in France, England, West Germany, Japan and India. Examples of research programs in Cu_xS/CdS solar cells carried out in the USA during 1978 are given in Table 2.

At present, at least two industrial organisations, namely the Solar Energy System Corporation of Newark, Delaware and the Photon Incorporation of El Paso, Texas are preparing to manufacture Cu_xS/CdS cells for terrestrial applications.

A plant capable of producing 500 kW annually of Cu_2S/CdS cells by a modified Clevite process was proposed to be designed in anticipation of supplying the market (Di Zio, 1976).

However, even though the Cu_xS/CdS cell has entered the "pilot plant" production stage, there are still many technical problems in the cell. These are related to the extreme sensitivity of the properties of the component materials (copper and cadmium sulfides) to the preparation conditions (Wendland, 1962; Dresner and Shallcross, 1963) as well as problems related to the stability and durability of the cell.

Solar Cell Configuration

The essential parts of the Cu_xS/CdS solar cell are

Table 2

Research programs in the field of Cu_2S/CdS solar cell, in the USA (US Dept. of Energy, Report, 1978).

Program Title	Organisation
1. Cadmium Sulfide/Copper Sulfide heterojunction cell research.	Institute of Energy Conversion, University of Delaware.
2. Research on Cu_xS(Cd, Zn)S photovoltaic solar energy converters.	Lawrence Berkely Laboratory, University of California.
3. Reactively sputtered thin film photovoltaics.	Lawrence Livermore Laboratory, University of California.
4. Cadmium Sulfide/Copper Sulfide heterojunction cell research.	Lockhead Palo Alto Research Laboratory.
5. Cadmium Sulfide/Copper Sulfide ternary-hetero-junction cell research.	Boeing Aerospace Company, Seattle.
6. CdS/Cu_xS ternary hetero-junction cell research.	Sperry Univac Defence Systems Division.
7. CdS/Cu_xS heterojunction cell research.	Westinghouse Electric Corporation, Research and Development Center.

illustrated in Fig. 1. They are a CdS base (either a single crystal slice or a thin film deposited onto a substrate), then a Cu_xS layer forming the intimate contact with the CdS; then ohmic contacts to both the Cu_xS and CdS.

The photovoltaically active part of the Cu_xS/CdS cell is the heterojunction between the p-Cu_xS and the n-CdS illustrated schematically in Fig. 2. The bandgap of CdS is 2.4 eV at 300 K. Sunlight falling on the earth contains very few photons having energies in excess of 2.4 eV and consequently CdS cannot absorb any significant fraction of the sun's energy.

Essentially all of the illumination current generated in the cell results from absorption in the Cu_xS film. Another reason why the Cu_xS/CdS cell should be illuminated from the Cu_xS side is related to the way the cell is constructed: the CdS is usually deposited on an opaque metal sheet; the Cu_xS layer is produced on the exposed surface of the CdS and, therefore, the sunlight must be incident on the Cu_xS side. Such cells are called frontwall cells.

Another cell configuration was proposed by Das et al, 1977; where the Cu_xS film was first deposited on a glass substrate having a gold grid layer previously deposited as bottom electrode. Thereafter CdS was deposited above the Cu_xS layer forming the p-n junction. In this geometry, the cell is illuminated also from the Cu_xS side, which is then protected from ambients by virtue of the CdS layer.

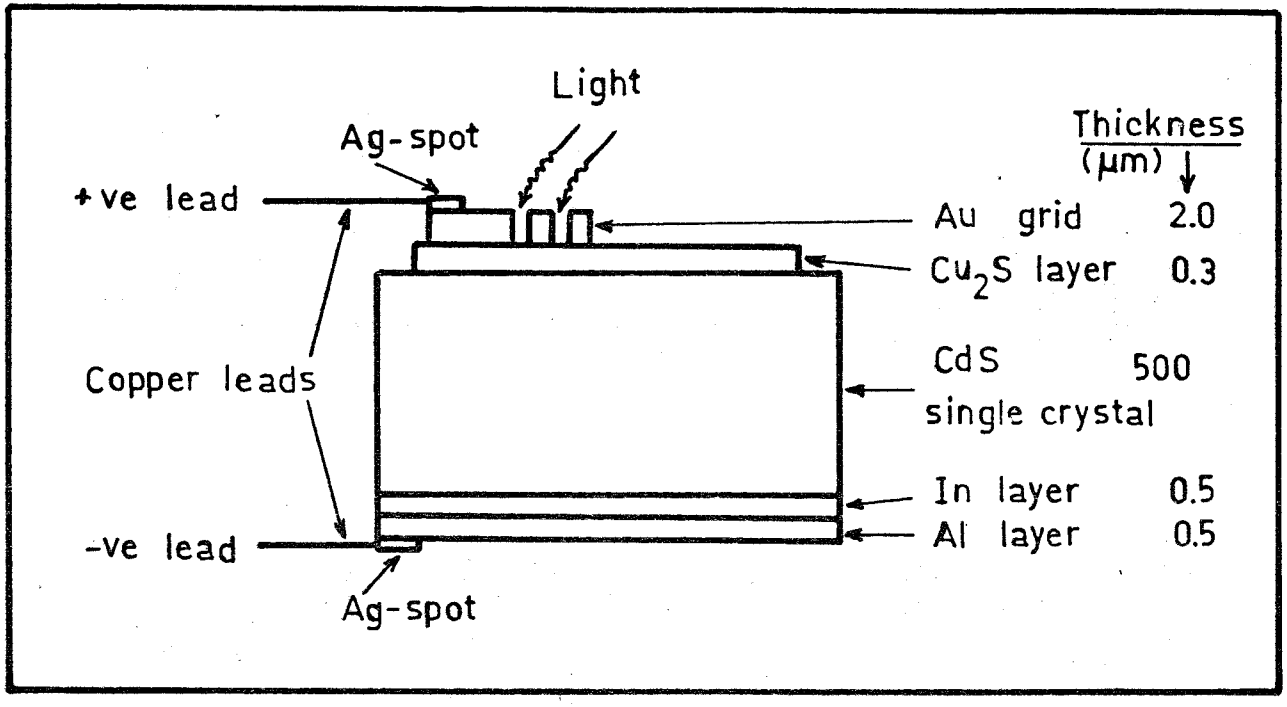

Fig. 1. Frontwall Cu_2S / CdS single crystal solar cell representation.

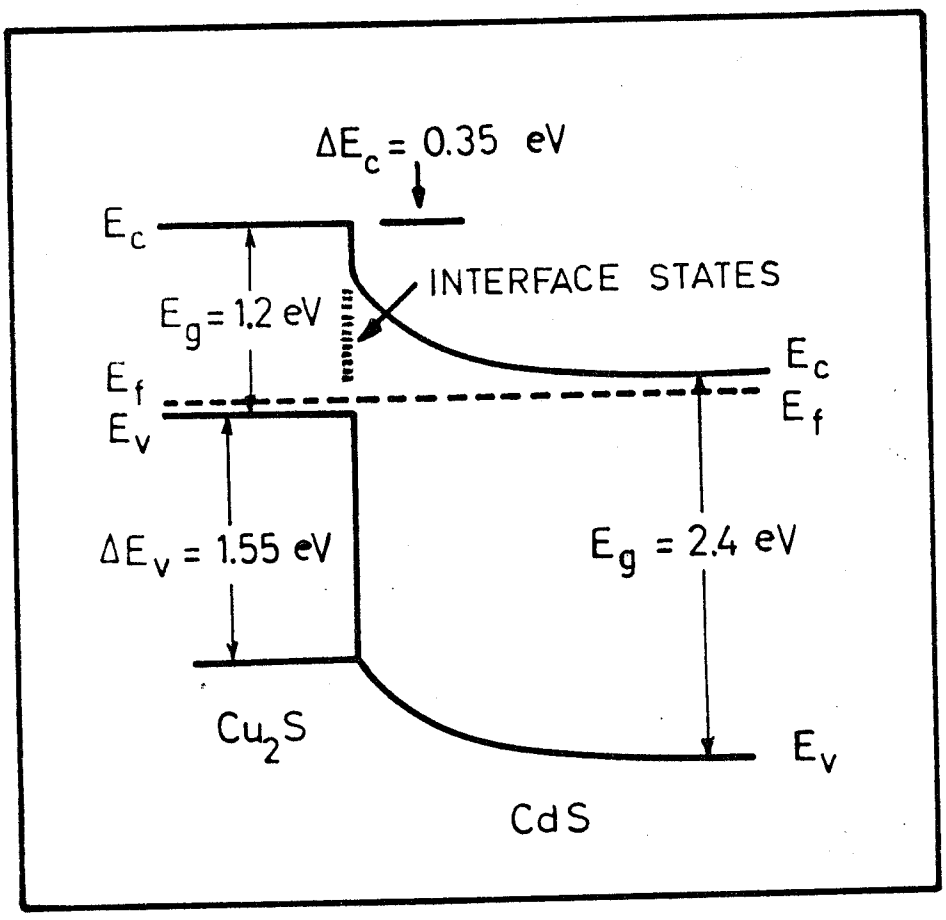

Fig. 2. Schematic representation of the energy band configuration in a cross-section through a p-Cu_2S / n-CdS cell.

Solar Cell Basic Parameters

Consider the I-V characteristic curve of a solar cell, Fig. 3.

I_{sc}, the short circuit current, is the maximum possible value of the generated photocurrent.

V_{oc}, the open circuit voltage, is the maximum possible value of the cell photovoltage.

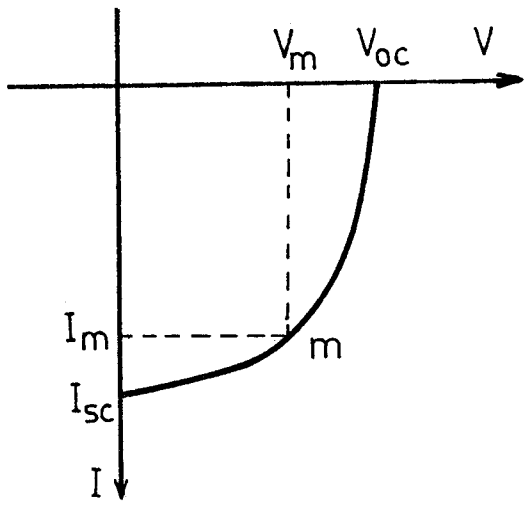

Fig. 3. Solar cell I-V curve and characteristic parameters

P_m, the cell power output, is the maximum power that can be delivered by the cell. Consider a point m on the I-V curve where the area of the rectangle that can be drawn between the curve and the coordinate axes is a maximum. The coordinates of that point m are V_m and I_m where $P_m = I_m \cdot V_m$

FF, the cell fill factor, is the ratio of the maximum power that can be delivered by a cell to the product of its short circuit current I_{sc}, and open circuit voltage V_{oc}; $FF = I_m V_m / I_{sc} V_{oc}$. The fill factor of a solar cell is a measure of the "sharpness of the knee" in the I-V curve.

η, the energy conversion efficiency, described as $\eta = I_m V_m / P_i A$ where P_i is the incident solar power density and A is the receiving area of the solar cell. The efficiency can also be expressed as $\eta = FF \cdot I_{sc} \cdot V_{oc} / P_i A$

3.3. OBJECTIVES

The three years project included the study and preparation of CdS / Cu_2S solar cells of the laboratory scale.

In order to develop this work, the prepared cells should have reasonable efficiencies (not less than 5%) for the economic usage.

After reaching this efficiency and achieving stable performance for certain life time period, a solar cell module can be constructed for electric power generation which can drive water pumps for irrigation.

This approach of solar energy utilization in water pumping meets the goals of environmental protection as well as of obtaining a renewable source of energy.

3.4. APPROACH AND KEY METHOD

The basic operations covered in the present work are shown schematically in Fig. 4.

Fabrication of the Solar Cell

We have produced and investigated three different types of the Cu_2S/CdS cells using different experimental techniques.

a) Single crystal CdS / thin film Cu_xS cell.

b) Thin film CdS / thin film Cu_xS cell.

c) Ceramic CdS / thin film Cu_xS cells.

Preparation of CdS layer. The n-type CdS thin films were produced by vapour decomposition under high vacuum (10^{-5} Torr) from 99.999% pure cadmium sulfide powder. We have used three different types of coating plants :

i. An EDWARDS coating unit Model 306 (British) with automatic digital film thickness monitor and deposition rate controller. The CdS powder was evaporated from Mo boats. This unit has also been used for the deposition of the Cu_xS as well as the electrode layers.

ii. A BALZERS (Swiss) coating unit was used for the deposition of CdS thin films at liquid nitrogen temperature (77 K).

iii. An EDWARDS coating unit model 610 was employed for preparing thicker CdS films (> 10 μm), using a specially designed graphite boat, Fig. 5. In this boat, the CdS vapours pass through the orifices in the quartz wool chamber, then through the quartz wool that is supposed to help in trapping

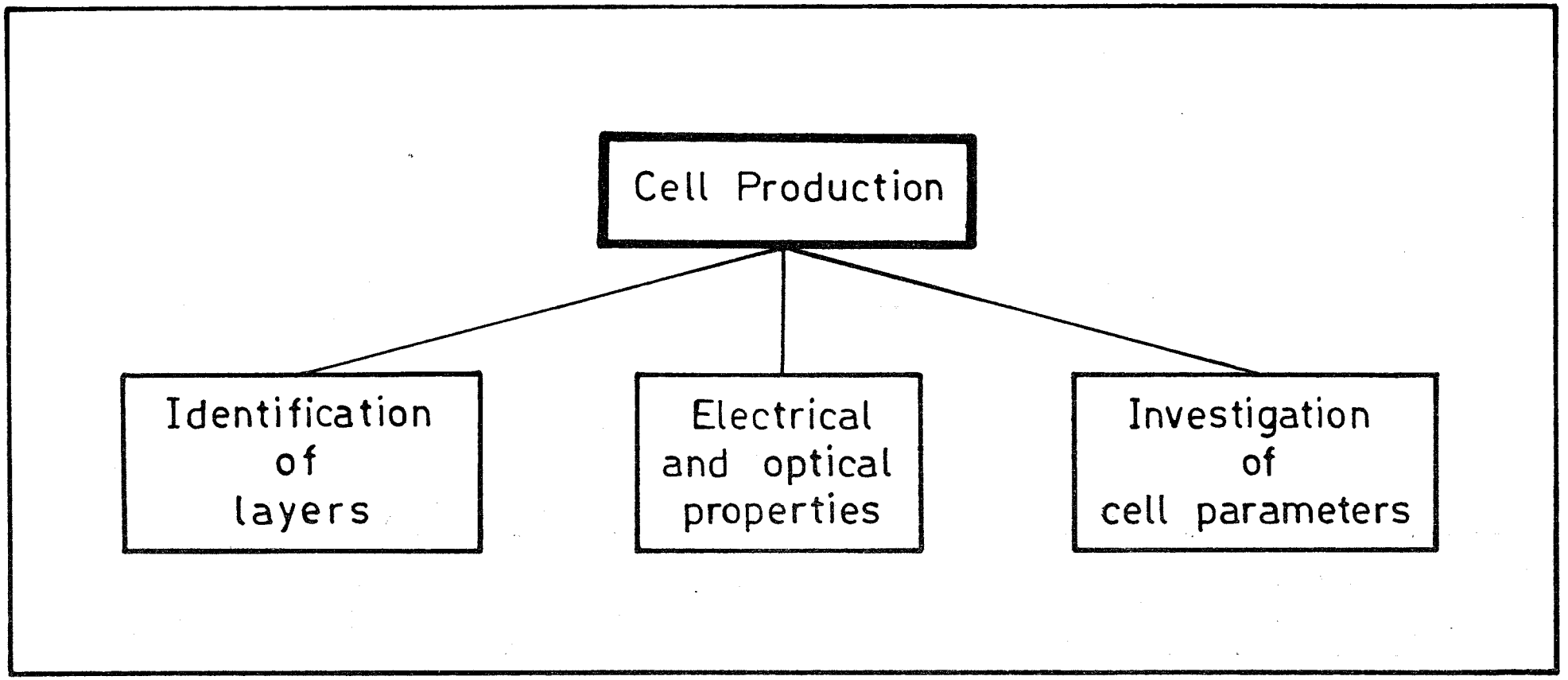

Fig. 4. Schematic representation of the Project's Master Plan.

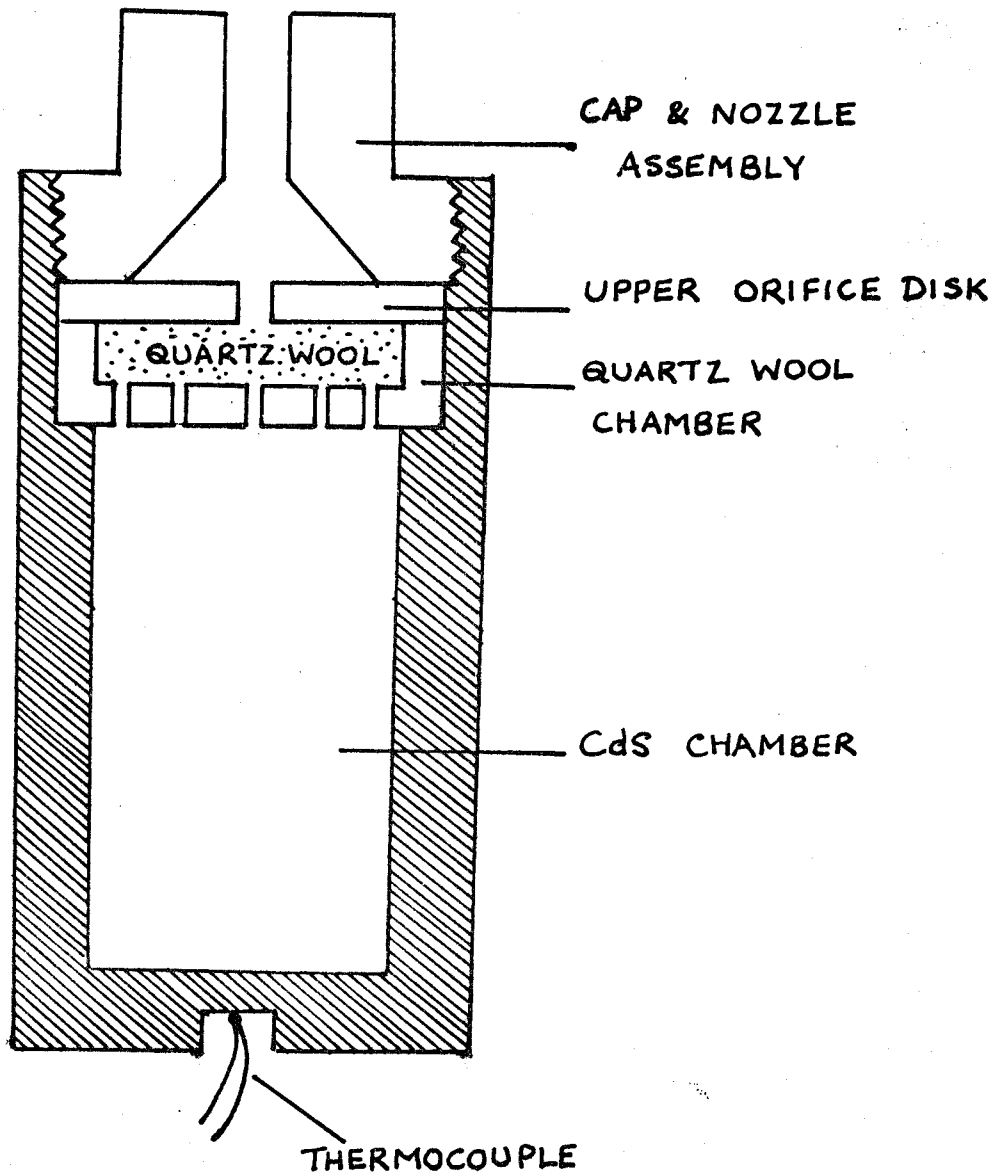

FIG. 5. DESIGN OF THE GRAPHITE BOAT ASSEMBLY.

any particles that may sputter out, and then finally the vapour is concentrated through the upper orifice disc and nozzle onto the substrate. A high current was needed (over 200 A) to heat the graphite boat.

We have also prepared n-type CdS in the form of ceramic discs. Such CdS/Cu_xS cells have been reported by Nakayama, 1969 and Matsumoto et al, 1976 to have high efficiency (over 9%). CdS powder of high purity (5N) was pressed in the form of discs (ϕ = 10 mm) with 300 μm thickness under a pressure of 4 Tons/cm^2 at room temperature and under vacuum. Such discs were then sintered at temperatures between 700°and 800°C in an inert atmosphere (Argon) using a silica glass tube furnace, for times ranging from one to five hours.

The p-type copper sulfide layer was prepared by substitutional reaction using either the "dipping" or wet technique or solid state reaction or the dry technique, or by direct vacuum deposition. In the chemical process, proposed by Shirland and Hietanen, 1965 and developed by Mytton, 1968, a substitutional reaction takes place, causing the displacement of one Cd ion by two Cu ions,

$$Cu_2^{2+} + CdS \rightleftharpoons Cu_2S + Cd^{2+}$$

or

$$2CuCl + CdS \longrightarrow Cu_2S + CdCl_2$$

The reaction takes place by dipping the CdS (ceramic disc or thin film) into a hot (90°C) acidic solution (pH ~ 2.5) of CuCl. A precise control of the dipping solution conditions (concentration, temperature, acidity and dipping time) is very important.

The dipping process is the most commonly used method for the formation of the Cu_2S layers for the Cu_2S/CdS solar cells. One obtains composition close to Cu_2S. However, as shown by Besson et al, 1975, the best composition for the cells is $Cu_{1.995}S$, Fig. 6.

The dry technique for barrier formation was developed by Te Velde 1973, for the fabrication of Cu_xS/CdS solar cells. In this case, high purity cuprous chloride (CuCl) is deposited under vacuum on CdS film. The cadmium sulfide with the film of cuprous chloride is then heated to 180 C in an inert atmosphere, and a solid state reaction occurs,

$$2\ CuCl + CdS \longrightarrow Cu_2S + CdCl_2 \quad . \ . \ . \ (1.1)$$

The reaction is completed after a certain time (usually few minutes). After cooling to room temperature, the surface layer of $CdCl_2$ is removed by washing in absolute alcohol.

The formation of Cu_xS layer by the technique of vapour deposition under vacuum required a primary synthesis of copper sulfide material. Copper sulfide is one member of the copper chalcogenide family of CuX, where X = S, Se or Te.

There are various methods of preparing copper chalcogenides. We chose the so-called "fusion method" which is generally used when the melting points of the reacting components differ largely. In this method, the reaction between the chalcogen vapour and the molten copper is allowed to take place gradually in an evacuated quartz tube. A two-section furnace operating at

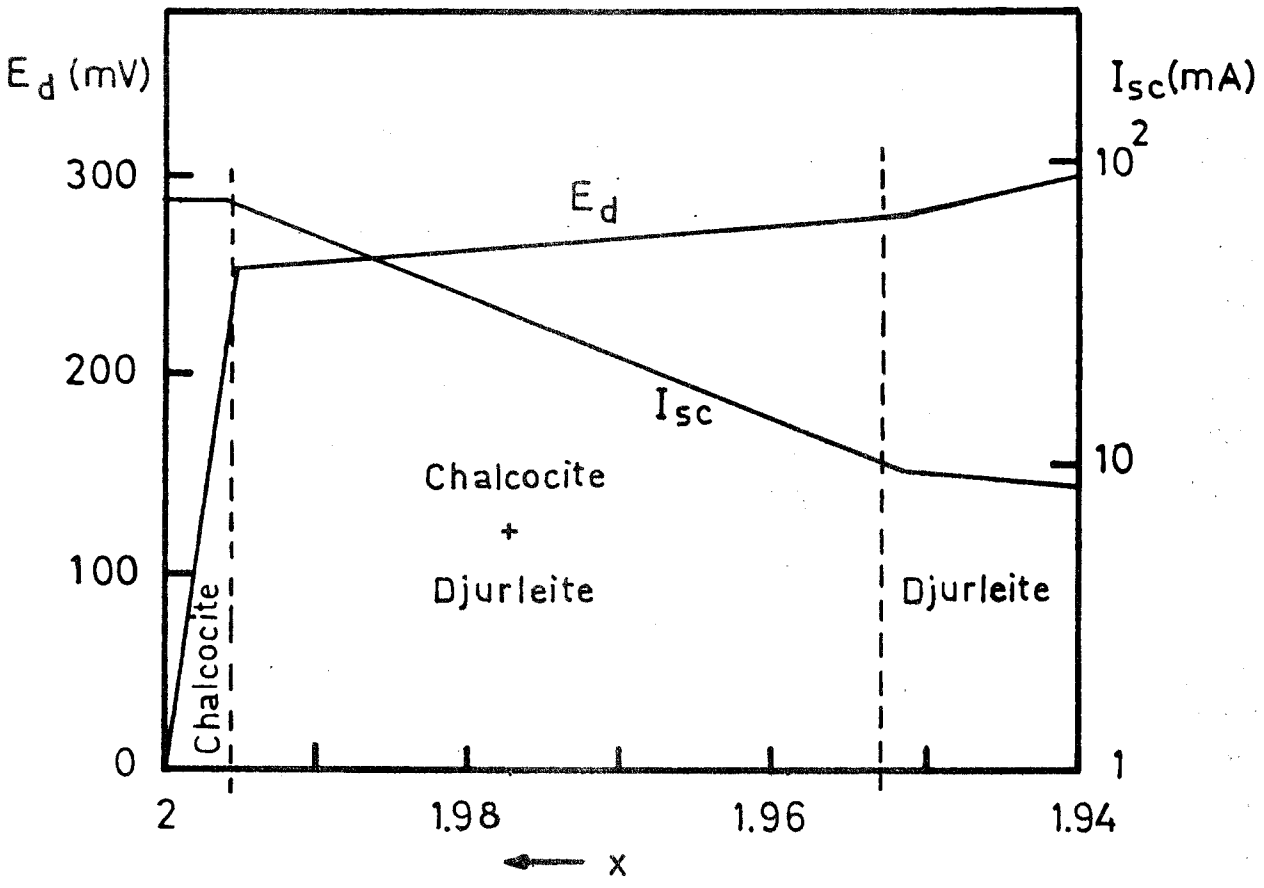

Fig. 6. Decomposition emf E_d and short-circuit current I_{sc} as function of x in $Cu_x S$.

1300°C (Heraus, West Germany) was used. The components (5N copper and sulfur) in stoichiometric proportion, were put into a silica tube which was then placed inside the furnace. The temperature of the mixture (Cu + S) in the hot section was raised gradually to 1200°C which is close to the melting temperature of copper. The "cold" section was kept at 200° C and then gradually heated to about 700° C (higher than the melting temperature of sulfur). After completion of the reaction (revealed by the disappearance of sulfur vapour) the temperature of the cold end was raised to 1200° C and the assembly was shaken to ensure homogeneity. The temperature was kept at 1200° C for about 5 hours and then slowly lowered down to 800° C at a rate of 30° C/h. The obtained material was in the form of a grey compact ingot of homogeneous structure as revealed by X-ray analysis.

After the formation of the Cu_xS layer, the next step in cell fabrication is the formation of the p-n junction. A heat treatment at a temperature in the range 150° - 200° C for a few minutes is usually needed to obtain a good p-n junction (Te Velde, 1973). After the annealing treatment, the top electrode is formed by vapour deposition in vacuum.

X-Ray and SEM Studies:

X-ray diffraction and scanning electron microscopy (SEM) were employed for identification of the CdS and Cu_xS layers. The X-ray analysis was carried out using Siemens D500 diffractometer operating at 36 kV - 20 mA. The diffractograms were

recorded automatically with a scanning speed of 2^{o} per minute and a scanning angular range of 10^{o} to 90^{o}. The charts were analysed with the aid of ASTM powder diffraction data cards (Cullity, 1978). The method consists of comparing the observed d_{hkl} values (calculated from Bragg equqtion, $2d_{hkl}\sin\theta = n$) with the standard d_{hkl} values from the ASTM cards.

For SEM analysis a scanning electron microscope was employed, operating at 15 kV. This analysis was confined to the ceramic CdS/Cu_xS cells, as the technique was introduced in the later stage of our work. Our initial analyses were carried out using X-ray diffraction only.

Measurement of Electrical Resistivity:

The electrical resistivity of deposited CdS films were carried out using the non-linear four-probe method. This method is used to measure the resistivity (ρ) of arbitrary shaped specimens as was shown by van der Pauw, 1958. The basic set up is shown in Fig. 7. Four electrodes 1, 2, 3 and 4 are connected to the four point contacts (indium is used for obtaining ohmic contacts) of the specimen. The resistance of the specimen is determined as the ratio of the potential difference between any two contacts to the current passing through the specimen between the remaining two contacts.

The basic equation for the specific resistivity (ρ) of a square sample of side s is given by

$$\rho = \frac{2\pi}{2-\sqrt{2}} \; s \; \frac{V}{I} = 10.7 \; s \; \frac{V}{I} \quad \ldots\ldots (2.1)$$

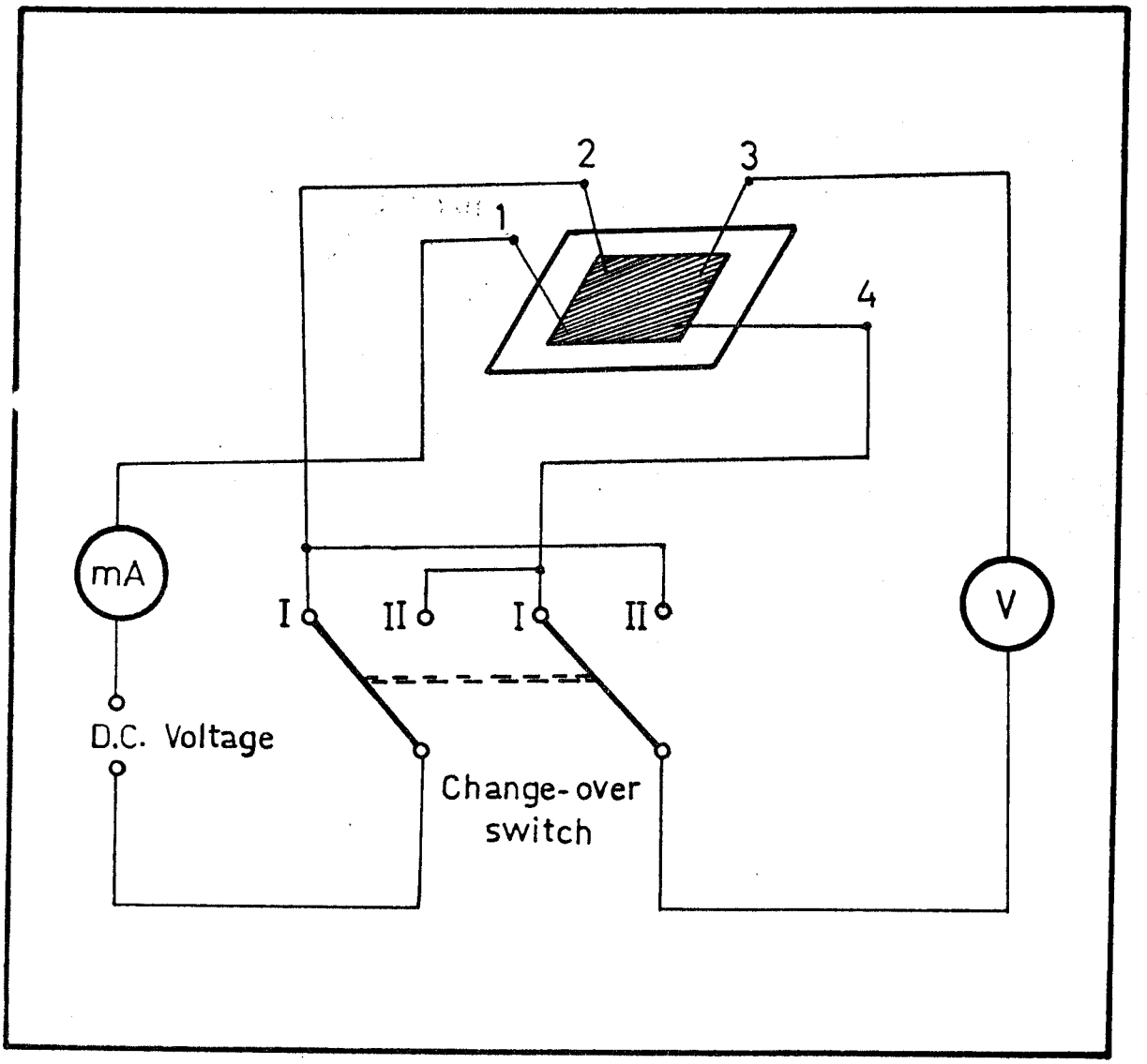

Fig. 7. Schematic diagram of measuring the specific resistance "ρ".

The above relation (Runyan, 1975) corresponds to the case of a square array resting on the surface of a semi-infinite medium.

The electrical resistivity of our samples was measured in dark at room temperature taking into consideration the various corrections developed for a square array.

Measurement of Optical Properties:

The study of the optical properties of the CdS and Cu_xS layers comprise an essential and equally important part of our studies. From reflectance and transmittance measurements one can determine important data relevant to solar cell studies like the energy gap ΔE_g, for example, as well as other important optical constants (n and k) of the materials.

Of the several experimental methods available, the most commonly employed one is the spectrophotometric method carried out at normal incidence. In our studies, the reflectance (R) and transmittance (T) for the spectral range of interest were measured using a spectrophotometer type VSU2, Germany.

Transmittance. The technique of transmittance measurement consists of coating one third of a glass substrate with an opaque aluminium layer, another third with the CdS/Cu_xS film under investigation and keeping the third part clean. The intensity of light passing through the film is measured relative to that passing through the clean part of the substrate, thus eliminating any existing light absorption in the substrate material.

The intensities I_f and I_g of light passing through the film-glass system and the glass, respectively can be expressed by the following relations:

$$I_f = I_o T (1 - R_g)(1 - A_g) \quad \ldots\ldots (3.1)$$

$$I_g = I_o (1 - R_g)^2 (1 - A_g) \quad \ldots\ldots (4.1)$$

where I_o is the intensity of light incident on the system,

T is the transmittance of the coating film,

R_g and A_g are the reflectance and absorptance of the substrate, respectively.

From equations (3.1) and (4.1) one obtains

$$T = (1 - R_g) \frac{I_f}{I_g} \quad \ldots\ldots\ldots (5.1)$$

Reflectance: A special attachment, Fig. 8, was used with the spectrophotometer for measuring the reflectance of the sample at normal incidence relative to the opaque aluminium coating. The reflectance is determined from the following expression given by Sklyarevskii and Korneeva, 1968,

$$R = \frac{I}{I_{Al}} R_{Al} - T^2 R_g (1 - A_g)^2 \quad \ldots (6.1)$$

where I is the intensity of the reflected light from the sample film,

I_{Al} is the intensity of the reflected light from the opaque Al layer,

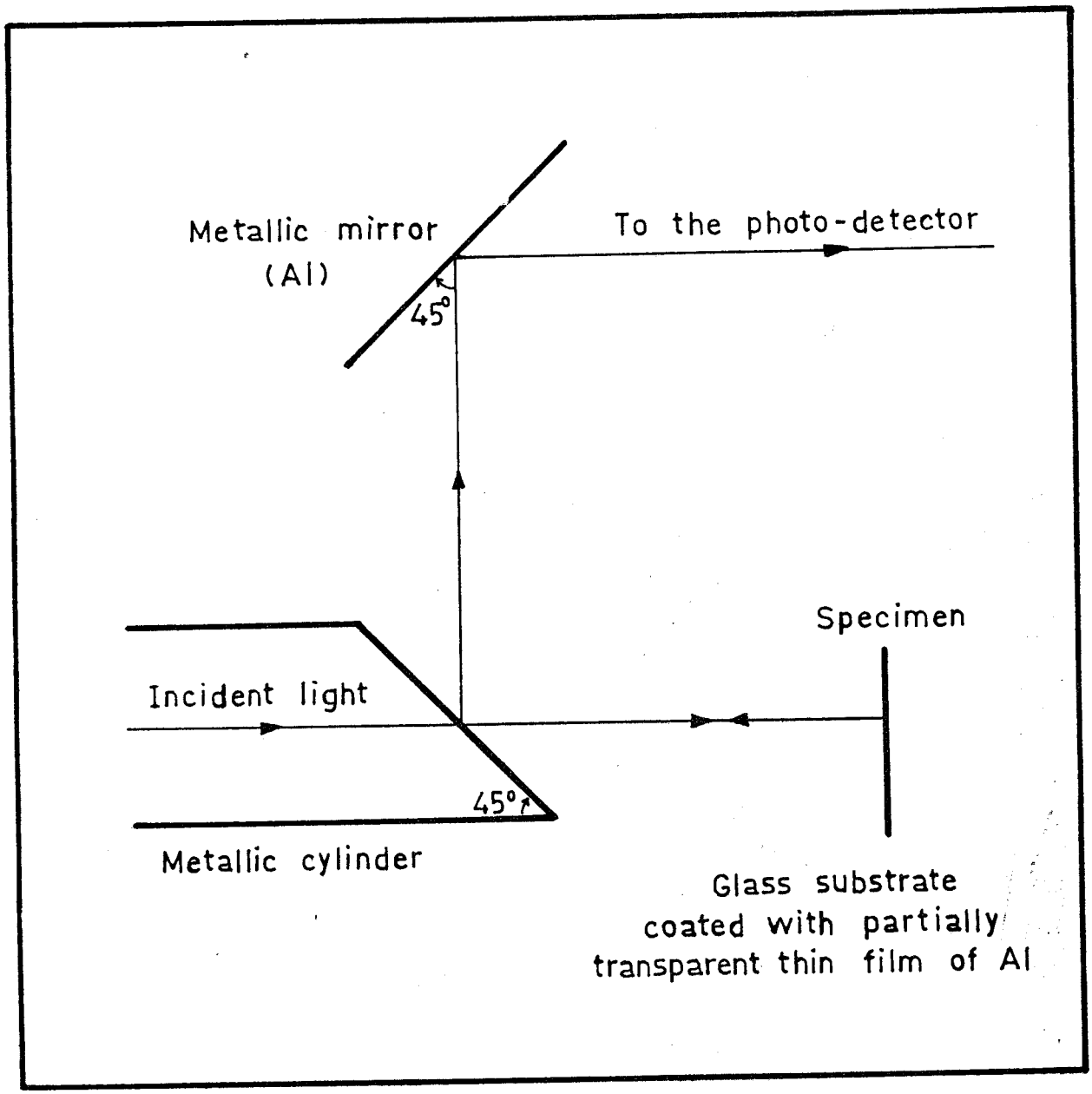

Fig. 8. Attachment for the reflectance measurement of thin films.

T is the transmittance through the film-substrate system, and R_g and A_g, the reflectance and absorptance of glass, respectively.

The reflectance of Al can be calculated from the formula,

$$R_{Al} = \frac{(n-1)^2 - k^2}{(n+1)^2 + k^2} \quad \ldots\ldots\ldots (7.1)$$

knowing n and k for Al. In the spectral region $\lambda = 0.4 - 1.1$ μm, we can neglect Ag. Thus equation (6.1) becomes,

$$R = \frac{I}{I_{Al}} - R_{Al} - T^2 R_g \quad \ldots\ldots (8.1)$$

Accordingly, measuring I and I_{Al}, the reflectance of the sample can be calculated.

Measurement of Photoconductivity:

This was carried out for both single crystal and thin film CdS samples possessing high resistivities. The single crystal samples were $\sim$ 10 x 5 x 0.5 mm^3 in size while the thin film samples had thicknesses lying between 0.8 and 2 μm. Before making measurements, the single crystal samples were always polished on their surfaces with fine diamond paste. Ohmic contacts were prepared by soldering pure indium.

The experimental arrangement is explained in many text-books (e.g. Ryvkin, 1964). The sample was illuminated with

monochromatic light using a Tungsten filament lamp (1000 W) and optical filters (in the range 0.4 to 0.8 μm). The intensity of the light was modulated by means of a mechanical chopper with frequencies (f) ranging from 20 to 1000 Hz. The spectral response characteristics were examined under 100 volt . The photocurrent was measured using a Kiethley Electrometer (type 610C). Samples were mounted in a thermally isolated and completely dark box. Measurements were carried out either in vacuum or in ambient atmosphere at room temperature.

The steady state photoconductivity $\delta\sigma_{st}$ (for $f = 0$) is given by

$$\frac{\delta\sigma}{\delta\sigma_{st}} = \tanh\left(\frac{1}{4\tau f}\right) \qquad \ldots\ldots (9.1)$$

where $\delta\sigma$ is the ac component of photoconductivity,

f is the measuring frequency and

τ is the effective relaxation time.

Investigation of Cell Parameters:

The various cell parameters of the p-Cu_xS / n-CdS heterojunction, viz., the open circuit voltage V_{oc}, the short circuit current I_{sc}, series resistance R_s, shunt resistance R_{sh}, fill factor FF, and efficiency η were determined from the current-voltage characteristics for different samples. The I-V characteristics were directly observed on a Tektronix curve tracer model 507D.

Another circuit, Fig. 9, was used to measure the loaded I-V characteristics in dark and under illumination (light illumination was provided by means of a pre-calibrated incandescent lamp) and also to study the spectral response of the I-V curves. A high impedance (10^8 Ohm) Philips Voltmeter type PM 2434 was used to measure the voltage across the cell. A 1.5 volts dc battery was used to compensate the voltage drop across the cell under illumination with zero load in order to determine I_{sc}. The series resistance R_s was determined by applying a sufficiently large forward bias. Measurement of I and V in this case allows R_s to be obtained directly.

To study the power output, an illuminated solar cell was connected to a resistive load, the value of which is varied from zero to infinity, as shown in Fig. 9. The maximum power that the cell can deliver under conditions of test can be obtained from this characteristic, as well as the shunt resistance, using the relation (Bryant and Glew, 1975),

$$R_{sh} = \left| \frac{\partial V}{\partial I} \right|_{V_L} = 0$$

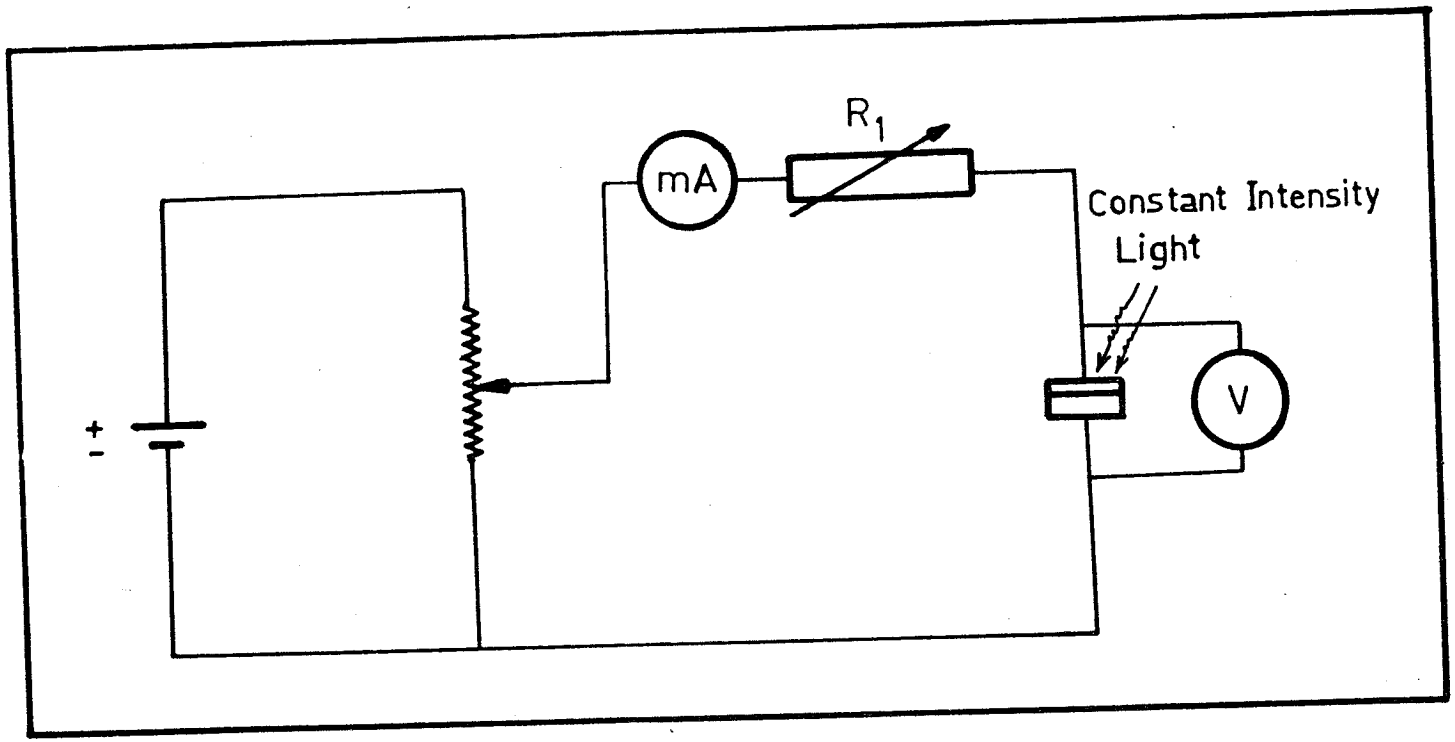

Fig. 9. The circuit used to measure cell parameters V_{oc}, I_{sc}, FF.

SECTION 4

RESULTS AND DISCUSSIONS

4.1. PHYSICAL PROPERTIES OF MATERIALS

a. Structure of CdS Films:

Cadmium sulfide is a binary $A_{II}B_{VI}$ compound which crystallizes in two allotropic forms (Aven and Prener, 1967) with the structures of zinc blende & wurtzite. The blende structure can be considered as the result of two interpenetrating cubic close packed lattice with lattice parameter a = 5.839 Å . The wurtzite structure is composed of two interpenetrating close packed hexagonal lattices with lattice parameters a = 4.613 Å and c = 6.716 Å .

Evaporated CdS films which were investigated on glass substrates were polycrystalline and the hexagonal structure was predominant. They showed the well-known characteristic peaks of the hexagonal phase of CdS. Fig. 10 represents a typical X-ray diffraction pattern for an evaporated CdS film. The observed peaks have been compared with those of ASTM cards. From such comparison, the calculated lattice parameters for the hexagonal wurtzite phase are a = 4.16 Å and c = 6.745 Å.

For the majority of the samples, the intense (002) peak in the diffraction pattern indicates a preferred orientation

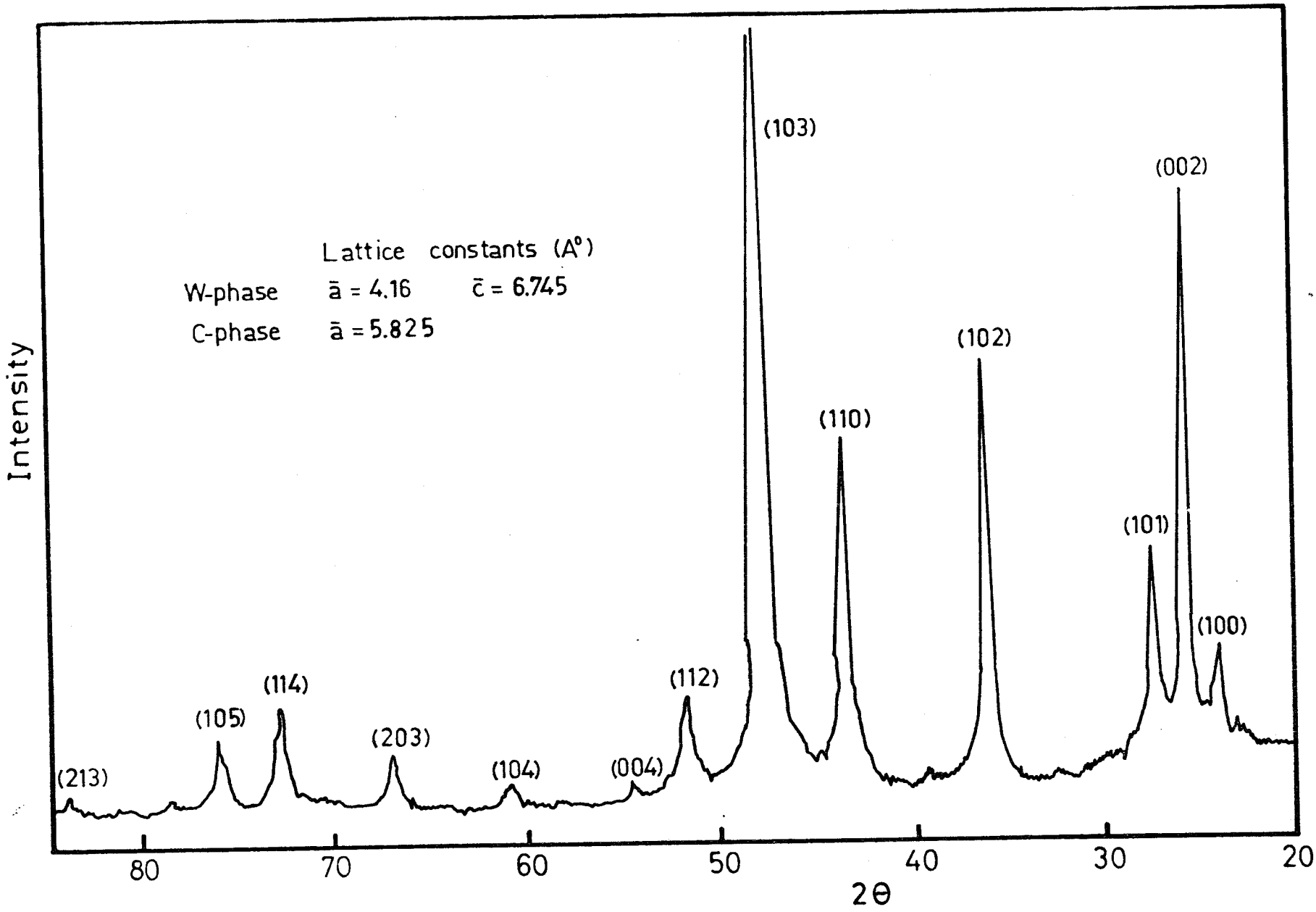

Fig.10. X-ray diffraction pattern of CdS film evaporated on glass substrate.

with the c-axis normal to the substrate surface. These results agree with the data published by Aven and Prener, 1967.

We have also investigated the effect of substrate temperature and film deposition rate on the X-ray diffractograms of CdS films. The effect of substrate temperature T_s on the orientation of CdS films (thickness 3 μm and deposition rate 0.3 μm/min.) is shown in Fig. 11, and obtained data are listed in Table 3. The substrate temperature ranged from -196°C to 300°C. The preferred orientation was referred to the intensity of the basal reflections (00ℓ), e.g., the (002) plane (Smith, 1978).

The data shows that the width and height of the diffraction peaks change with substrate temperature. This change is more appreciable for the (002), (103) and (105) planes. When the substrate is kept at room temperature, the peaks are broad and less intense compared to the results at higher substrate temperatures. This indicates a lesser degree of crystallinity due to the relatively abrupt cooling of the vapour. At 150°C, an increase in the intensity of the (002) reflections and a decrease in the (101) reflections take place; this may be attributed to changes in the stoichiometry of the CdS structure.

The maximum intensity of the (002) plane was obtained at 250°C, Fig. 12, accompanied by the disappearance of the (101) plane, indicating that the film achieved maximum degree of preferred orientation. In this case, the ratio of the intensity of (101) peak to that of (002) peak is very small. This indicates that $Cd^{++} < S^{--}$, i.e., no free cadmium exists in

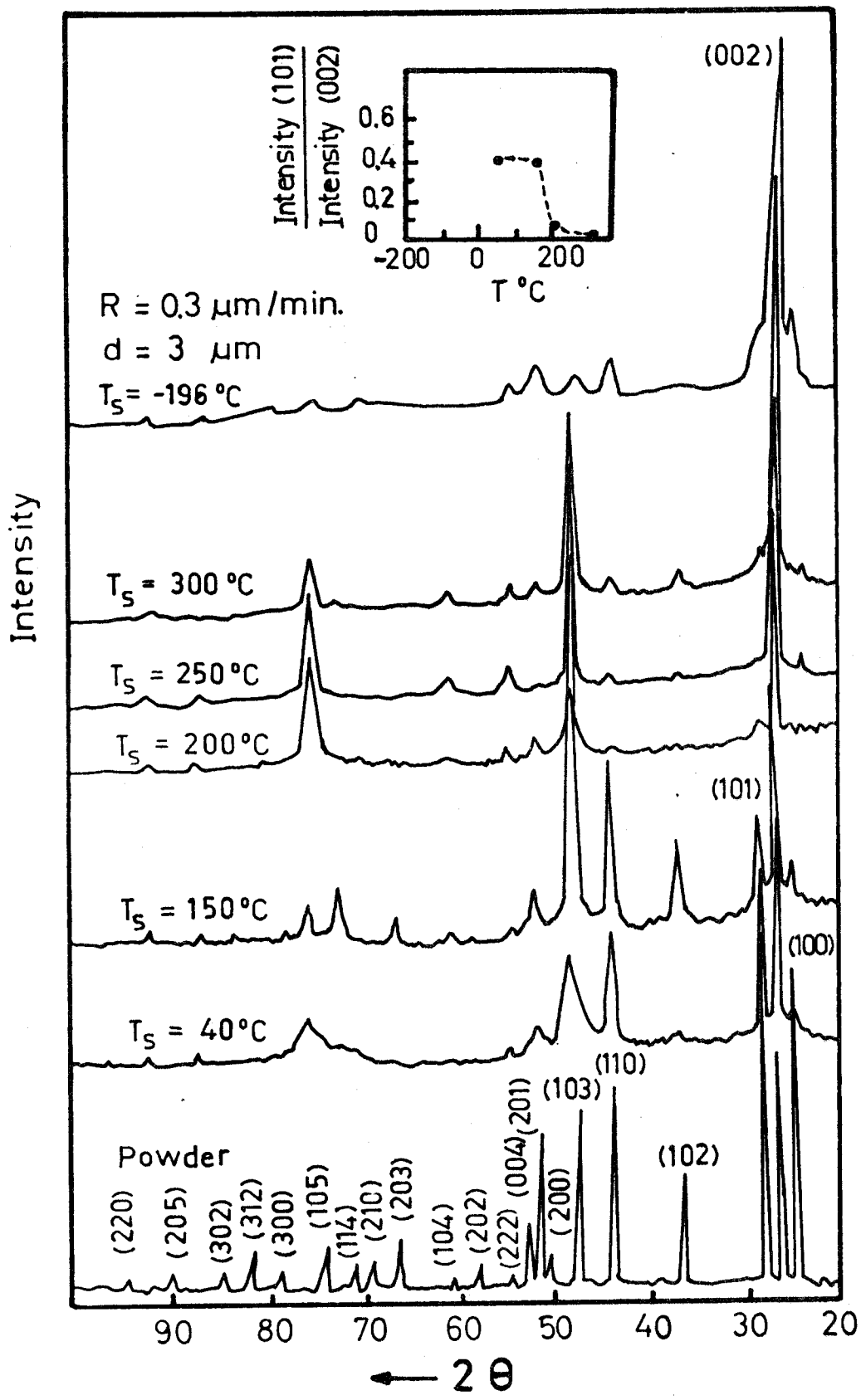

Fig. 11. X-ray diffractograms as a function of substrate temperature for CdS thin films.

Table 3

X-Ray data of thin film CdS evaporated at different substrate temperature

A.S.T.M.			CdS thin films evaporated at substrate temperature (T_s)																	
			T_s = - 196 °C			T_s = 40 °C			T_s = 150 °C			T_s = 200 °C			T_s = 250 °C			T_s = 300 °C		
d A°	I/I_o	(hkl)	$d_{obs.}$ A°	I/I_o	(hkl)	$d_{obs.}$ A°	I/I_o	(hkl)	$d_{obs.}$ A°	I/I_o	(hkl)	$d_{obs.}$ A°	I/I_o	(hkl)	$d_{obs.}$ A°	I/I_o	(hkl)	$d_{obs.}$ A°	I/I_o	(hkl)
3.583	75	(100)	3.558	14	(100)	3.58	14	(100)	3.56	11.8	(100)	3.544	1.8	(100)	3.558	3	(110)	3.558	4	(100)
3.357	59	(002)	3.323	100	(002)	3.348	100	(002)	3.35	59	(002)	3.335	56	(002)	3.323	100	(002)	3.347	100	(002)
3.16	100	(101)	3.15	12	(101)	3.15	4	(101)	3.15	22.7	(101)	3.139	2	(101)				3.139	6	(101)
2.45	25	(102)							2.44	19	(102)	2.433	6	(102)				2.433	3	(102)
2.068	57	(110)	2.055	7	(110)	2.065	40	(110)	2.058	37.8	(110)	2.0555	14	(110)	2.055	1	(110)	2.0555	3	(110)
1.898	42	(103)	1.886	4	(103)	1.894	34	(103)	1.89	100	(103)	1.886	100	(103)	1.893	19	(103)	1.893	31	(103)
1.791	17	(200)																		
1.761	45	(112)	1.7565	6	(112)	1.763	10	(112)	1.76	10.5	(112)	1.7565	3	(112)				1.753	3	(112)
1.731	18	(201)																		
1.679	4	(004)	1.6732	4	(004)	1.678	4	(004)	1.671	2.5	(004)	1.6704	3	(004)	1.6704	5	(004)	1.6704	3	(004)
1.581	7	(202)																		
1.52	2	(104)							1.515	3.4	(104)	1.515	5	(104)	1.515	2.5	(104)	1.513	2	(104)
1.398	15	(203)							1.4	5.5	(203)									
1.3536	6	(210)																		
1.3271	11	(211)	1.33	1.6	(211)															
1.303	7	(114)							1.3	10.5	(114)	1.299	2	(114)				1.301	1	(114)
1.257	11	(105)	1.2535	2	(105)	1.255	14	(105)	1.255	6.7	(105)	1.2535	13	(105)	1.2535	18	(105)	1.2535	10	(105)
1.194	8	(300)																		
1.1585	12	(312)																		
1.1249	8	(302)							1.12	2.1	(302)	1.115	1	(302)	1.117	1	(302)	1.117	1	(302)
1.074	6	(205)							1.07	2.1	(205)	1.069	2	(205)	1.067	2	(205)	1.0671	1	(205)
1.034	4	(220)																		

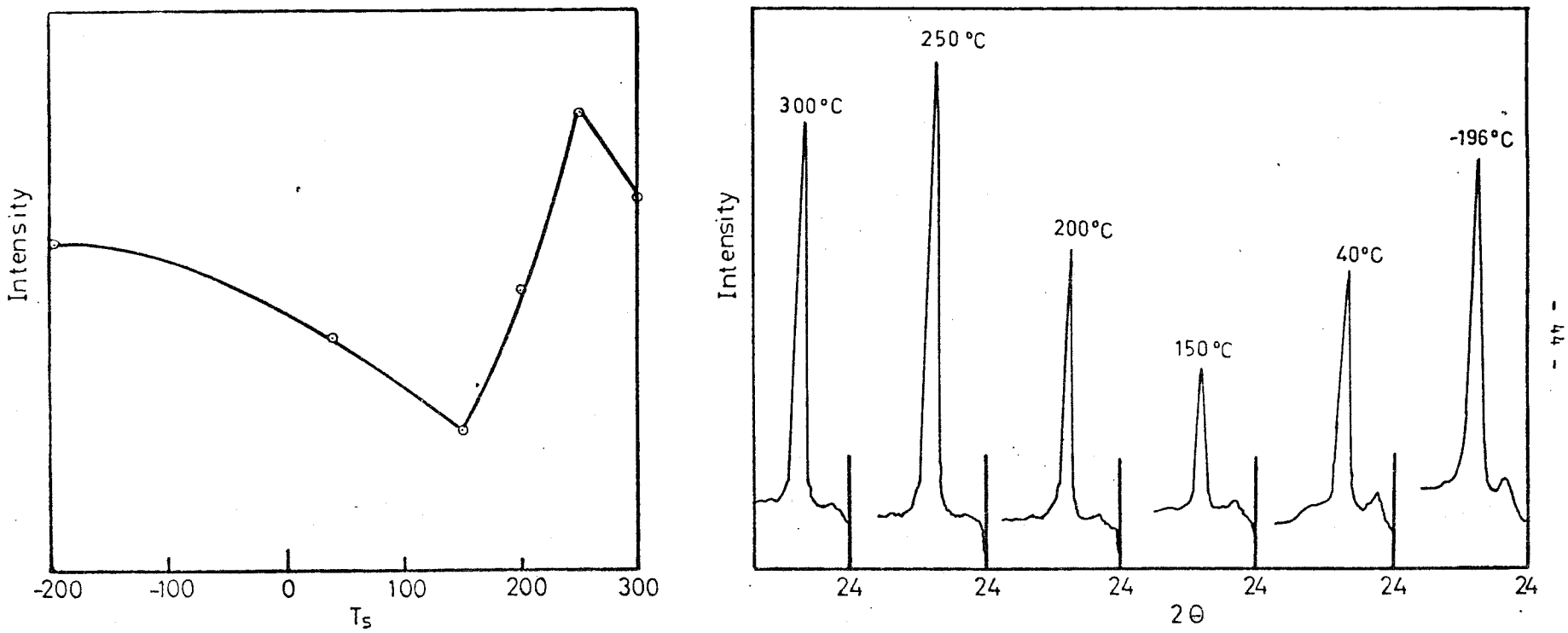

Fig.12. Variation of the maximum intensity of (002) plane for CdS thin film with substrate temperature T_s.

the film, as reported by Savelli and Bougnot, 1979. At T_s = 300°C, the intensity of the (002) plane begins to decrease and the (101) plane appears again indicating a lesser degree of preferred orientation.

It is worthy to mention that when the substrate is at liquid nitrogen temperature, the intensity of the (002) reflection is higher than in the case of T_s = room temperature, but still lower than the corresponding intensity at T_s = 250°C. The (101) plane has an appreciable intensity, but the broadening of the peak makes the latter appears as a shoulder compared to the former. These results agree with those published in the literature (Tyagi et al, 1975; Wilson and Woods, 1973; Okamoto, 1965 and 1966).

To investigate the effect of the film deposition rate, both the substrate temperature and the thickness were kept constant at 200°C and 3 μm respectively. The resulting diffractograms are shown in Fig. 13. and the data is presented in Table 4. It was found that at a low deposition rate, 0.06 μm/min., a better preferred orientation results. The increase in the intensity of the (002) plane and the decrease in the intensity of the (101) plane indicates that the Cd^{++}/S^{--} ratio decreases with increasing the rate of deposition. The present results are in close agreement with other published data (e.g. Foster, 1967).

The relation between the film thickness and the preferred orientation has been satisfactorily studied by Hossain, 1974.

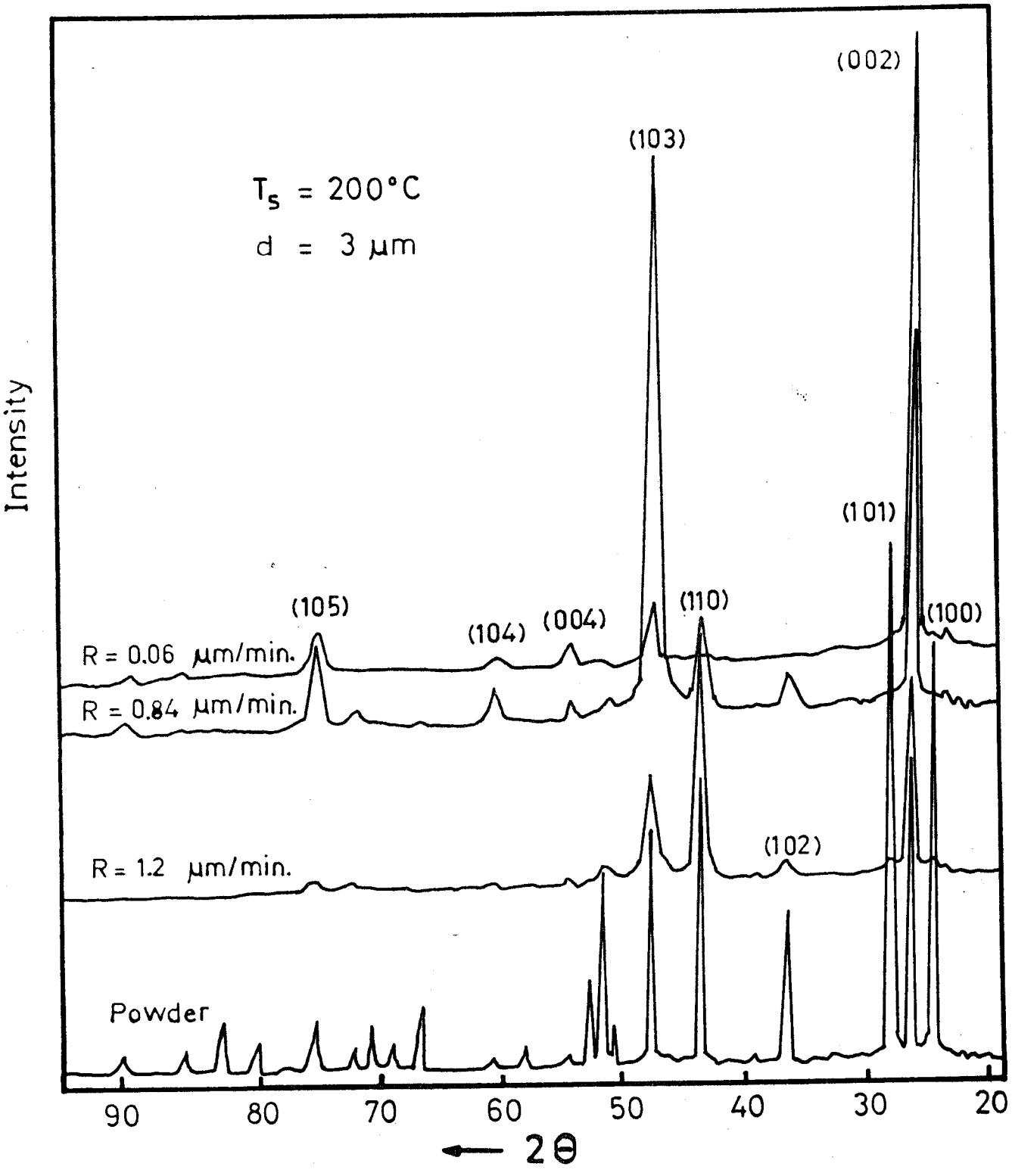

Fig. 13. X-ray diffractograms as a function of deposition rate for CdS thin film.

Table 4

X-Ray data of thin film CdS at different evaporation rate:

A.S.T.M.			R = 10 A°/Sec.			R = 80 A+/Seq.			R = 200 A°/Sec.		
d A°	I/I_o	(hkl)	$d_{obs.}$ A°	I/I_o	(hkl)	$d_{obs.}$ A°	I/I_o	(hkl)	$d_{obs.}$ A°	I/I_o	(hkl)
3.583	95	(100)	3.558	1.5	(100)	3.544	1	(100)	3.558	9	(100)
3.357	59	(002)	3.335	100	(002)	3.335	56	(002)	3.323	73	(002)
3.16	100	(101)				3.139	2	(101)			
2.45	25	(102)	2.427	0.4	(102)	2.433	6	(102)	2.433	7	(102)
2.068	57	(110)	2.0555	1.5	(110)	2.0555	14	(110)	2.0555	100	(110)
1.898	42	(103)	1.8865	8.2	(103)	1.886	100	(103)	1.889	43	(103)
1.791	17	(200)									
1.761	45	(112)				1.7565	3	(112)	1.7565	7	(112)
1.731	18	(201)									
1.679	4	(004)	1.6732	3	(004)	1.6704	3	(004)	1.6704	2	(004)
1.581	7	(202)									
1.52	2	(104)	1.5126	1	(104)	1.515	5	(104)			
1.398	15	(203)									
1.356	6	(210)									
1.3271	11	(211)									
1.303	7	(114)				1.299	2	(114)			
1.257	11	(105)	1.2535	5	(105)	1.2535	13	(105)	1.2507	4	(105)
1.194	8	(300)									
1.1585	12	(312)									
1.1249	8	(302)				1.115	1	(302)			
1.074	6	(205)				1.069	2	(205)			
1.034	4	(220)									

He concluded that preferred orientation occurs at film thicknesses above 0.5 μm.

Thus one can finally conclude that with increasing the substrate temperature (in the range 150 - 250°C) and decreasing the film deposition rate (in the range 1.2 - 0.06 μm/min) better results can be obtained with respect to the preferred orientation of CdS films.

Crystallite size. For estimating the CdS crystallite size of deposited films, the half band width of the (002) peak in the X-ray diffractogram was measured. The crystallite size was then calculated from the simple formula (Wilson and Woods, 1973),

$$L = \frac{\lambda}{D \cos \theta} , \qquad \ldots\ldots\ldots (4.1)$$

where λ is the X-ray wavelength,

D is the angular half width at half the peak height

and θ is the Bragg angle.

It is well known that the X-ray line broadening arises from many factors such as crystallite size, lattice strains and instrumental broadening. During the course of analysis, the instrumental broadening was considered constant. Therefore, the change in the value of the line broadening is a measure of the crystallite size.

For accurate estimation of the crystallite size "L" , the width of the reflecting plane of quartz (annealed at 400°C for one hour) was taken as a reference and Scherrer's equation

(Cullity, 1978) was applied to determine the average crystallite size,

$$L = \frac{k \lambda}{B \cos \theta} , \qquad \ldots\ldots (4.2)$$

where $B = \sqrt{B_s^2 - B_q^2}$, is the increase in the line width,

B_s is the experimentally measured half width of the sample under investigation,

B_q is the measured half width of a line produced under similar conditions by a standard substrate (α-quartz),

λ is the X-ray wavelength (Å),

and k is a constant known as the "shape factor" (numerically, $k \sim 0.95$).

The crystallite size was determined as a function of the substrate temperature and the film deposition rate. The crystallite size was found to increase regularly with the increase of the substrate temperature from - 196°C to room temperature, at a constant deposition rate of 0.06 μm/min., Fig. 14. Above room temperature, the crystallite size increased more rapidly to a maximum value of 1.67 μm at T_s = 200°C , above which the crystallite size decreased again.

The effect of the deposition rate on the crystallite size is presented in Fig. 15. The grain size decreases with the increase of the deposition rate to a certain limit. Above 0.5 μm/min., the change in the grain size is very slight with deposition rate change.

Fig. 14. Grain size of evaporated CdS films as a function of substrate temperature.

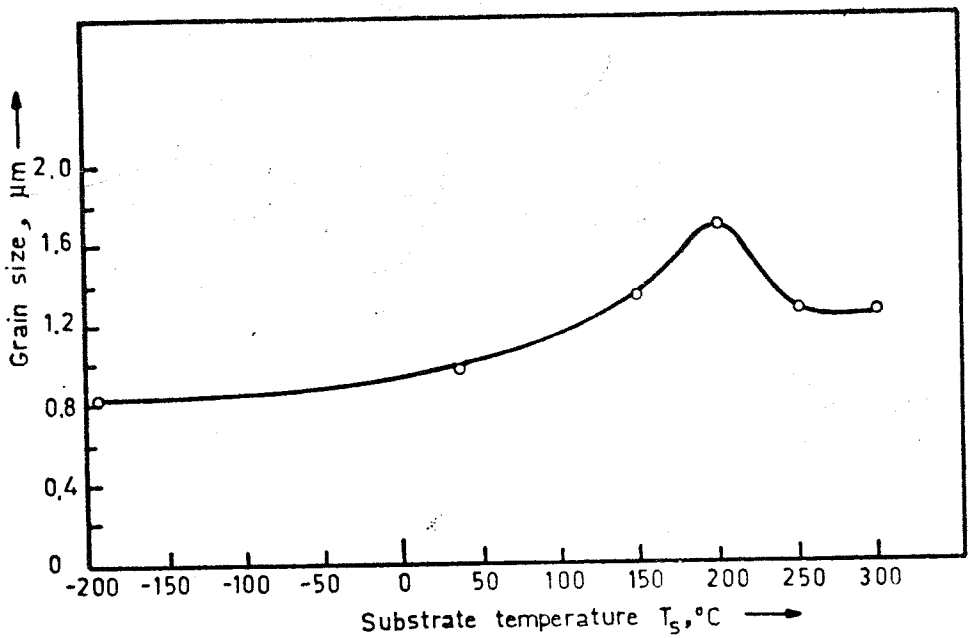

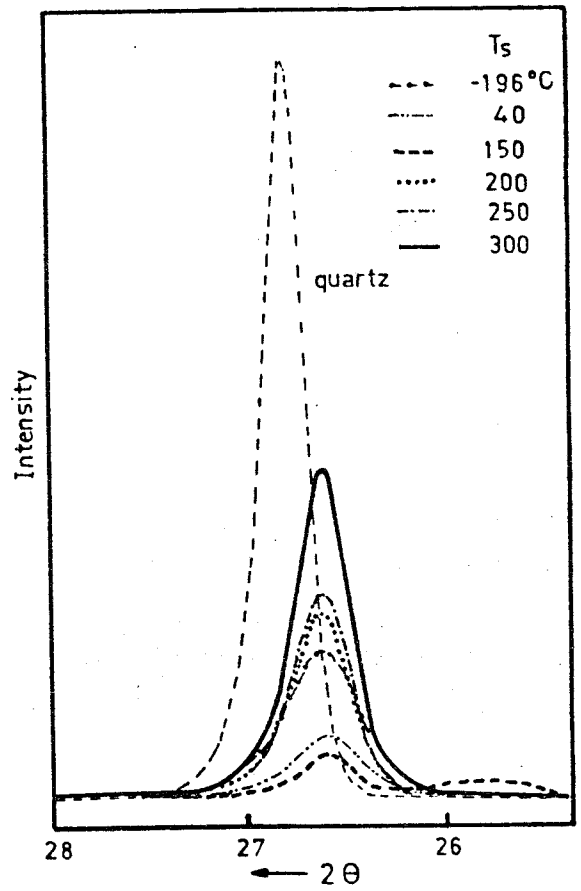

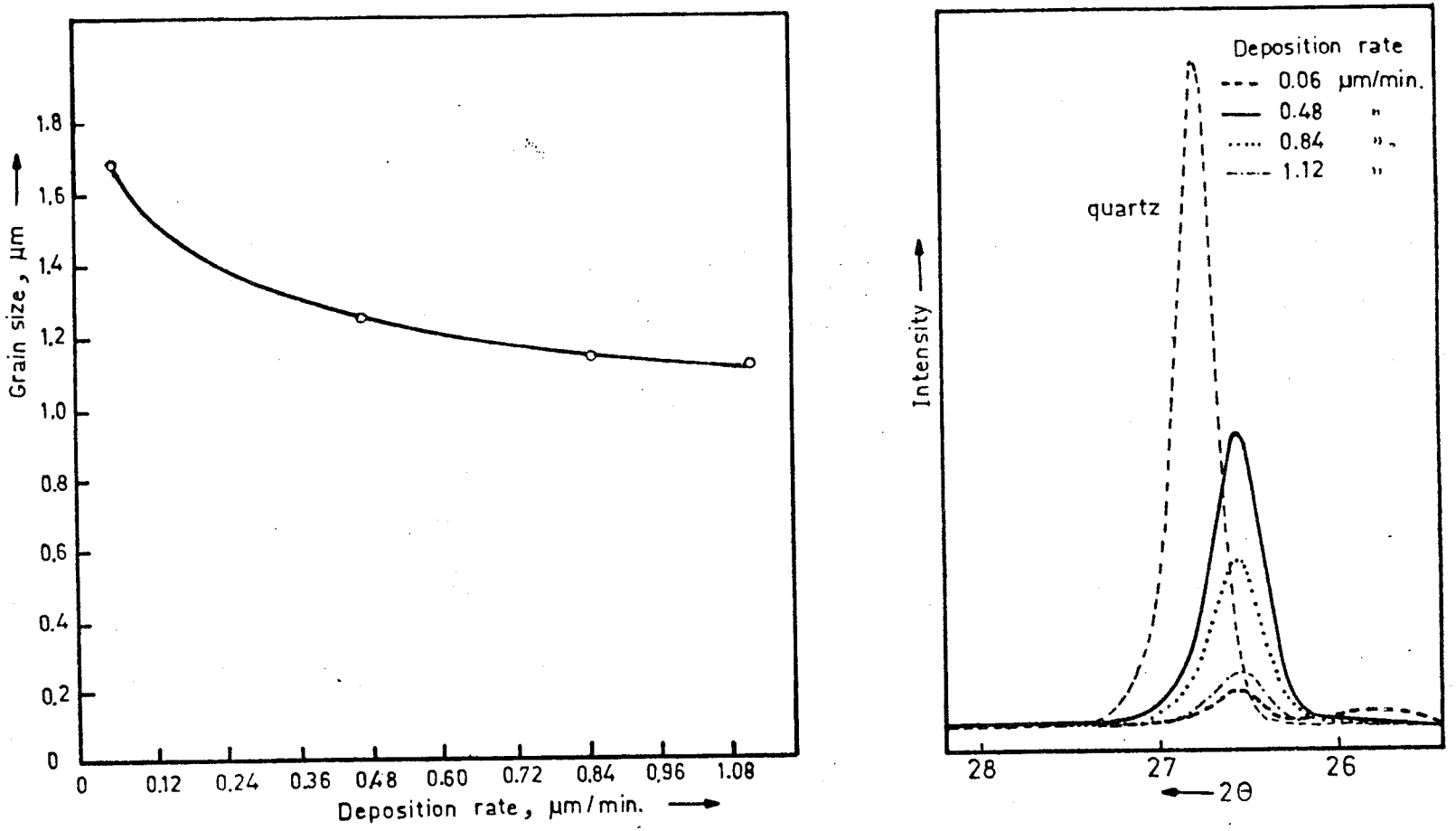

Fig.15. Grain size of evaporated CdS films as a function of the deposition rate.

b. Structure of Cu_xS Thin Films:

The phase diagram of Cu_xS system is enough complicated. The range Cu_2S-$Cu_{1.75}S$ is not well defined and is still a subject of debate in the literate (Savelli and Bougnot, 1979). At room temperature , stable phases are the chalcosite (γ-Cu_2S), the djurleite Cu_xS (x = 1.96 - 1.93), the digenite Cu_xS ($1.765 < x < 1.78$), the anilite $Cu_{1.75}S$ and the covellite CuS.

The chalcocite phase has a very narrow existence range. At room temperature, it crystallizes in orthorohmbic form. The unit cell containing 96 molecules of Cu_2S with the dimensions a = 11.881 Å, b = 27.323 Å and c = 13.491 Å. Chalcocite Cu_2S is a p-type semiconductor with three forms: α-(cubic), β (hexagonal) and γ(orthorohmbic). This material, in the form of thin film, is used together with cadmium sulfide to form the p-n junction used as a solar cell.

Copper sulfide thin films have been prepared by three different methods : by direct evaporation from bulk copper sulfide material, or by substitutional reaction using either the solid state reaction (dry technique) or the dipping (wet) technique.

X-ray diffraction pattern of copper sulfide prepared by vapour deposition on glass substrate is shown in Fig. 16. The d-values were calculated and compared with the standard d-values for bulk orthorohmbic Cu_2S. The calculated average lattice constants are: a = 11.817 Å, b = 27.08 Å and c = 13.35 Å.

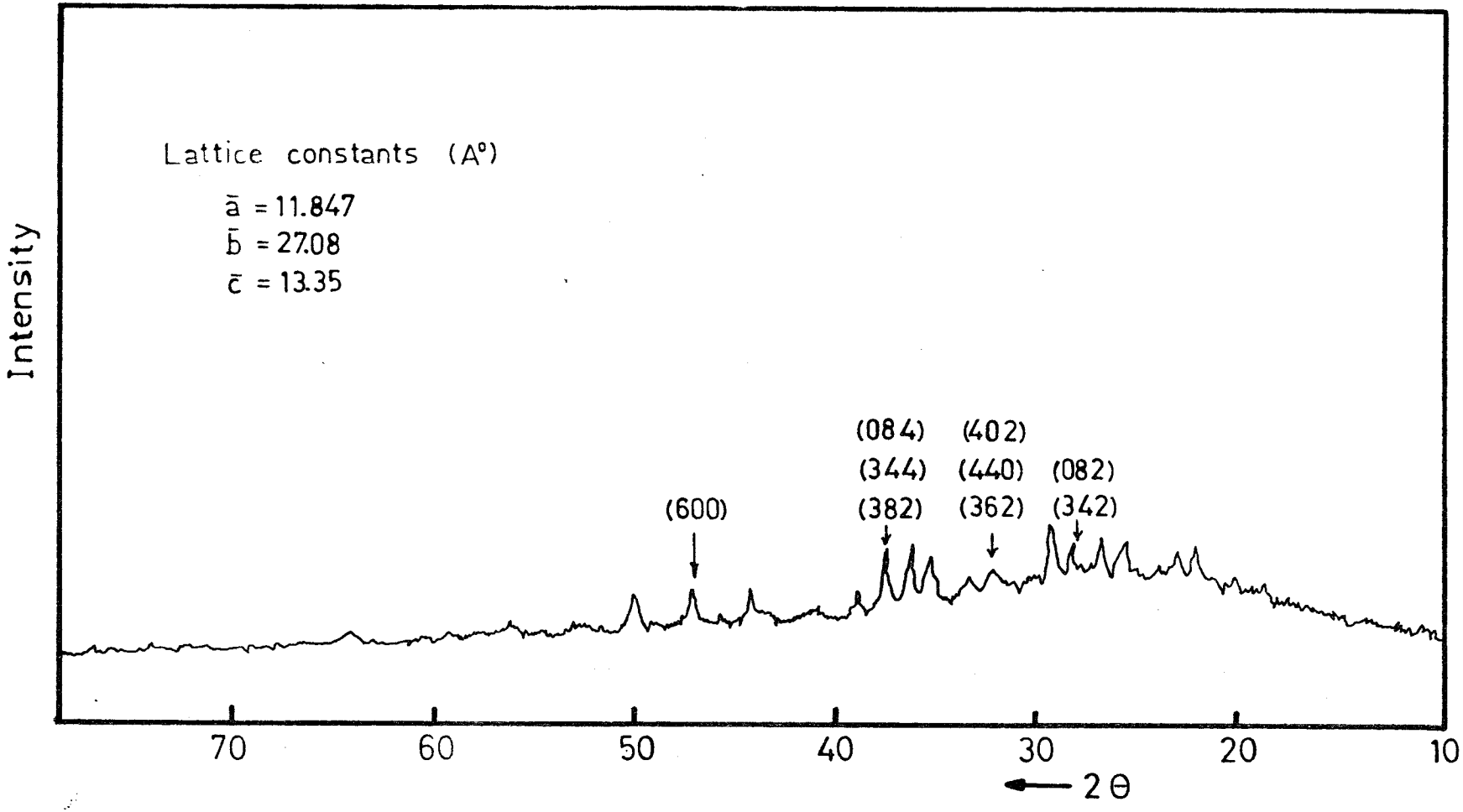

Fig.16. X-ray diffraction pattern of Cu_2S film evaporated on glass substrate.

These values are very close to the standard values for the bulk Cu_2S (Savelli and Bougnot, 1979). Fig. 17 illustrates the diffractograms of Cu_2S film evaporated on CdS thin film.

Cu_xS films could also be obtained by the dipping technique discussed previously with x very close to 2. In our first experiments, the dipping time used was few minutes according to Mytton, 1968. The X-ray diffractograms, however, showed no trace of Cu_2S and, in fact, were representative of typical CdS patterns although such samples exhibited I-V characteristics. Based on this, it was initially concluded (Multidisciplinary Environmental Studies, Report No. 3, Feb. 1981) that X-ray technique is unsuitable for the identification of Cu_2S layer with very small thickness (t) as formed by the wet technique for dipping time of 5 minutes only($t < 1\,\mu$).

It is of interest to note that Böer et al, 1973, have reported the use of a new X-ray diffraction fluorescence method to obtain the structure of the Cu_2S layer. The diffraction patterns obtained were different from expected patterns of standard material and a positive structure identification was not possible. Radler et al, 1979, also reported that X-ray diffraction patterns obtained for most Cu_2S samples were usually not well defined and the diffraction peaks were often broadened or totally smeared.

However, further samples from CdS sintered tablets were dipped in cuprous chloride solution for longer periods of time ranging from 30 to 120 minutes (Nakayama, 1969). Although

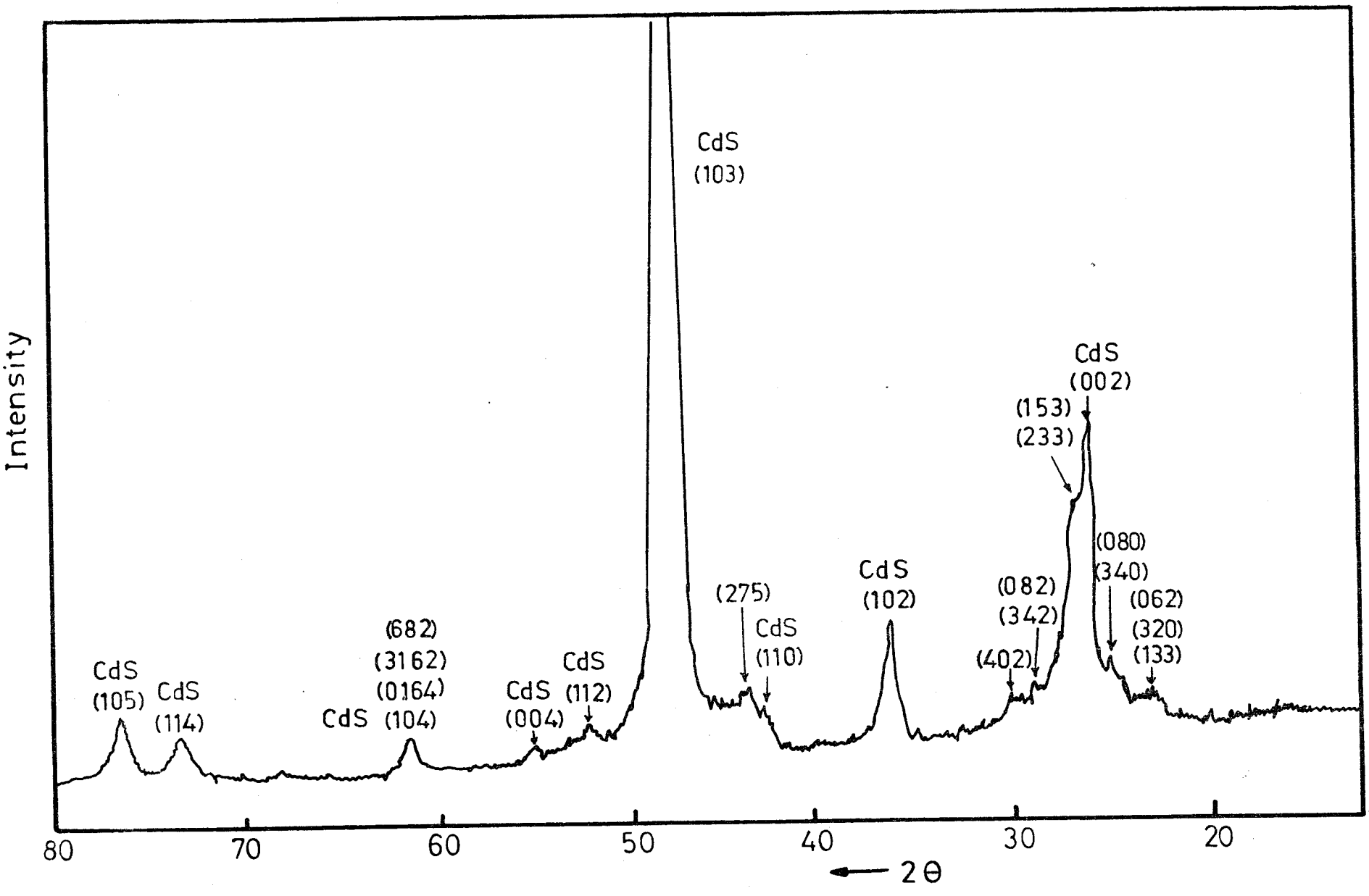

Fig. 17. Cu_2S film evaporated on CdS film.

the sample with dipping time t = 30 minutes showed the characteristic copper sulfide peaks, Fig. 18, the CdS patterns were predominant. An increase in the dipping time from 30 to 120 minutes resulted in a large increase in the copper sulfide peak intensities which can be interpreted as an increase in the abundance of the Cu_2S. At the same time, the CdS reflections were seen to decrease in their relative intensities as the dipping time was increased. These results are presented in Tables 5 and 6.

Table 5

Increase of the relative intensities of some Cu_2S reflections with increase in the dipping time, for Cu_2S layer on sintered CdS base.

Cu_2S peaks	Relative intensity I/I_o		
	30 min	60 min	120 min
(342) (082)	21	52	69
(440) (404) (362)	14	52	59
(600)	11	30	30

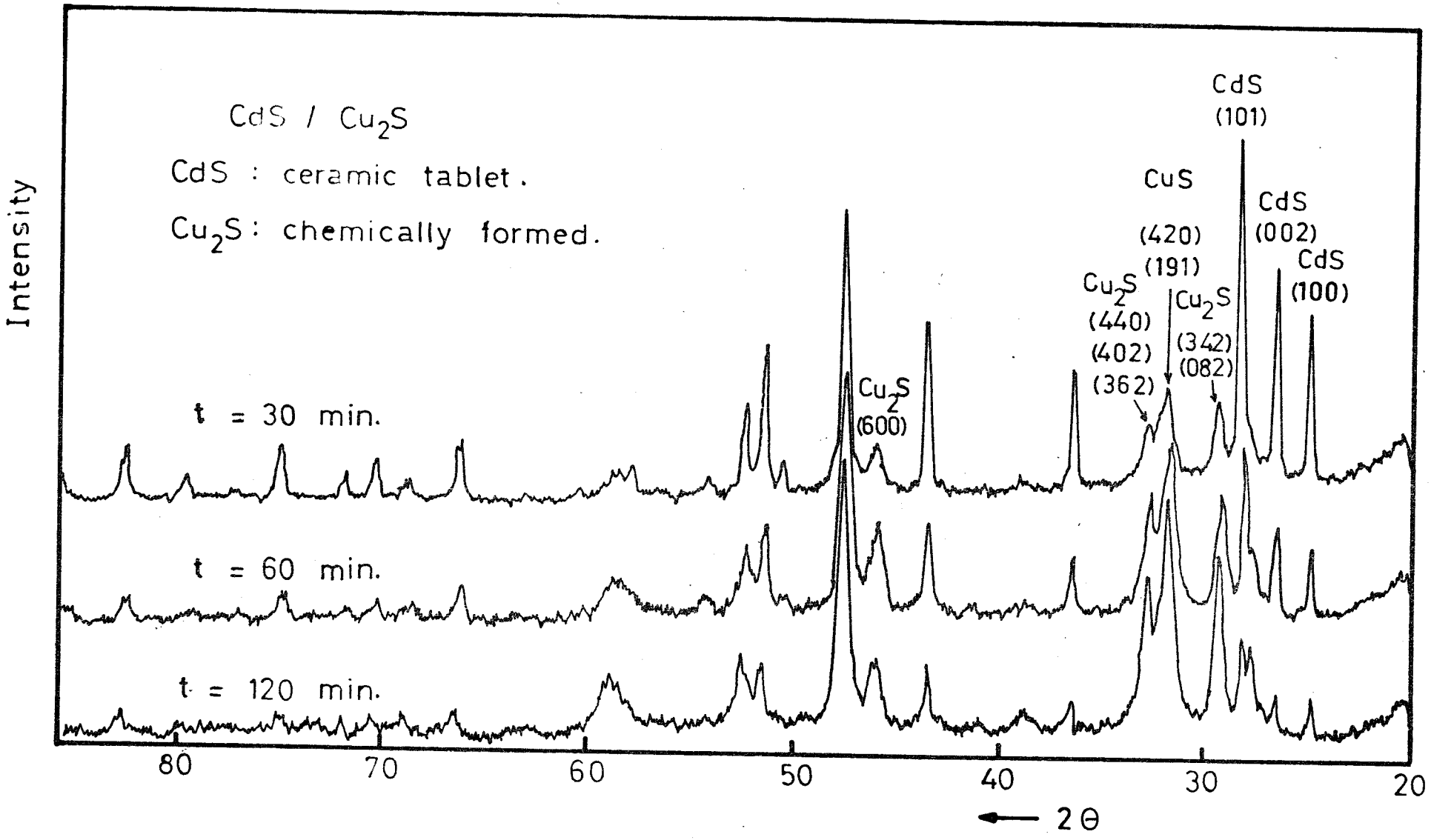

Fig. 18. X-ray diffractograms for Cu_2S/ CdS samples for various dipping times, t.

Table 6

Decrease of the relative intensities of some CdS reflections with increase in the dipping time, for sintered CdS tablet.

CdS peaks	Relative intensity I/I_o		
	30 min	60 min	120 min
(100)	48	30	15
(002)	61	39	17
(101)	100	72	38

Dipping times over 90 minutes, however, led to the formation of CuS which is not desirable. Nakayama, 1969, reported that the surface resistance of the Cu_2S p-layer increases markedly for chemical treatment times over 90 min.

The lattice constants for Cu_2S formed by the dipping process were calculated for various samples and the values for dipping time 30 minutes are: a = 11.784 Å, b = 27.214 Å and c = 13.729 Å. In general, the lattice parameters are found to vary slightly (in the second place of decimal) from the standard values for Cu_2S obtained from ASTM data. These changes clearly indicate a non-stoichiometry and therefore the Cu_2S obtained by the dipping reaction is not strictly Cu_2S.

In our investigation we have used the scanning electron microscope, since it is well established now (Müller et al, 1979 ; University of Delaware, IEC Report, 1981) that SEM is the most direct tool for the systematic investigation of the topographical characteristics and morphology of the different layers in every step of the cell production process.

Representative examples of scanning electron micrographs taken of the Cu_2S surface and fractured side views of the dipped ceramic CdS tablets are given in Photos 1 - 3.

Photos 1 and 2 show the Cu_2S surface features for samples dipped for 30 minutes each but sintered for 1 and 2 hours, respectively at 750°C in Argon atmosphere. Grain growth is clearly observed with change in sintering time and densification of the structure occurs with increased sintering periods.

Photo 3 is a representative micrograph of a fractured side view of a dipped Cu_2S / CdS sample. The Cu_2S and CdS layers are clearly visible. One can notice the intrusion of the Cu_2S into the CdS layer through cracks in the grain boundaries.

c. Transmittance and Reflectance of CdS and Cu_xS Thin Films.

Representative reflectance and transmittance curves of a CdS thin film (thickness 2 μm and deposition rate 0.15 μm/min) as a function of light wavelength λ , are presented in Fig. 19. It is clear from the figure that, a sharp optical transmittance cut-off occurs at $\lambda = 0.515$ μm. This value corresponds to an optical energy gap $\Delta E_g = 2.42$ eV.

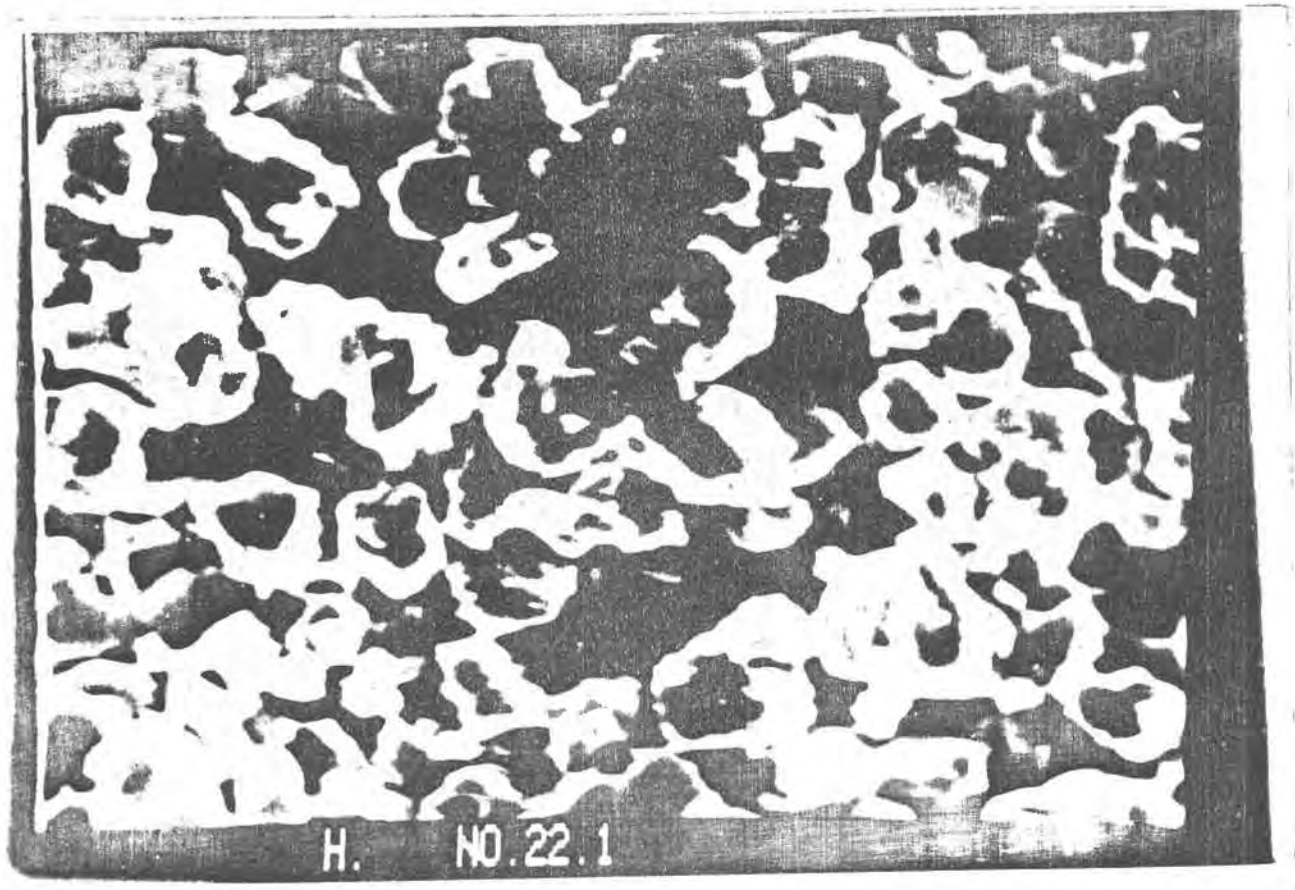

Photo 1. Scanning electron micrograph of Cu_2S surface of a dipped CdS ceramic tablet sintered in argon atmosphere at 750°C for 1 hour and dipping time 30 min. The average grain size of the CdS grains lies between 4 - 7 μm. (4000X)

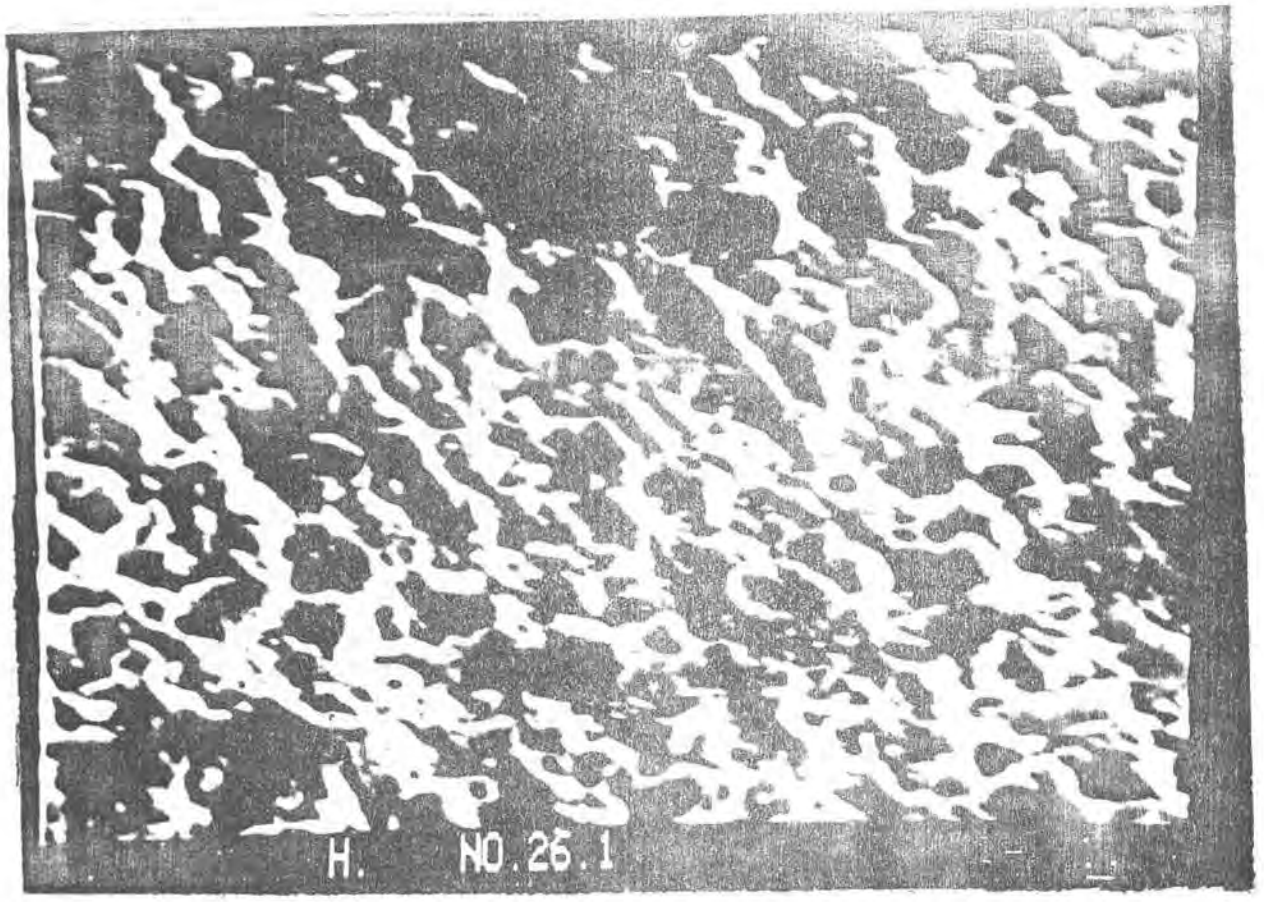

Photo 2. Scanning electron micrograph of Cu_2S surface of a dipped CdS ceramic tablet sintered in argon atmosphere at 750°C for 2 hours and dipping time 30 min. Note the densification of the structure with increased sintering time as compared to Photo 1. (4000X)

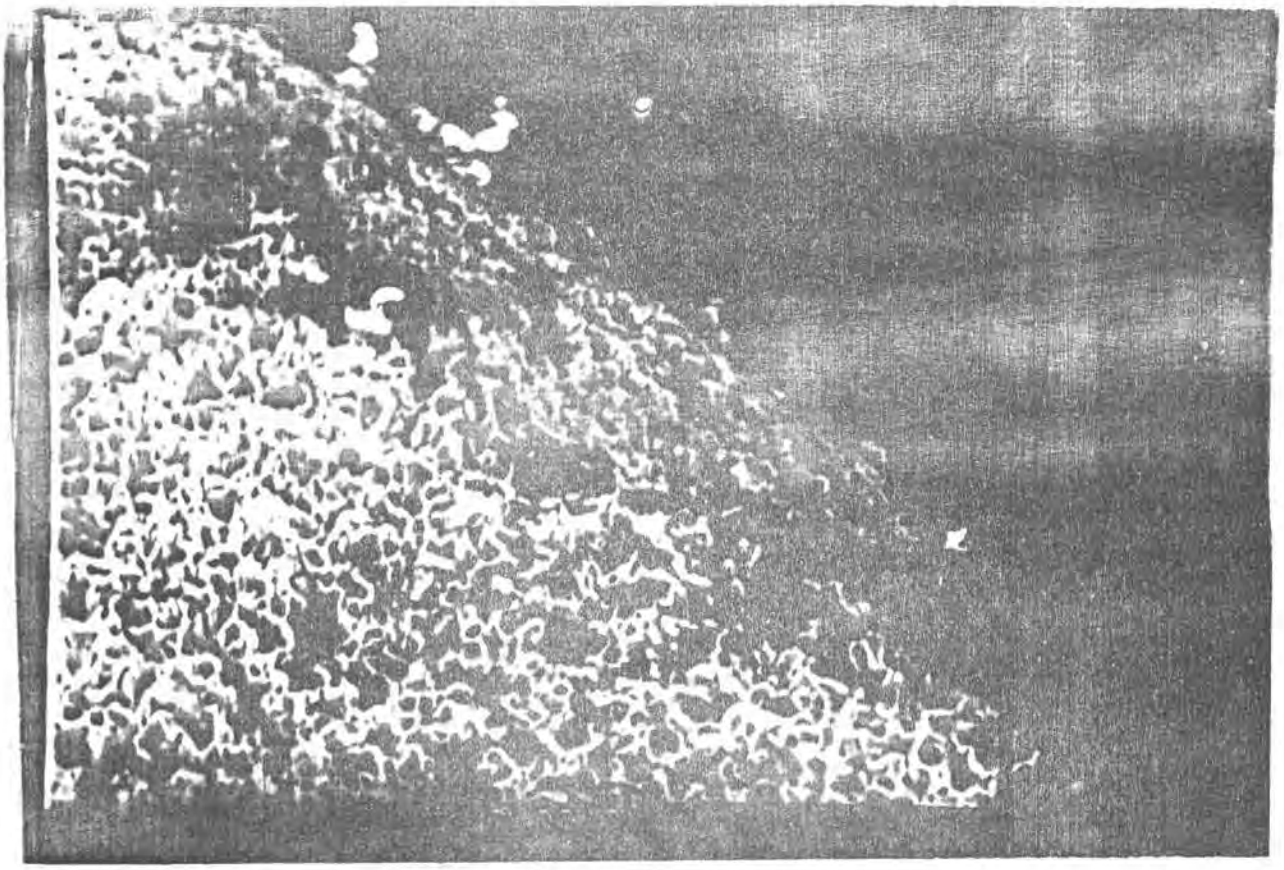

Photo 3. Scanning electron micrograph of a fractured CdS ceramic / Cu_2S dipped tablet showing the two constituents: CdS with Cu_2S layer covering it. Notice the intrusions of Cu_2S along cracks in the CdS layer. (4000X)

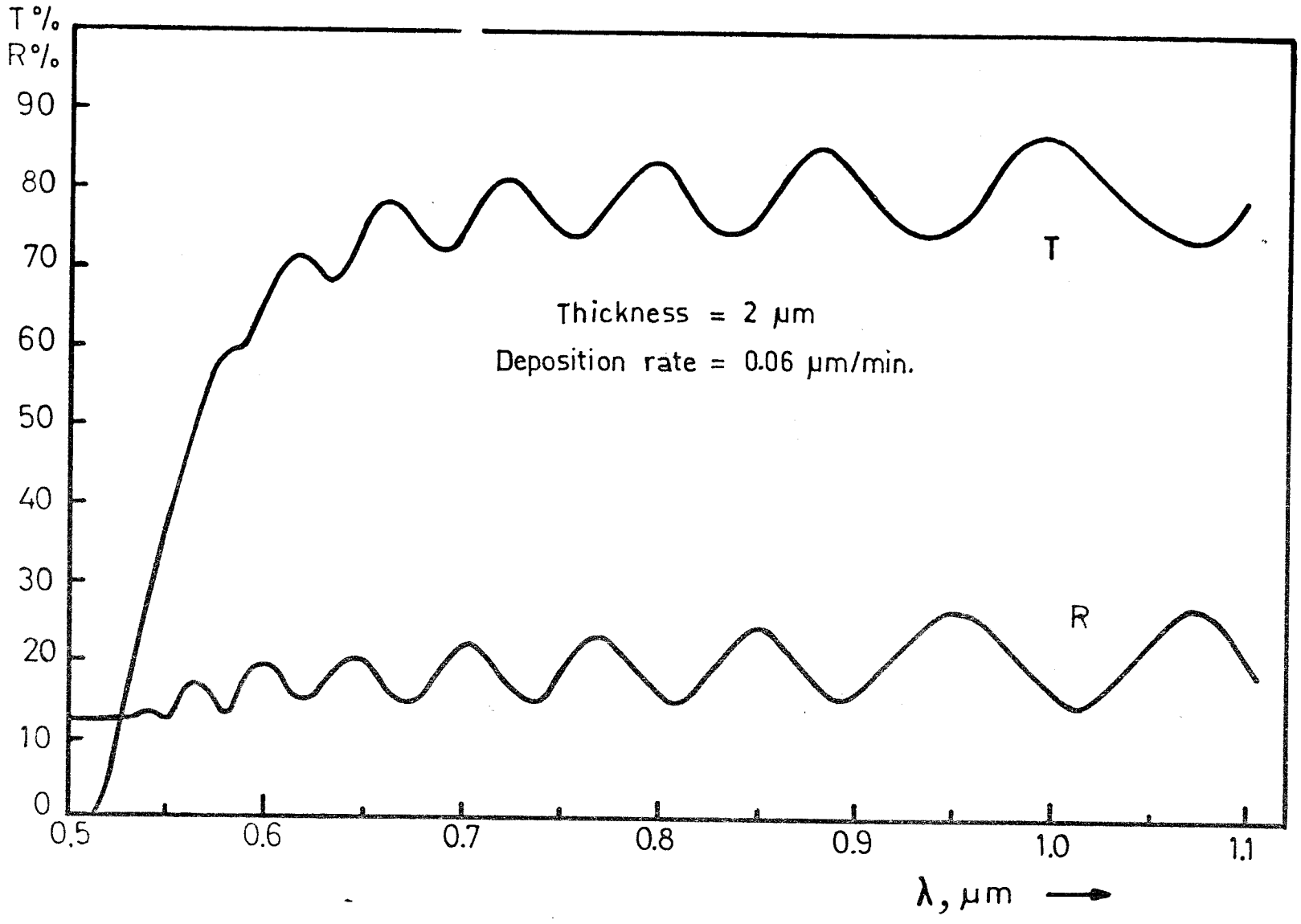

Fig.19. Spectral dependence of transmittance T and reflectance R for CdS film on glass substrate.

The transmittance and reflectance curves of Cu_2S thin films (thickness 0.25 μm and deposition rate 0.06 μm/min) deposited on glass substrate are shown in Fig. 20. From calculations based on the results exhibited in Fig. 20, two optical edges for Cu_2S thin films exist at 1.1 and 1.7 eV, corresponding to two optical energy gaps. In literature, there is a large disparity between the different results concerning the value and the nature of the energy gaps in copper sulfide (Savelli and Bougnot, 1979).

d. Electrical Resistivity of CdS Films.

The electrical res stivity of CdS layers is one of the principal parameters which determine the operation of the Cu_2S / CdS solar cell. Mainly, it represents the series resistance of the cell itself which affects the I-V characteristics of the junction. The electrical resistivity (ρ) of CdS layers used in solar cells lies in the range 10 - 100 Ohm.cm (Wilson and Woods, 1973; Das et al, 1979; Savelli and Bougnot, 1979).

The electrical resistivity of undoped evaporated CdS films is usually high, and is controlled mainly by the existence of natural defects and impurities (Das et al, 1978). The dark electrical resistivity of the film depends upon the film thickness, t, the substrate temperature, T_s, the film deposition rate, R, as well as the annealing temperature, T_a.

Effect of film thickness, t. The values of the electrical resistivity of CdS films obtained by thermal evaporation at a

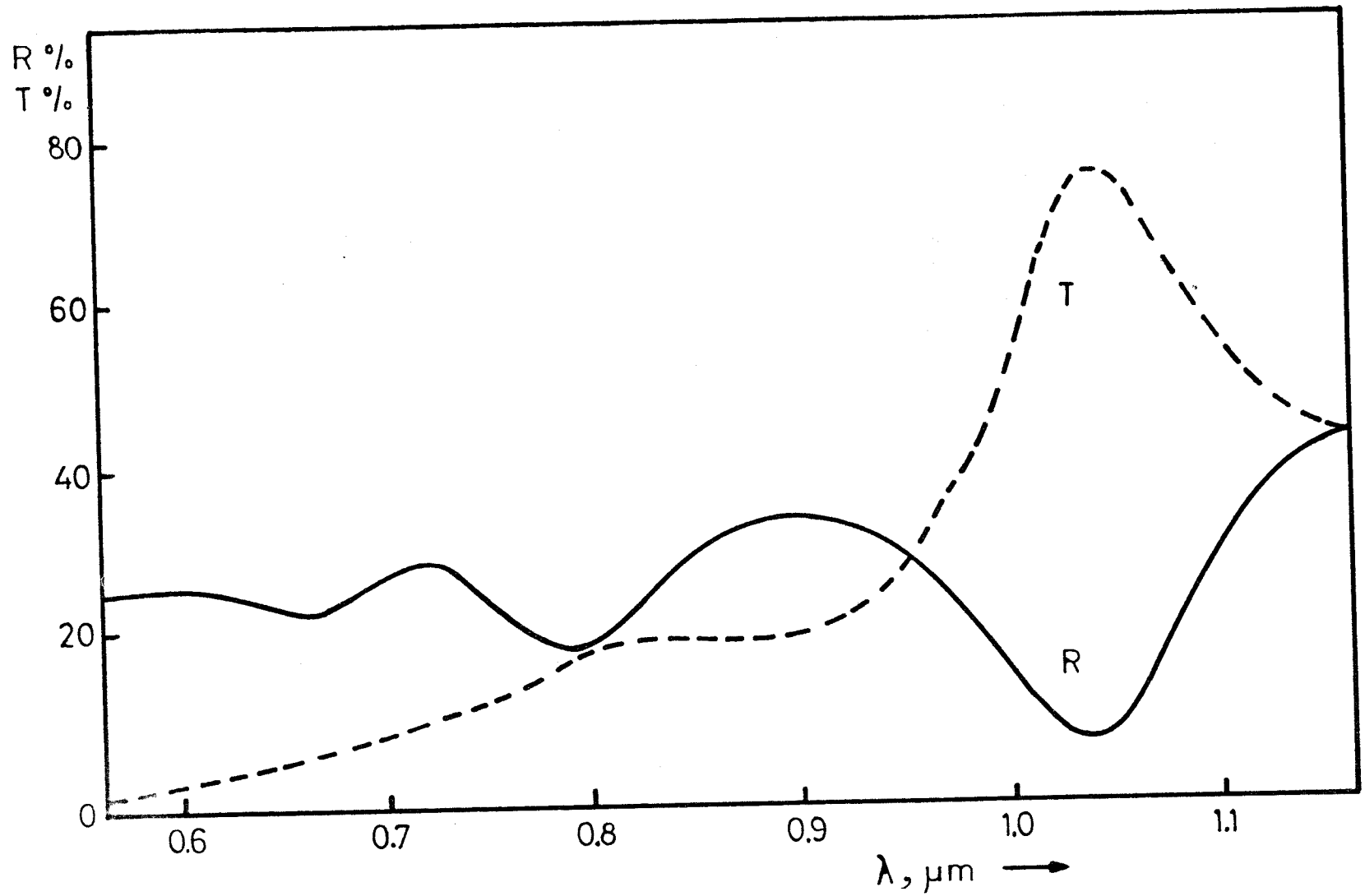

Fig. 20. Spectral dependence of transmittance T and reflectance R for Cu_2S films on glass substrate.

fixed substrate temperature, T_s = 40°C and evaporation rate, R = 0.15 μm/min as a function of the thickness, t are shown in Fig. 21. Such behaviour can be understood in the light of an increasing degree of preferential orientation taking place with thickness increment. Wilson and Woods, 1973, however, explained the resistivity variation with film thickness in terms of free carrier concentration.

Effect of substrate temperature, T_s. CdS films of thickness 2 μm and deposition rate 0.48 μm/min were deposited under vacuum on glass substrates having temperatures ranging from -196°C to 300°C and the resistivity was measured for these films. The results are presented in Fig. 22. It was observed that the change of resistivity was accompanied by a colour change of the film. Thus, at low substrate temperature, the film resistivity is small and its colour is dark grey which changes to yellow for films deposited at high substrate temperatures.

This is explained by a stoichiometric departure from the usual CdS form. Most probably these films contain excess Cd and this is the reason for the high electrical conductivity. However, X-ray diffraction experiments show that they still exhibit the CdS structure.

Experiments with $T_s > 300°C$ were not successful as a destruction of the evaporated films took place and also re-evaporation of the material from the substrate was intensive.

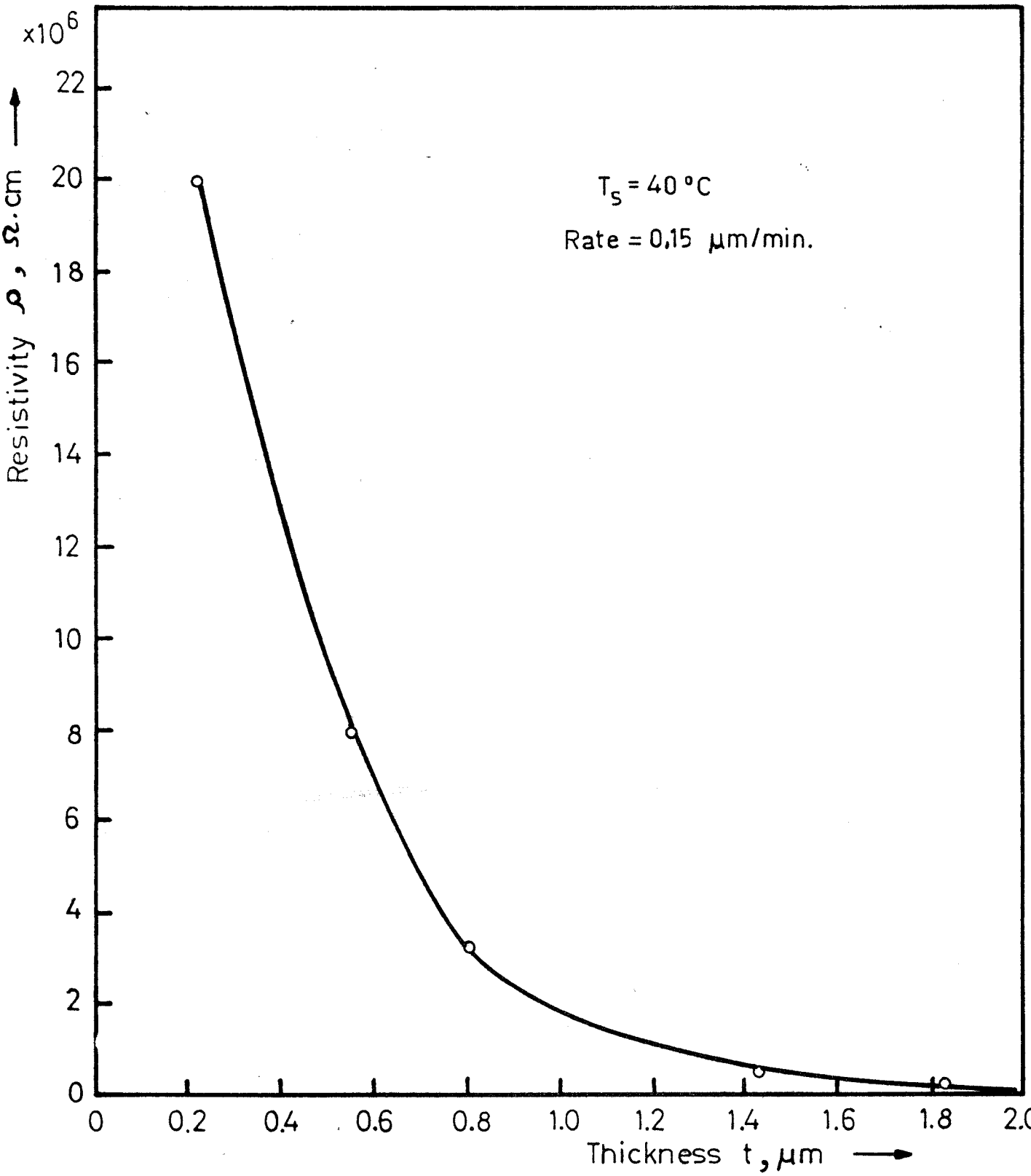

Fig. 21. Resistivity at room temperature of CdS films as a function of thickness.

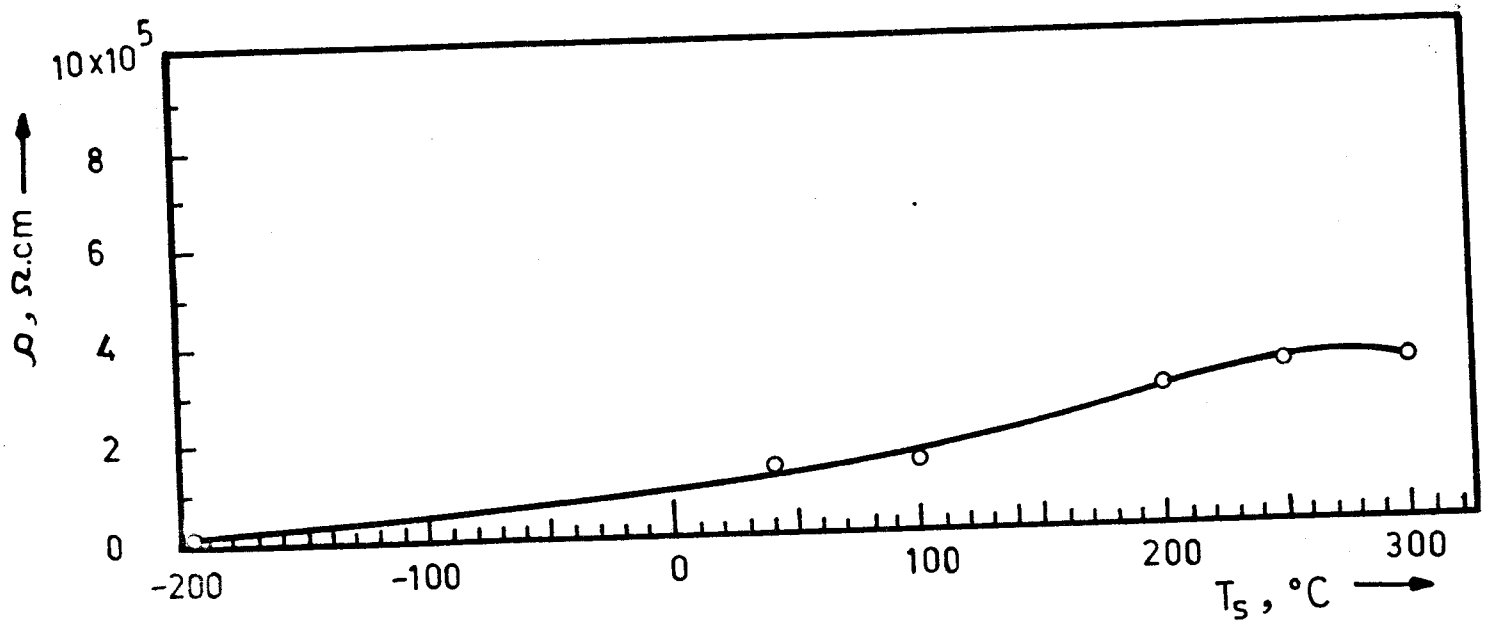

Fig. 22. Resistivity ρ vs substrate temperature T_s for Cd S film.

Effect of deposition rate, R. The dependence of the dark electrical resistivity of CdS films of thickness 2 μm and deposited at T_s = 150°C, is illustrated in Fig. 23. One can observe that an increase in the deposition rate leads to an increase in the resistivity of the film. This behaviour agrees with the results of Wilson and Woods, 1973, and is confirmed by the results of X-ray diffraction, where the degree of preferential orientation of crystallites increases with decreasing deposition rates.

Effect of annealing in air. A large decrease in the resistivity with annealing at high temperatures (one hour at each temperature) in air is illustrated in Fig. 24 for CdS films. Similar results have been previously reported and Savelli and Bougnot, 1979, attribute such a decrease to a higher degree of crystallinity after annealing.

e. Photoconductivity of CdS.

Photoconductivity of CdS single crystals. AC photoconductivity measurements have been carried out for CdS single crystals for samples 10 x 5 x 0.5 mm^3. Surfaces of the samples were mechanically polished with fine diamond paste. Ohmic contacts were prepared by soldering pure indium.

Fig. 25 illustrates the spectral distribution of photoconductivity for two samples. It is clear that the photoconductivity spectra consist of two regions: the well known intrinsic region at $\lambda \sim 0.5 - 0.53$ μm, and another broad band (extrinsic)

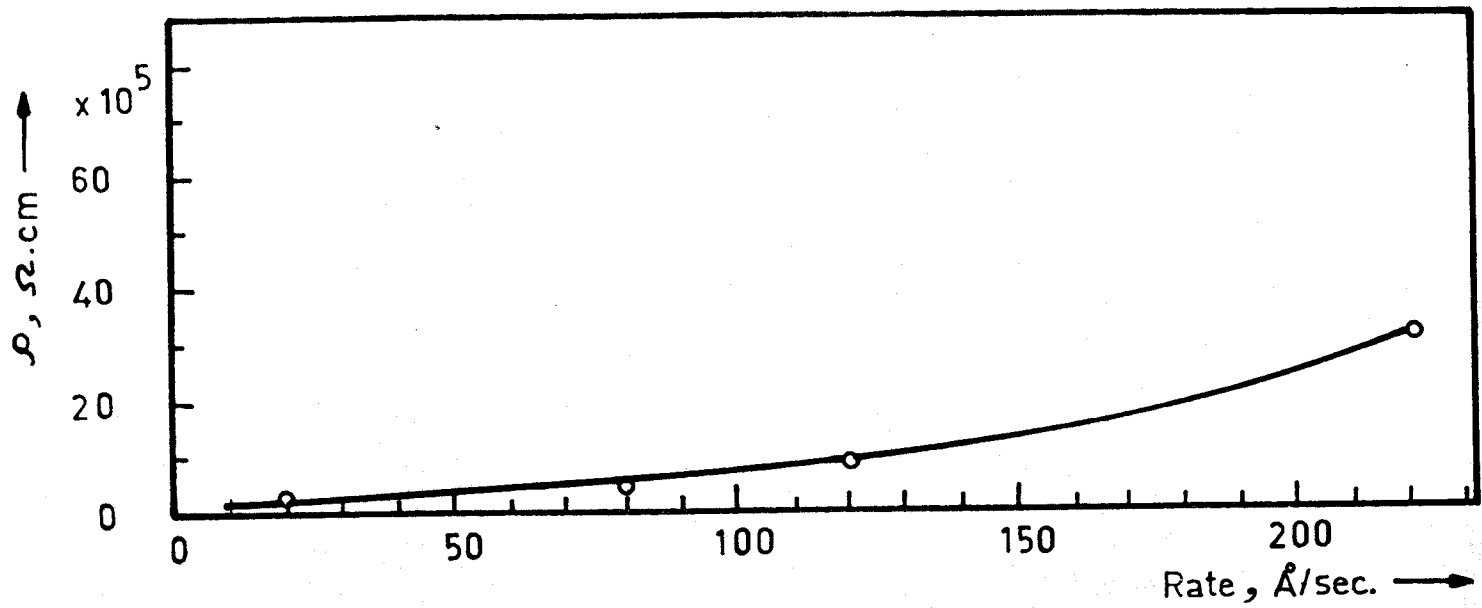

Fig. 23. Resistivity ρ vs film rate of deposition for CdS film.

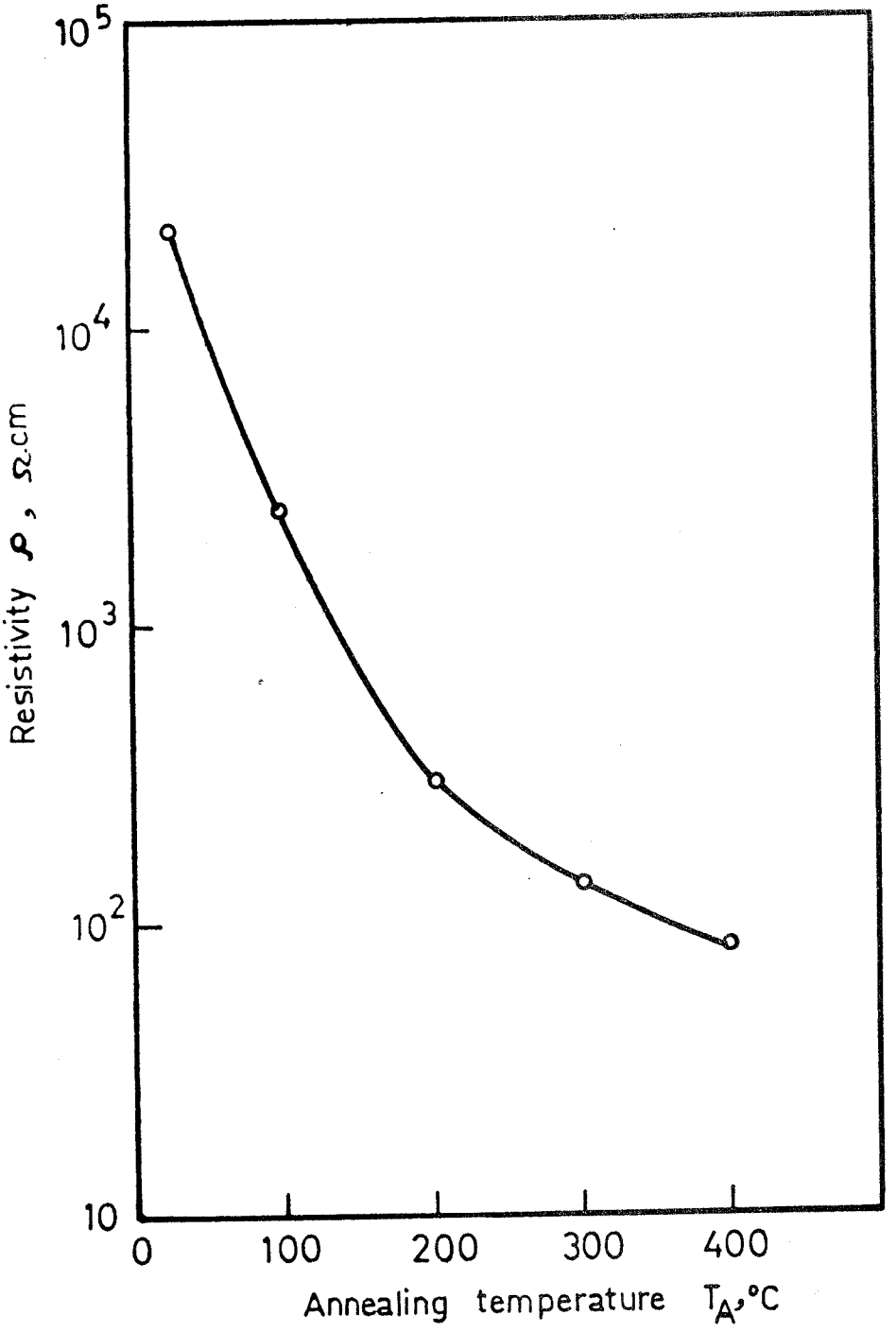

Fig. 24. Resistivity at room temperature of CdS films evaporated on glass at R.T. as a function of annealing temperature in air.

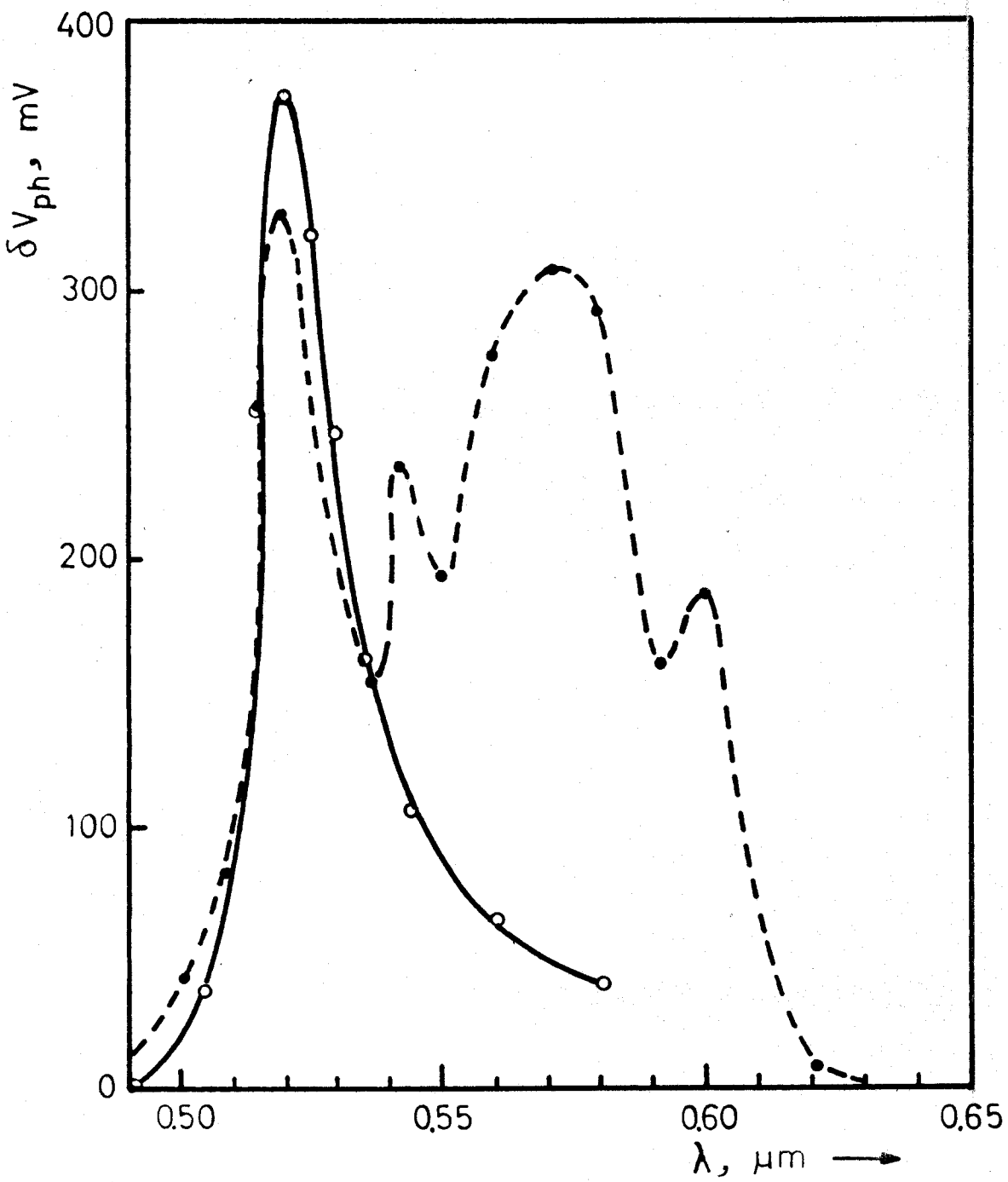

Fig. 25. AC photoconductivity of CdS single crystals.

- o pure sample.
- • impure sample.

extending from 0.53 to 0.65 μm. For pure samples (solid curve) the intensity of the intrinsic peak at $\lambda_{max} \sim 0.515$ um is larger than that for the extrinsic (dashed curve) or comparable with each other. Sometimes the intrinsic range in "dirty" crystals is suppressed by the extrinsic one, solid curve of Fig. 26, and appears only after surface retreatment, dashed curve.

Photoresponse of CdS appearing at wavelengths (0.53 - 0.65 μm) higher than that corresponding to intrinsic transition has been observed and studied several years ago (Bube, 1960). This phenomenon has been explained by the presence of impurities or structural defects of acceptor type lying above the valence band. Impurities of acceptor type which mainly exist in CdS are Cu, Ag and Au. The intensity of extensive peak due to Cu impurities in CdS largely increases with the quantity of copper introduced (Aven and Prenery, 1967).

Another origin of defects, which influences the photoresponse of CdS is the structure of the surface. It is well known that defects introduced by mechanical damages in the surface layer of a crystal can act as traps for carriers. The thickness of such damaged layers ranges from a fraction of a micron to nearly 100 μm depending upon the mechanical properties of the crystal and the type of mechanical treatment: sawing, lapping or polishing. Such damaged surface layers influence the electrical and optical properties. It leads to the appearance of the "dead layer" on the surface (Leonov et al, 1976).

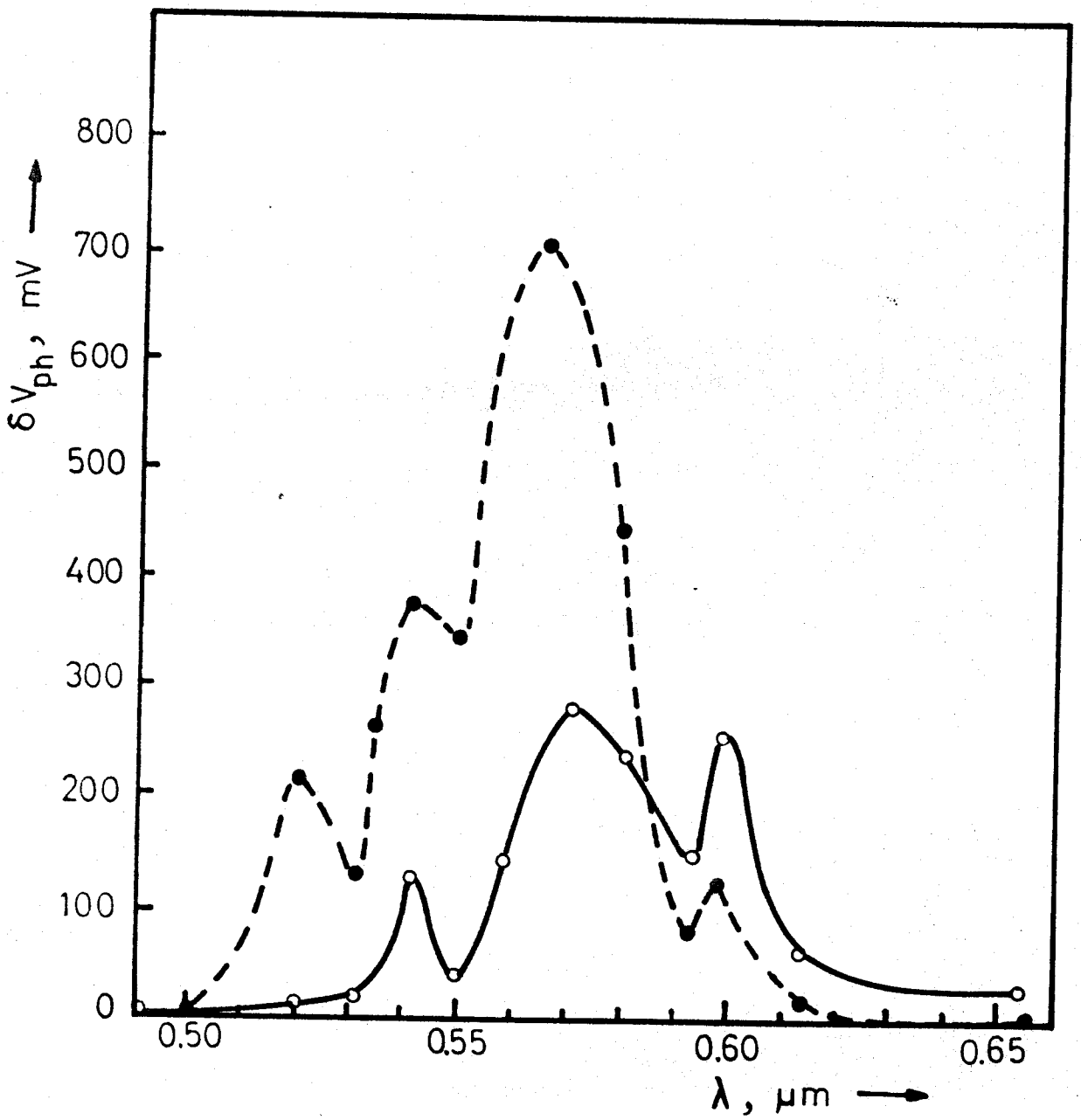

Fig. 26. AC photoconductivity of CdS single crystal.

o sample without surface treatment.

● same sample after » »

It has been also mentioned, that the introduction of local defects of high concentration leads to the deformation of the surface bands, similar to that occurring due to the introduction of impurities.

Chemisorped oxygen on the surface of CdS can also affect the photoconductivity especially when measurements are carried out in the ambient atmosphere. In this case photoconductivity decreases with increasing the amount of adsorped oxygen (Gross, 1977).

The observed photoconductivity in our experiments is of complicated origin (impurity, surface defects and adsorped atoms). It is necessary to control the doping level of impurities, surface treatment and ambient atmosphere which act as trap levels for carriers and is indicated by long life time of carriers. Such study is important to understand some effects related to the diffusion of Cu from the Cu_xS to the CdS layer of the solar cell. It is known that one of the reasons of degradation of the Cu_xS / CdS solar cell is the decomposition of the upper layer and the diffusion of Cu ions through the structure of CdS film which leads to short circuiting of the cell as well as changing the spectral response of the cell itself.

Photoconductivity of CdS thin film. DC photoconductivity of CdS thin films of electrical resistance in the order of mega-ohms was studied. CdS films (0.8 - 2 μm thick) were deposited on glass substrate at T_s = 150°C under vacuum with deposition

rate 200 Å/sec. Indium electrodes were evaporated onto the CdS film. Such samples showed to be photosensitive in the spectral region 0.40 - 0.70 μm. The relation between the photocurrent and the incident light wavelength for CdS film is shown in Fig. 27. Such a relation shows a maximum response at about 0.5 μm corresponding to the excitation across the 2.42 eV forbidden band gap (Mochizuki and Igaki, 1979).

4.2. SINGLE CRYSTAL CdS/Cu_xS SOLAR CELL

The following is a brief description for the experimental procedure adopted to fabricate this cell.

a. CdS as substrate. Pure wafers (5 x 5 x 0.5 mm^3) of undoped CdS single crystals were used, with the c-axis perpendicular to the plate surfaces. The faces of the platelets were mechanically polished using 0.3 um alumina, then etched for 30 sec. in 1N HCl solution to remove any possible oxide layer (Caswell et al, 1975).

b. Ohmic contacts. This was made to one of the faces by the vacuum deposition of indium (0.5 μm thick) followed by the deposition of an aluminium thin layer (0.5 μm thick) as a protection and negative electrode. The CdS plates were then heat-treated at 180°C for some hours.

c. Cu_2S layer. The other polished surfaces of the CdS plates were masked from the edges, then etched for 30 sec. in a solution of 1N HCl to remove any possible oxide layer. The p-Cu_2S

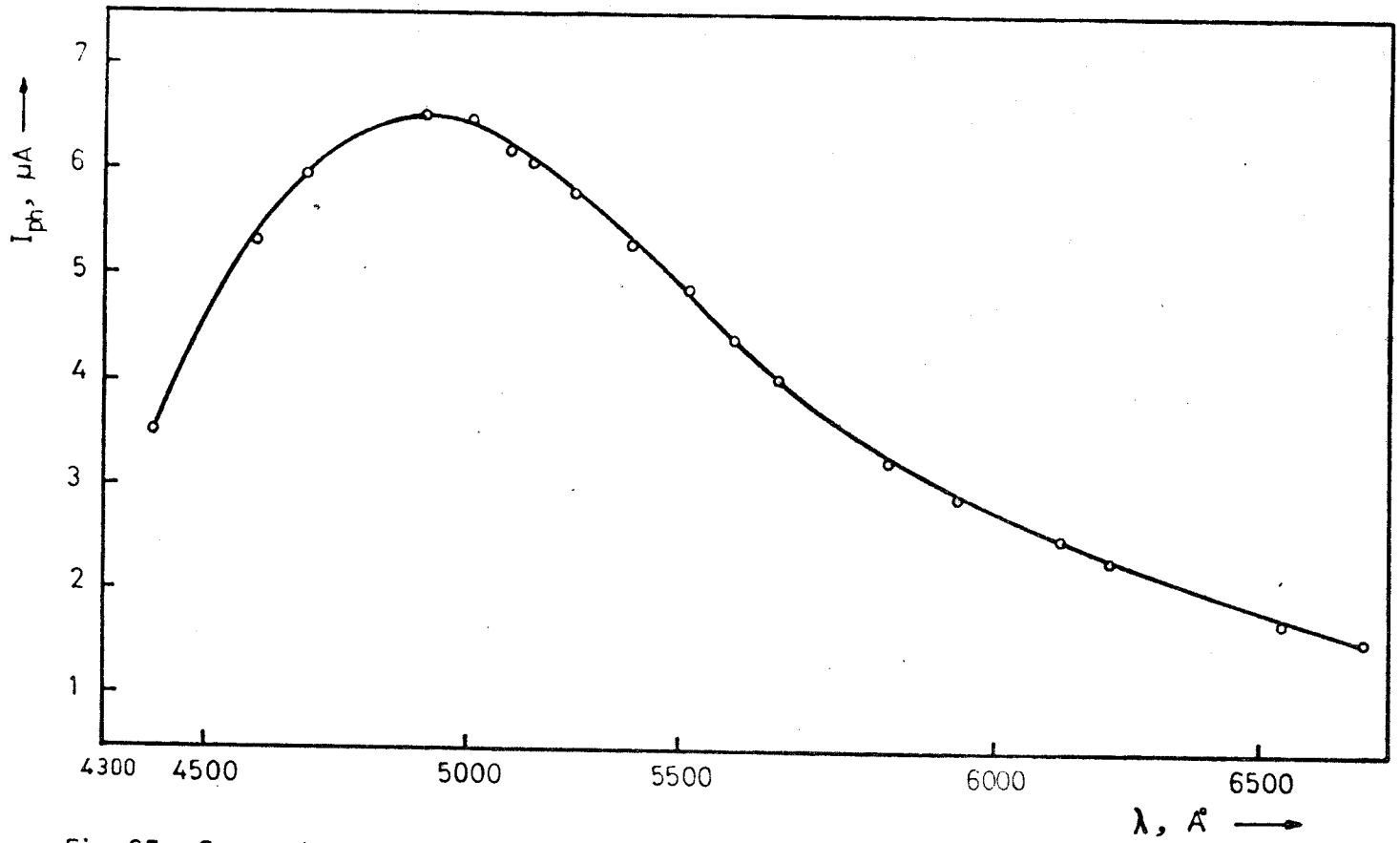

Fig 27 Spectral response of photoconductivity current I_{ph} for CdS thin film.

layer was formed by direct evaporation of copper sulfide synthesized by the methods previously described. The thickness of Cu_2S layer was 0.2 μm as measured by the thickness monitor attached to the coating unit.

d. Heat treatment. After the deposition of the Cu_2S layer, the next step is the complete formation of the cell itself by heat treatment. Meakin et al, 1976, as well as Fahrenbruch and Bube, 1974, have shown that a vacuum heat treatment of the completed cell is a major factor in the performance reproducibility. They found that such heat treatment eliminated much of the variability observed immediately after barriering, and moreover, heat treatment improved the stoichiometry towards the ideal copper sulfide for solar cells. Heat treatment was performed under vacuum at 200°C for ten minutes.

e. Top electrode. A simple linear grid of evaporated gold lines was used as top +ve electrode. The optimum grid line spacing was calculated according to Wyeth, 1977. Gold was evaporated in a poor vacuum (10^{-4} Torr) to prevent puncturing of the Cu_2S layer.

f. Cell encapsulation. Since Cu_2S is unstable in the presence of oxygen and water vapour and reacts to form a surface film of copper oxide in contact with a reduced stoichiometry copper sulfide layer, the formation of only one or two monolayers of oxide in the very thin Cu_2S to film is sufficient to change the carrier concentration by orders of magnitude. This manifests itself as a loss in the short circuit current, which is a

parameter affecting directly the efficiency of the cell. To reduce this problem a plastic film for encapsulation was applied to the Cu_2S film.

Fig. 1 shows a configuration of the "frontwall" p-Cu_2S/ n-CdS solar cell in which the light is absorbed directly by the Cu_2S layer.

Diode Characteristics of the
CdS / Cu_2S Heterojunction :

a. Effect of light. Typical results of current-voltage characteristics in dark and under illumination are illustrated in Photo 4, photographed directly from the screen of the oscilloscope. We observe that the two curves have a crossover point. This behaviour may be accounted for by the photoconductive process in CdS which leads to a decrease in the series resistance of the cell (Gill and Bube, 1970). The same behaviour has been reported also for Ga As-Zn-Se (Bolch and Anderson, 1972) and Zn Te-CdSe (Gashin et al, 1973).

b. Power output of the cell. An illuminated solar cell (using Tungesten lamp of 1000 Watt power) was connected to a series load resistance R_l, the value of which varied from zero to infinity as shown in Fig. 9. The result is the I-V curve shown in Fig. 28. From this graph we obtained the following values for the cell parameters:

Open circuit voltage V_{oc} = 0.405 Volts

Short circuit current I_{sc} = 3.75 mA

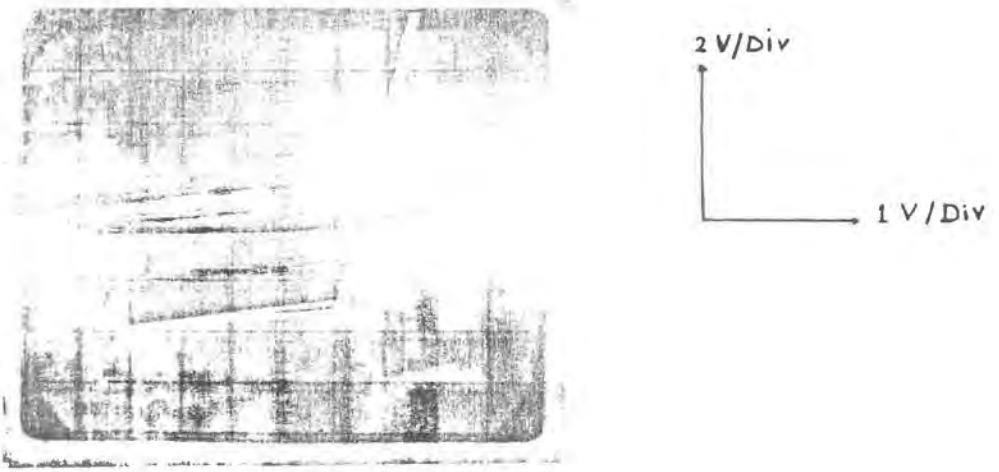

Photo 4. Oscilloscope display of I-V characteristics in dark and under illumination for single crystal CdS / Cu_2S solar cell.

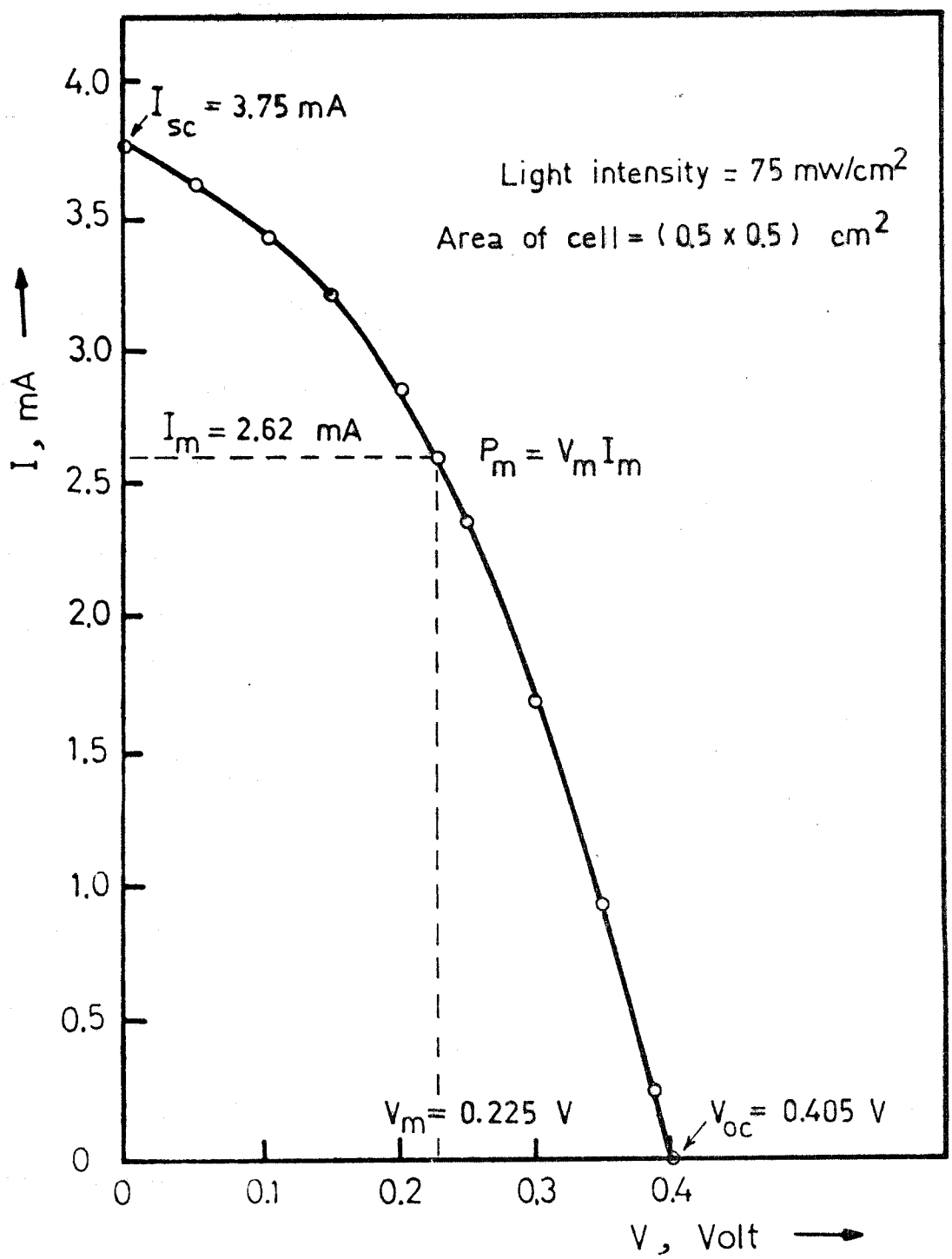

Fig. 28. Light I-V characteristic of $Cu_2S_{thin\ film}/CdS_{single\ crystal}$ solar cell.

Fill factor $FF = 0.385$

Cell efficiency $\eta = 2.34\ \%$

The series resistance R_s and the shunt resistance R_{sh} of the cell were calculated from

$$R_s = \left|\frac{\partial V}{dI}\right|_{V=V_{oc}} , \qquad R_{sh} = \left|\frac{\partial V}{dI}\right|_{v=0}$$

Their numerical values are $R_s = 46.5\,\Omega$ and $R_{sh} = 375\,\Omega$.

As it is shown, the ratio R_s/R_{sh} plays a great role in producing high efficiency solar cells. For an ideal cell both R_s and R_{sh} must tend to zero and infinity, respectively. Actually, both R_s and R_{sh} have certain values. This gives rise to low values for both the fill factor and accordingly, the efficiency of the cell.

c. Effect of different light intensities. This is represented by the I-V curves in Fig. 29. For each of these curves the cell temperature was kept at 28°C. As expected, the open circuit voltage rises with increasing light intensities and starts to saturate, while the short circuit current increases approximately linearly. However, the slopes of the curves at the current axis became less horizontal with increasing light intensity, which means a decrease of the internal shunt resistance. We can also conclude that the fill factor FF decreases slightly with the increase of the light level. The variation of the cell parameters: V_{oc}, I_{sc}, FF, P P_{max} and with light levels are tabulated in Table 7.

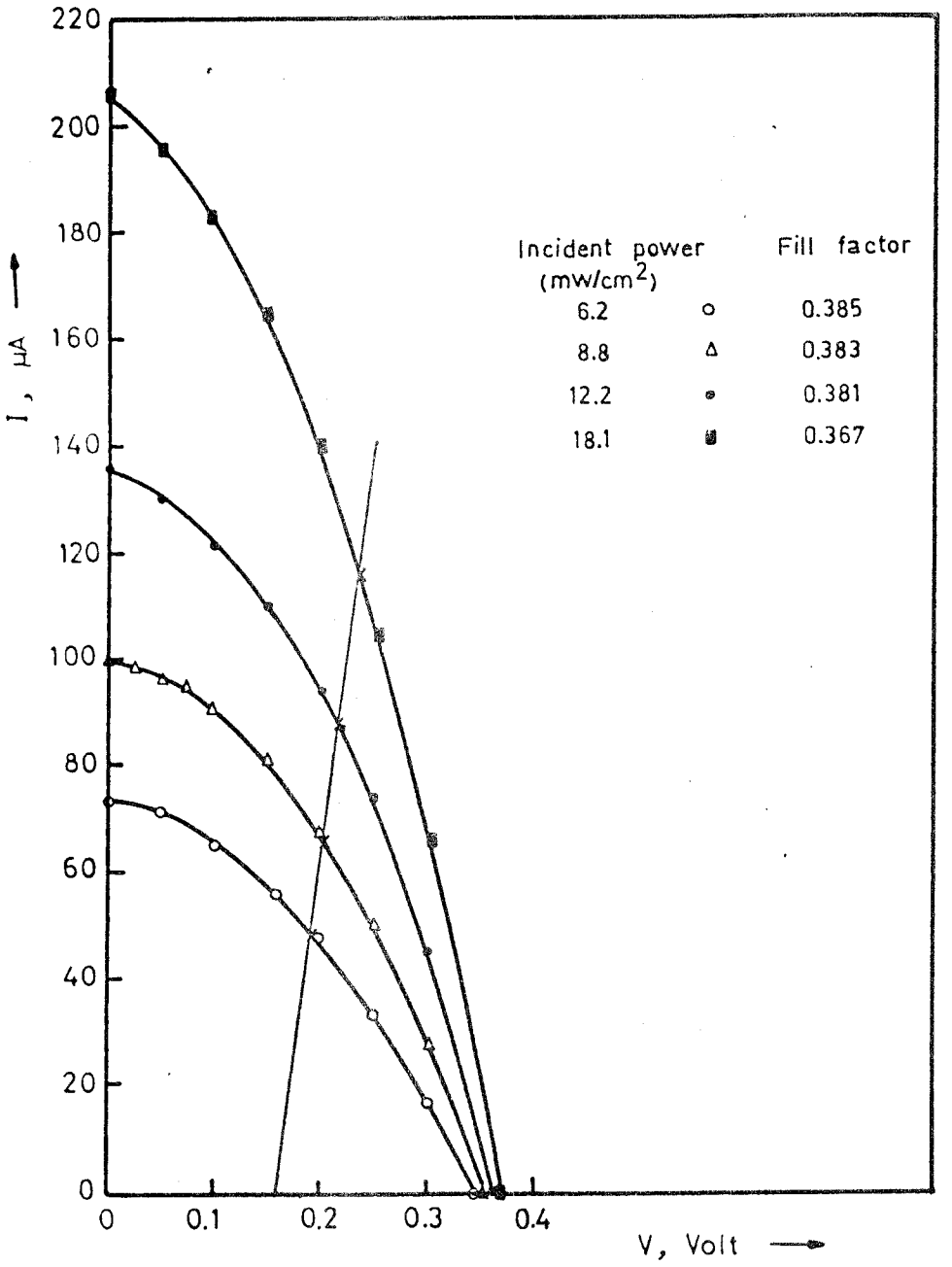

Fig. 29. Effect of variation of incident light power on I-V characteristics of CdS/Cu_2S single crystal solar cell

Table 7

Variation of Cu_2S / CdS single crystal solar cell output with light intensity (5 x 5 mm^2 cell).

Intensity of light (mW/cm^2)	V_{oc} (Volt)	I_{sc} (uA)	J_{sc} (mA/cm^2)	FF	η
6.2	0.345	71.5	1.190	0.385	2.55
8.8	0.355	100	1.670	0.383	2.58
12.2	0.365	136	2.267	0.381	2.58
18.1	0.370	206	3.433	0.367	2.58

d. Temperature effect. The current-voltage characteristics of the CdS/Cu_2S heterojunction were also studied in the temperature range 30 - 150°C. Measurements were carried out in a dark furnace having a temperature regulator. In each case, the temperature was kept constant during the course of the I-V measurements in both directions. The effect of temperature on the I-V characteristics of a CdS/Cu_2S cell is shown in Fig. 30. From this figure we notice that the saturation current I_o decreases with increasing the temperature under which the I-V curves are measured. This leads to the improvement of the open-circuit voltage V_{oc} of the cell (Prince, 1955).

e. Spectral response. Charge carriers in Cu_2S/CdS heterojunction are generated in the Cu_2S by photons with energy greater than 1.1 eV, and such carriers are created in CdS by intrinsic

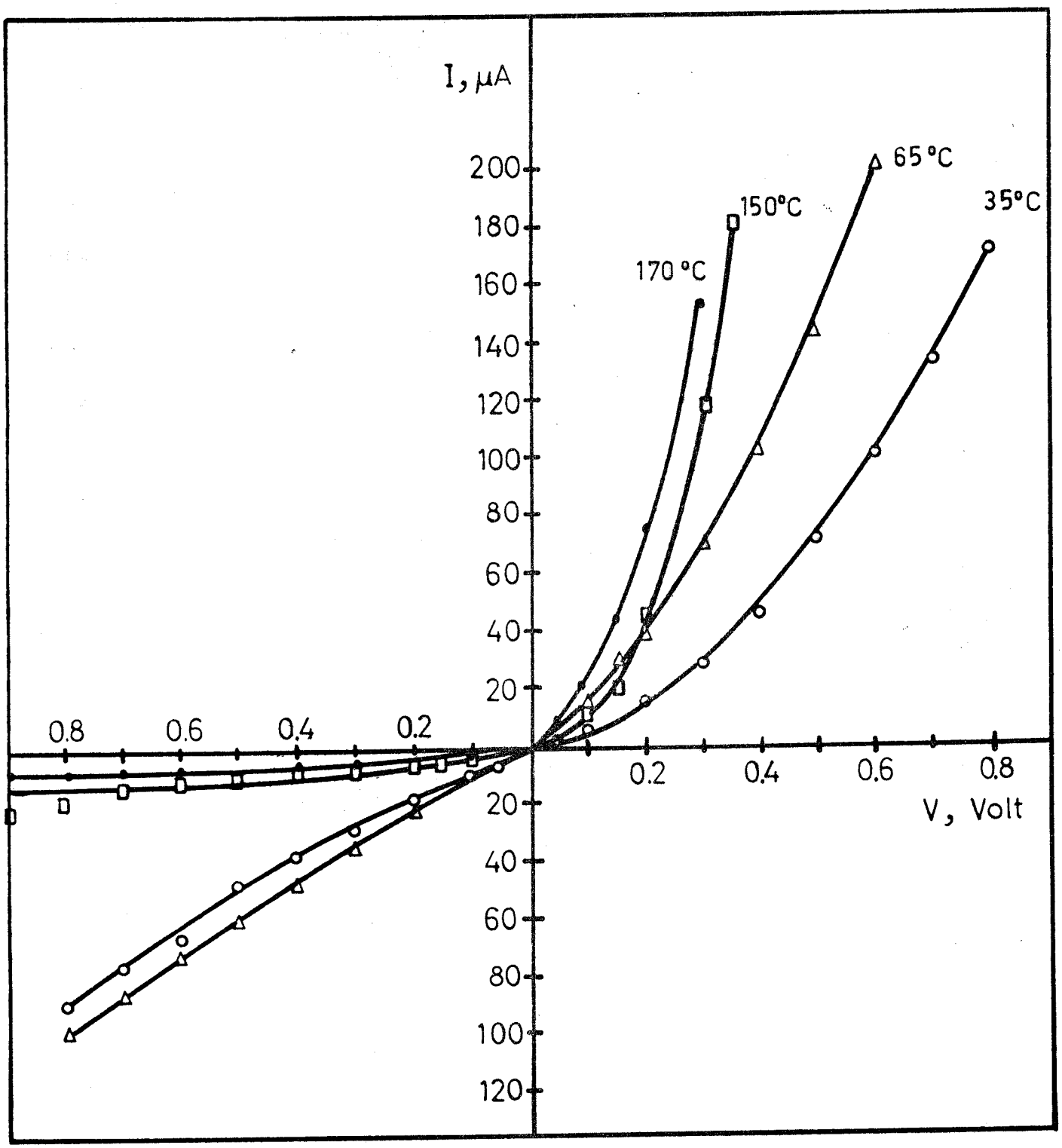

Fig. 30. I-V curves for CdS / Cu_2S single crystal solar cell at different

excitation at energies greater than 2.45 eV.

When the cell is illuminated from the CdS side (back-wall cell), the spectral response appears between wavelenths ranging from 0.5 - 1 μm. When illuminating from the Cu_2S side (frontwall cell), the maxima will be shifted to the less energy side, i.e., the response will spread out to the shorter wavelenths. Different cells exhibit different response patterns within these limits, but most CdS cells show a major peak at about 0.5 um which is apparently associated with the band edge of CdS, and a second major peak at about 0.67 - 0.70 μm.

These results are in agreement with those published by Shirland, 1966. The dependence of I_{sc} on λ has been investigated in the range from 0.40 to 0.80 μm using interference filters. Results are shown in Fig. 31.

4.3. THIN FILM CdS/Cu_xS SOLAR CELL

In this case glass substrates were used. They were cleaned by chemical and ultrasonic methods then coated with two layers of chromium and indium, each of 0.5 μm thickness and deposited under vacuum (10^{-5} Torr). The chromium layer acts as an intermediate adherance layer while the indium or aluminium layer provides a good ohmic contact with the next deposited CdS thick layer (Douglas et al, 1973).

The thick CdS film (> 10 μm) was formed by direct evaporation of 5N CdS powder from a graphite boat. As mentioned before, it is of great importance to control the evaporation

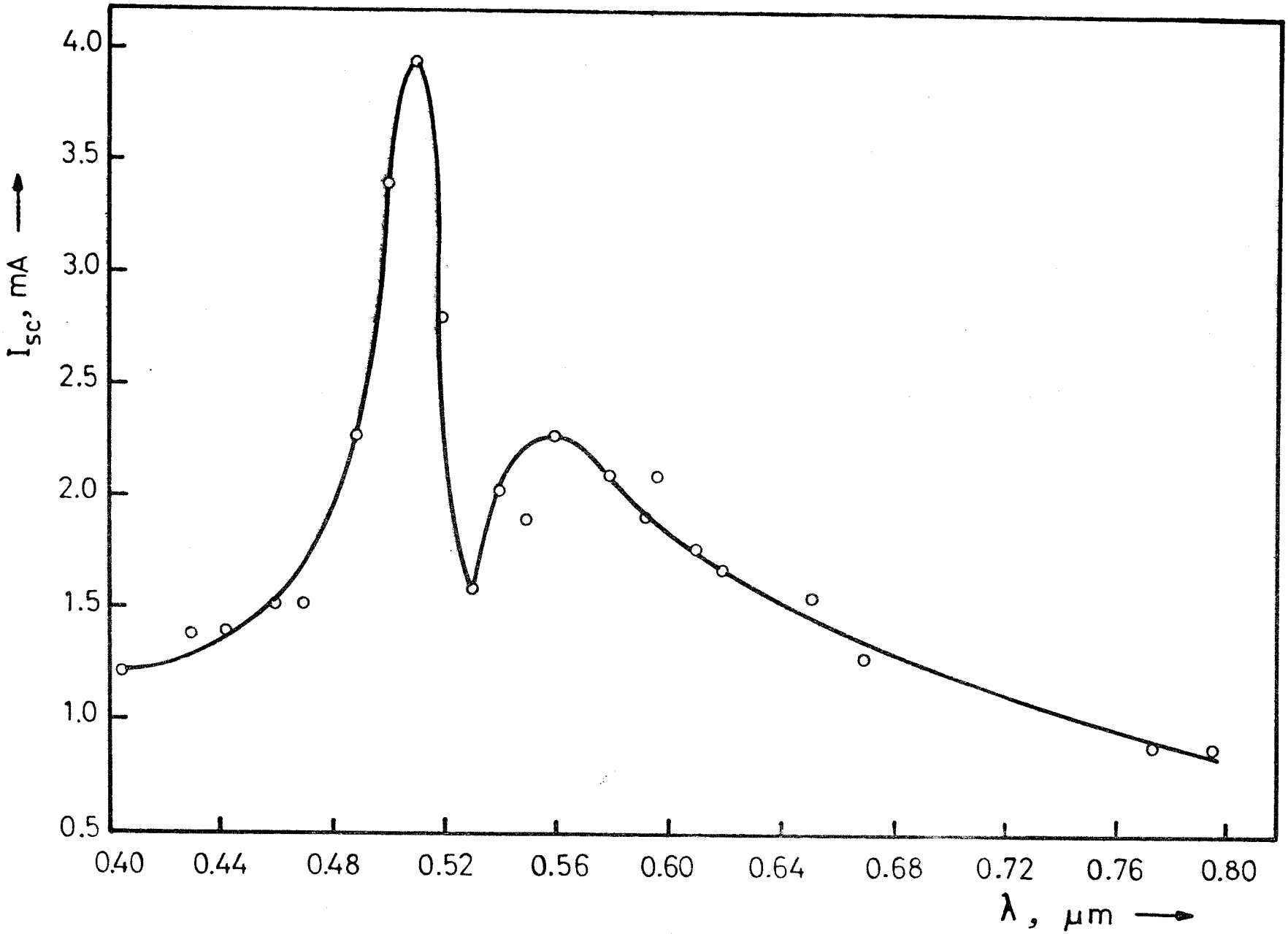

Fig. 31. Spectral response of I_{sc} for a single crystal CdS / Cu_2S solar cell.

conditions (rate of evaporation, film thickness and substrate temperature). Such conditions have a direct influence on the physical and structural properties of the formed films. This influence is, in turn, reflected on the efficiency of the fabricated solar cell. The freshly prepared CdS films were then annealed under vacuum at 300°C for about one hour to reduce the electrical resistivity of the films and to improve the ohmic contact between In and CdS (Smith, 1955). Prior to the formation of the Cu_xS thin film, the prepared CdS films were again etched for 10 seconds in 1N HCl solution to obtain a smooth fresh CdS surface.

The Cu_xS film was formed either by direct evaporation of bulk Cu_xS or by the dry technique. The next step was the heat treatment of the p-n junction (baking) under vacuum or in air at 180°C for about 10 minutes. The top gold finger-shaped electrode was then deposited. Thin copper wires attached to both lower and upper electrodes using silver paste acted as leads for the cell. The cell was finally encapsulated using a glass cover plate and a suitable adhesive material.

Study of the Thin Film Cu_2S/CdS Heterojunction Characteristics:

a. Effect of temperature. The I-V characteristics of the p-n heterojunction were studied using the circuit shown in Fig. 9. These measurements were carried out at different temperatures ranging from 30°C to 170°C in a dark furnace equipped with a temperature regulator. Fig. 32 shows the I-V characteristics for the Cu_2S/CdS thin film solar cell, while Fig. 33 presents

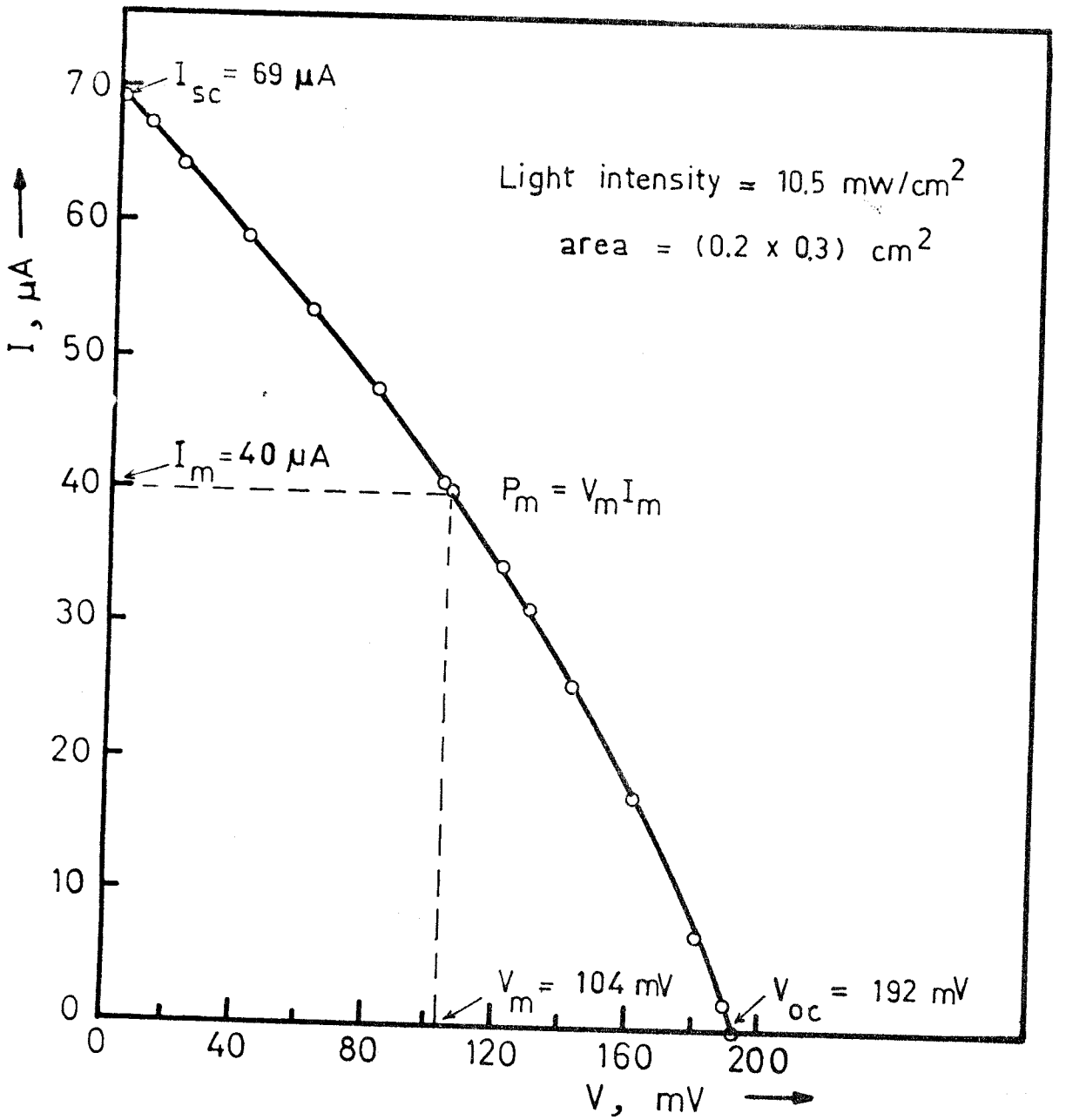

Fig. 32. Light I-V characteristic of $Cu_2S_{thin\ film}$ / $CdS_{thin\ film}$ solar cell.

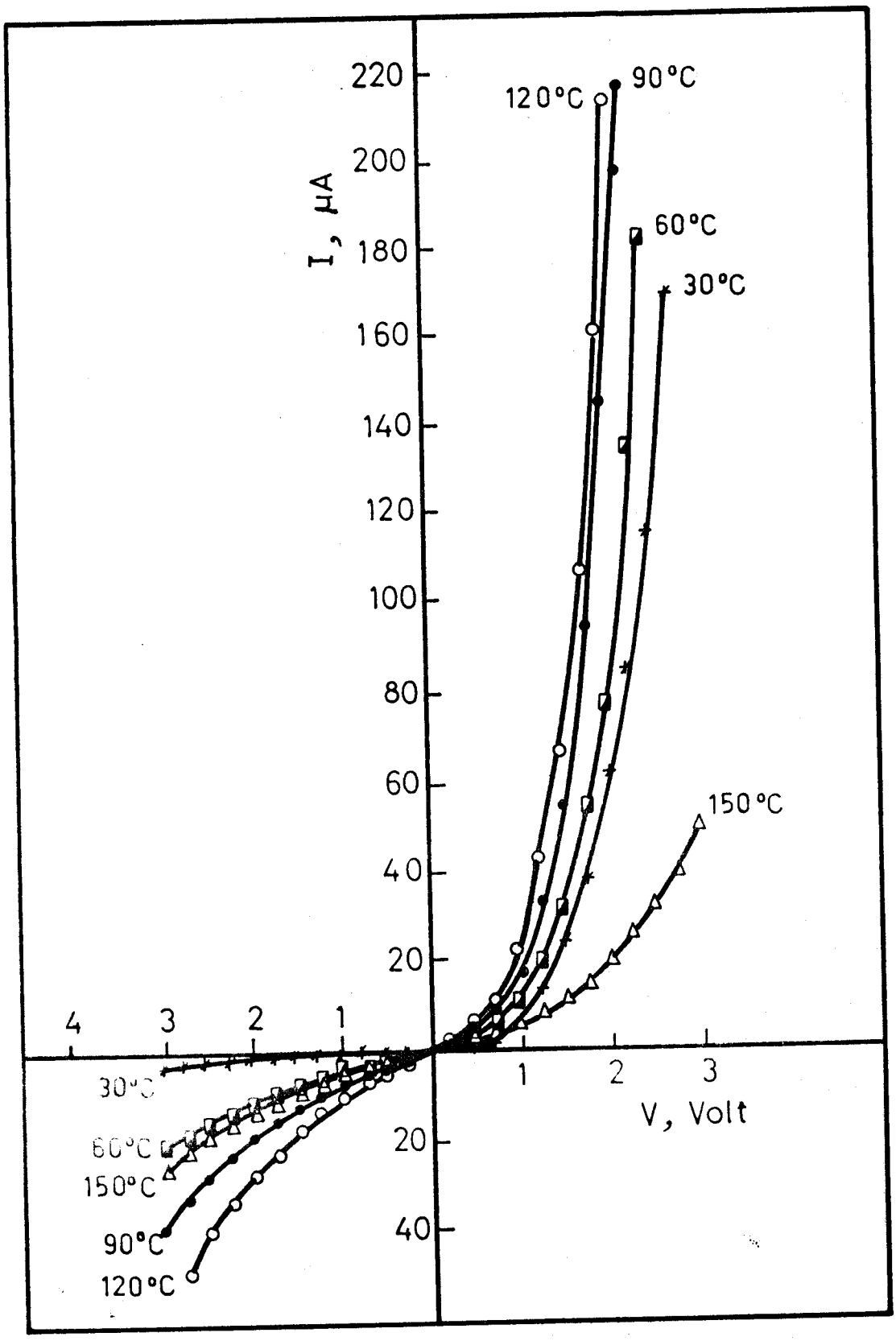

Fig. 33. Dark I-V characteristics as a function of temperature for $Cu_2S_{thin\ film}/CdS_{thin\ film}$ heterojunction.

the effect of temperature on these curves. The activation energy ΔE of the junction was calculated by plotting ln I vs 1/T at constant voltage, Fig. 34, with a value E=0.7 eV (this value amounted to 0.68 eV for the single crystal CdS/Cu_xS cell).

In order to calculate the series resistance R_s, we have plotted ln I vs V , Fig. 35. At larger forward voltages the horizontal displacement V (for a given current I) between the actual curve and the extrapolation of the linear region gives the voltage drop, IR_s , across the neutral region and by plotting ΔV against I, Fig. 36 , the value of R_s may be determined. It was found to be 7.5 kΩ.

b. Effect of illumination. Fig. 37 shows a comparison between the I-V characteristics in dark and under illumination for the CdS/Cu_2S thin film junction. The cell parameters were calculated from Fig. 32 and the values are:

Open circuit voltage	V_{oc} = 0.192 V
Short circuit current	I_{sc} = 69.0 μA
Fill factor	FF = 31.4%
Efficiency	η = 0.66%

These numerical values are arranged in Table 8 together with the corresponding values for the single crystal cell.

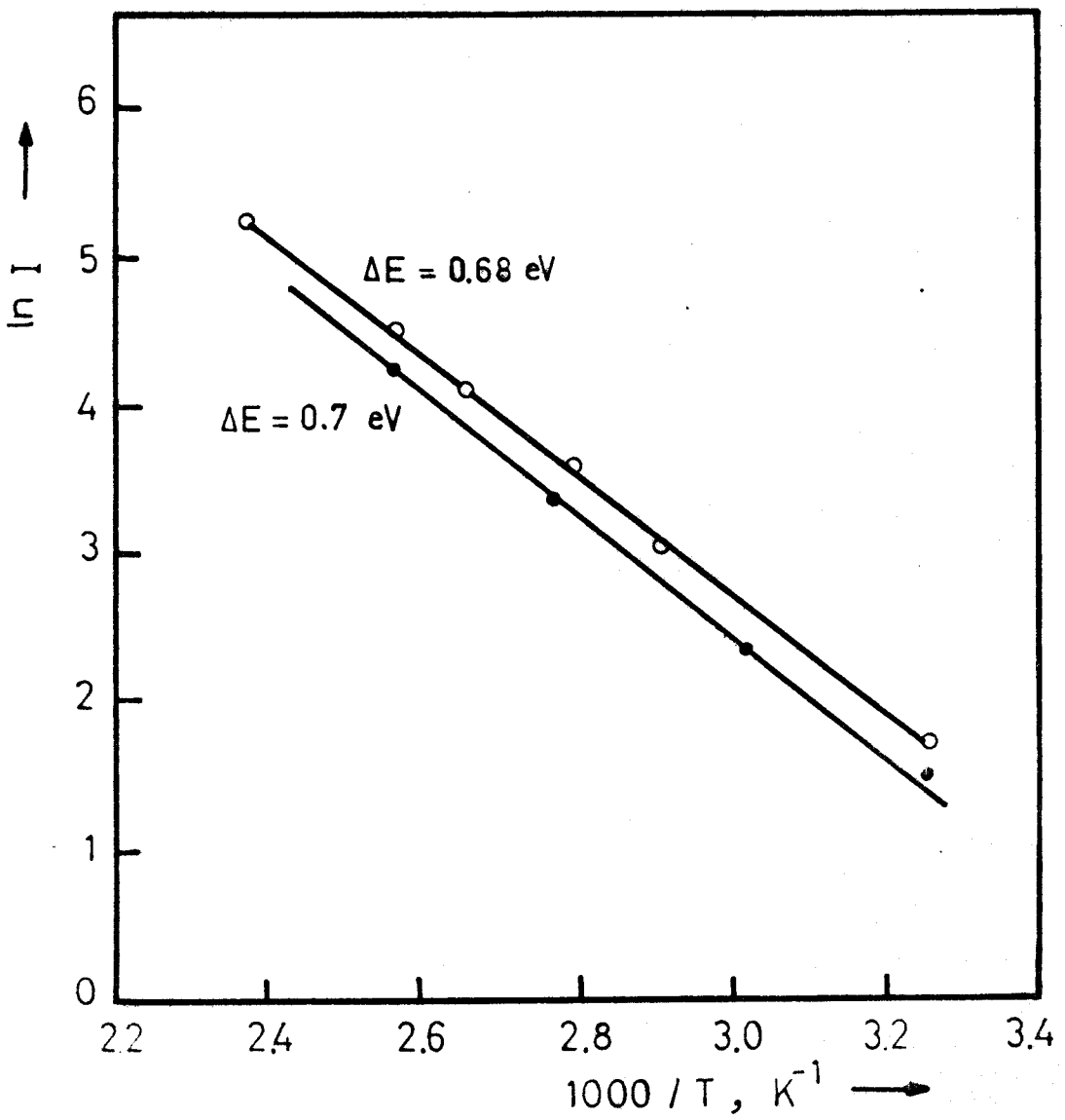

Fig. 34. Activation energy measurement.

(•) Cu_2S_{film} / CdS_{film} heterojunction.

(o) Cu_2S_{film} / $CdS_{single\ crystal}$ heterojunction.

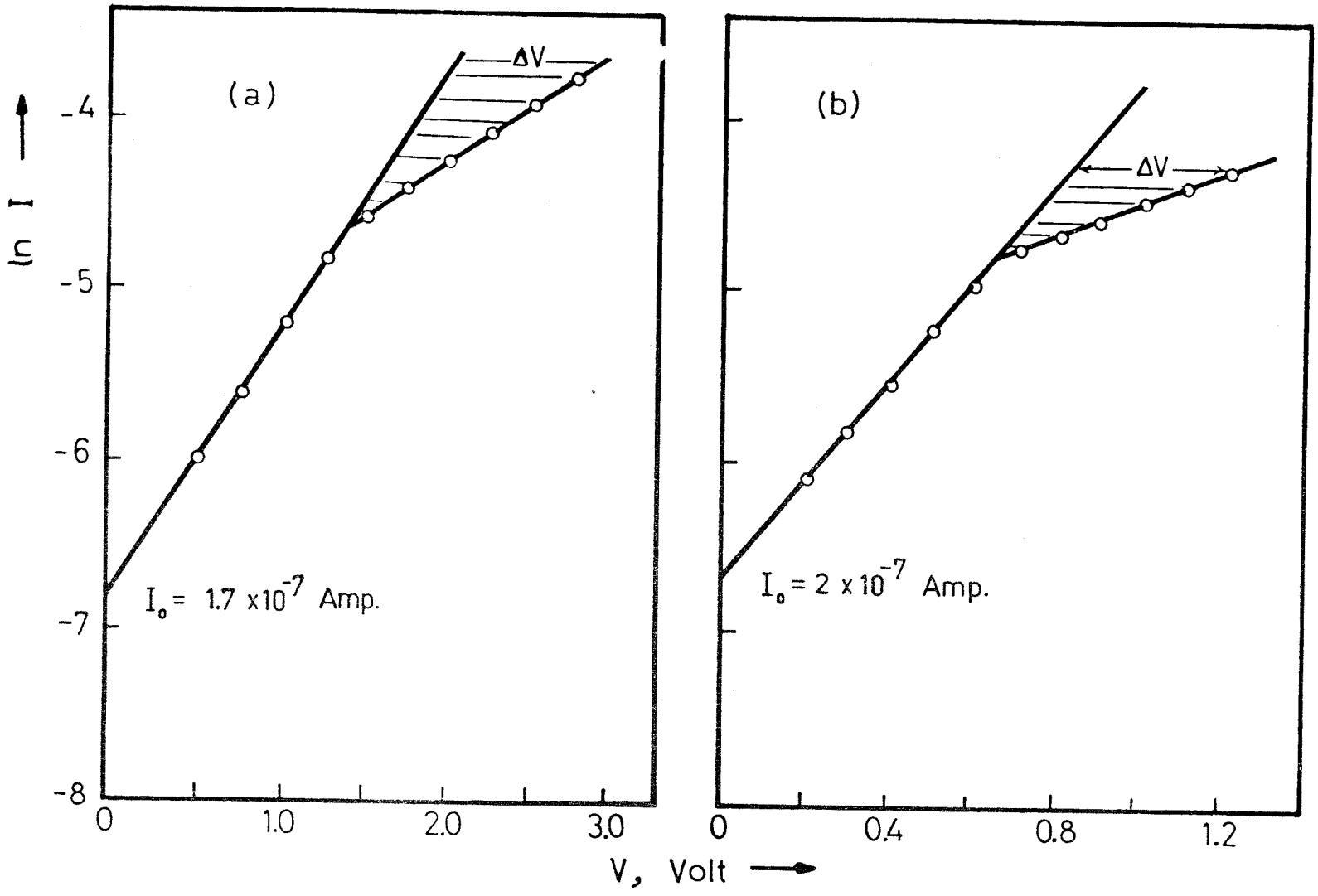

Fig. 35. I-V characteristic of Cu_2S_{film}/CdS_{film} (a) and $Cu_2S_{film}/CdS_{single\ crystal}$ (b) heterojunction showing the effect of series resistance.

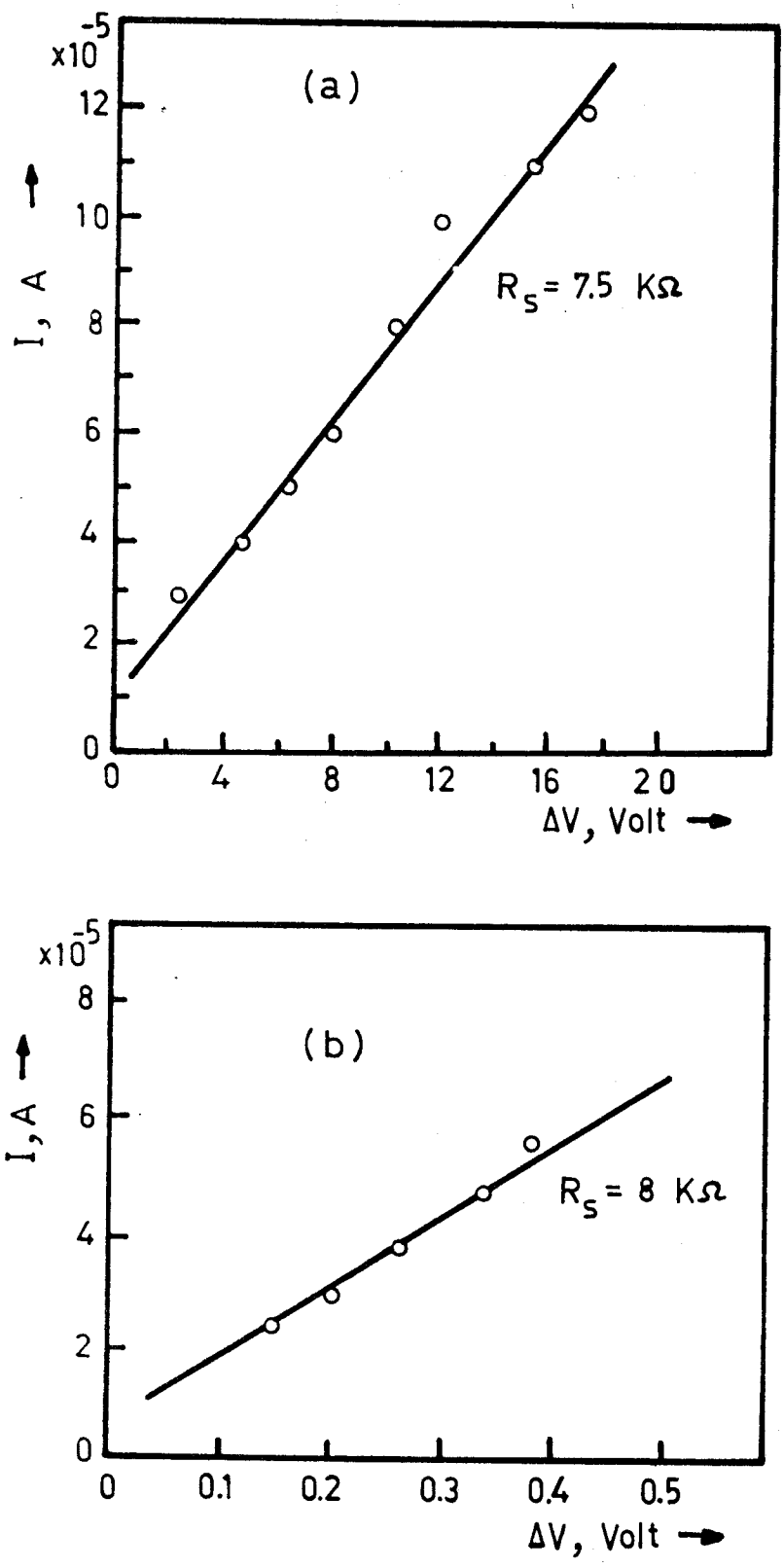

Fig.36. Series resistance measurements.

(a) Cu_2S_{film}/CdS_{film} heterojunction.

(b) $Cu_2S_{film}/CdS_{single\ crystal}$ heterojunction.

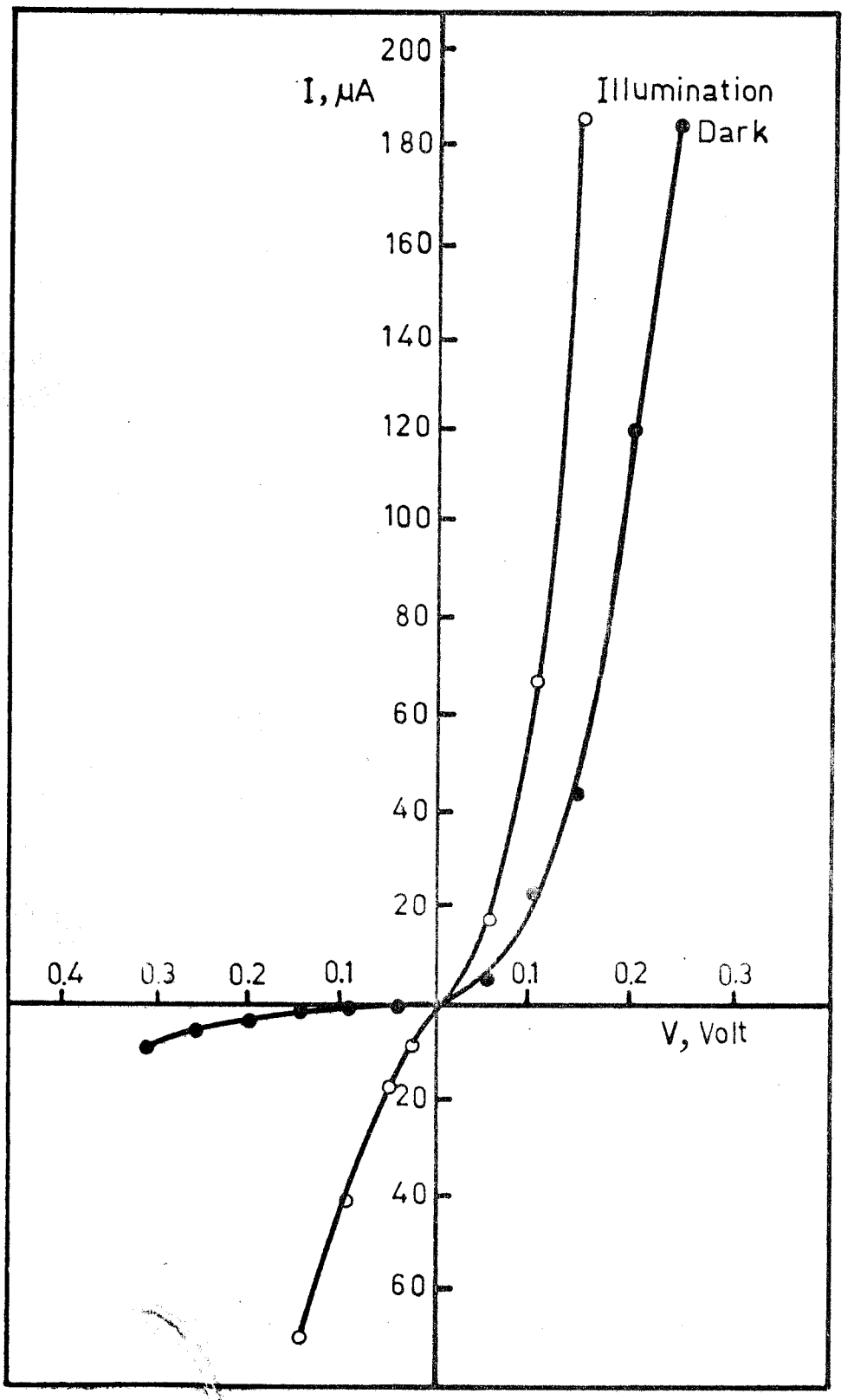

Fig.37. Dark and illuminated I-V characteristics for $Cu_2S_{thin\ film}$ / $CdS_{thin\ film}$ solar cell.

Table 8

Comparison between the single crystal and thin film Cu_2S/CdS cell parameters.

Cell parameter	Single crystal Cell	Thin film Cell
V_{oc}	0.405 V	0.192 V
I_{sc}	3.75 mA	69.0 μA
FF	0.385	0.314
η	2.34 %	0.66 %

c. Effect of light intensity. This is represented in Fig. 38 and Table 9.

Table 9. Variation of Cu_2S/CdS thin film cell output with incident light intensity (3x3 mm^2 cell).

Light intensity (mW/cm^2)	V_{oc} (mV)	I_{sc} (μA)	J_{sc} (mA/cm^2)	FF	η %
6.2	100	27	0.3	0.306	0.148
8.8	140	57	0.633	0.298	0.300
12.2	170	105	1.167	0.310	0.504
18.1	202	180	2.00	0.306	0.683

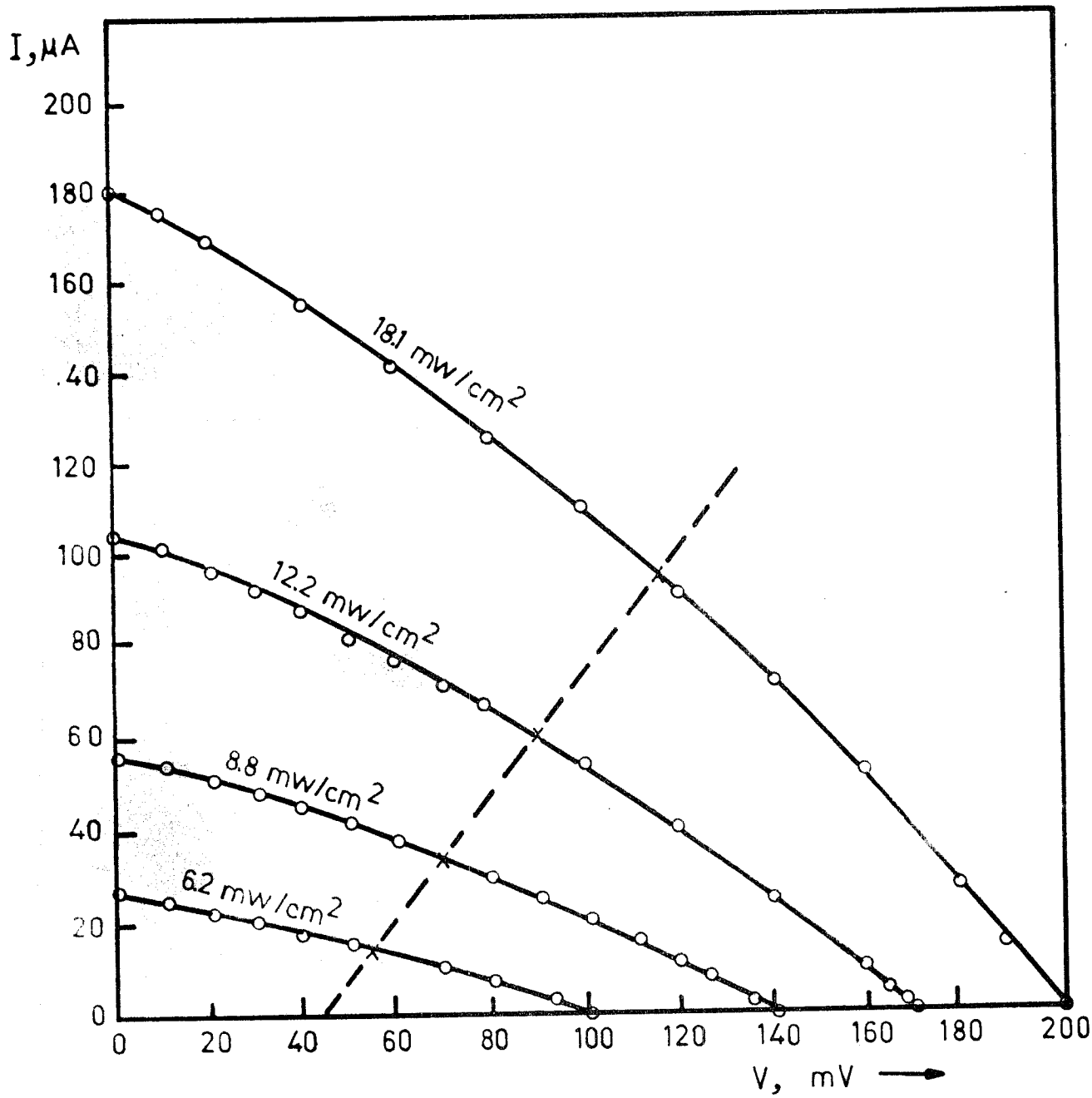

Fig. 38. Effect of illumination intensity for $Cu_2S_{thin\ film}$ / $CdS_{thin\ film}$ solar cell.

From theoretical considerations discussed by Rothwarf and Barnett, 1977, a significant increase in V_{oc} can be expected if a smooth junction with small effective area is used. Such junctions can be obtained by forming the Cu_2S on evaporated , unetched CdS using a solid state reaction between evaporated CuCl and CdS.

A major factor determining I_{sc} is the photon loss due to reflection at the outer Cu_2S surface. These losses can be reduced by the use of effective anti-reflection coatings.

4.4. CERAMIC CdS/Cu_xS SOLAR CELL

Ceramic CdS cells are considered one of the modifications of CdS/Cu_2S cells which has been studied and proved to be of high efficiency (Nakayama, 1969; Matsumoto et al, 1976). In addition to thin film solar cells which compose the major line of research in this project, we have also studied ceramic CdS cells. This was motivated by the simplicity of their preparation as well as the reliability to study the Cu_2S layer formed by the dip technique.

We have already given in this report (p.26) the details of the experimental procedure adopted to prepare the ceramic CdS tablets and the Cu_2S layer by the dip technique.

Preliminary results on this type of cells indicate reasonable I-V characteristic curves with conversion efficiency

of about 3%. However, this type of cells, is material consuming (thickness of each CdS tablet $\sim$ 500 μm) compared with thin film cells, but it has some other prospects. This type of cells is still under investigation as well as development.

REFERENCES

Aven, M. and Prener, J.S. (Eds.);
"Physics and Chemistry of II-VI Compounds", North Holland Publ. Co., Amesterdam (1967).

Barnett, A. and Rothwarf, A.;
Proc. IEEE 12th Photovoltaic Spec. Conf., Baton Rouge, La., p. 544 (1976).

Besson, J., Nguyen Duy, T., Gauthier, A. and Martin, C.;
Proc. IEEE 11th Photovoltaic Spec. Conf., New York, p. 468 (1975).

Böer, K.W., Birchenall, C.E., Greenfield, I., Hadley, H.C., Partani, T.L.W., Phillips, J.E., Schultz, J. and Tseng, W.F.;
Proc. IEEE 9th Photovoltaic Spec. Conf., Palo Alto, Calif., p. 77 (1973).

Bolch, J.W. and Anderson, W.W.;
Phys. Stat. Solidi (a) 9, 567 (1972).

Bragagnolo, J.A.;
Proc. IEEE 13th Photovoltaic Spec. Conf., New York, p. 412 (1978).

Bryant, F.J. and Glew, R.W.;
Energy Conversion 14, 129 (1975).

Bube, R.H.;
"Photoconductivity of Solids", John Wiley & Sons, Inc., New York (1960).

Carlson, D.E. and Wronski, C.R.;
Appl. Phys. Lett. 28, 671 (1976).

Caswell, B.G., Russel, G.J. and Woods, J.;
J. Phys. D: Appl. Phys. 8, 1889 (1975).

Chu, S.S., Chu, T.L. and Yang, H.T.;
Proc. IEEE 13th Photovoltaic Spec. Conf., New York,
p. 956 (1978).

Cullity, B.D.;
"Elements of X-Ray Diffraction", Addison Wisely, 2nd Edition,
Chapter 3 (1978).

Cusano, D.A.;
Rev. de Phys. Appl. 1 , 195 (1966).

Das, S.R., Nath, P., Banerjee, A. and Chopra, K.L.;
Solid State Communications 21, 49 (1977).

Das, S.R., Vankar, V.D., Nath, P. and Chopra, K.L.;
Thin solid Films 51, 257 (1978).

DiZio, S.F.;
Proc. Joint Conf. Amer. Sect., International Solar Energy
Society (ISES) and Solar Energy Society of Canada Inc.,
Winnipeg, USA, p. 108 (1976).

Douglas, D.M. Allan, Alastair, J. Hay and Malcolm, A. Reid;
Solid State Electronics 16, 951 (1973).

Dresner, J. and Shallcross, F.V.;
J. Appl. Phys. 34/8, 2390 (1963).

Fahrenbruch, A.L. and Bube, R.H.;
J. Appl. Phys. 45, 1264 (1974).

Fan, J.C., Bozler, C.O. and Chapman, R.L.;
Appl. Phys. Lett. 32, 390 (1978).

Foster, N.F.;
J. Appl. Phys. 38, 149 (1967).

Gashin, P.A., Simas, A.V. and Kerich, H.;
Phys. Stat. Solidi (a): 19, 615 (1973).

Gill, W.D. and Bube, R.H.;
J. Appl. Phys. 41, 3731 (1970).

Gross, E.F.;
Uzpek. Fiz. Nauk. 76, 433 (1977).

Hossain, S.B.;
Thin Solid Films 22, S5 (1974).

Hovel, H.J. and Woodall, J.M.;
Proc. IEEE 10th Photovoltaic Spec. Conf., Palo Alto,
Calif., p. 25 (1973).

Hovel, H.J.;
J. Solar Energy 19, 605 (1977).

Hunt, L.P., Dosaj, V.D., McCormik, J.R. and
Crossman, L.D.;
Proc. IEEE 12th Photovoltaic Spec. Conf., Baton Rouge, La.,
p. 125 (1976).

Kazmerski, L.L., White, F.R. and Morgan, G.K.;
Appl. Phys. Lett. 29, 268 (1976).

Leonov, V.M., Molchanov, A.G., Popov, Yu.M. and
Talat, G.H.;
Sov. Phys. Semiconductors 10, 852 (1976).

Macsumoto, H., Nakayama, N., Yamaguchi, K. and Ikegami, S.;
Jap. J. Appl. Phys. 15, 1849 (1976).

Meakin, J.D., Baron, B., Böer, K.W., Burton, L.,
Devaney, W., Hardley, H., Phillips, J., Rothwarf, A.,
Storti, G. and Tseng, W.;
Proc. Joint Conf. Amer. Sect., International Solar Energy
Society (ISES) and Solar Energy Society of Canada Inc.,
Winnipeg, USA, p. 113 (1976).

Meakin, J.D.;
University of Delaware, Institute of Energy Conversion, USA, Technical Report No. IEC/PV/TR/79/8, February (1979).

Mochizuki, K. and Igaki, K.;
Jap. J. Appl. Phys. 18, 1447 (1979).

Müller, W., Frey, H., Radler, K. and Schuller, K.H.;
Thin Solid Films 59, 327 (1979).

Mytton, R.J.;
Brit. J. Appl. Phys. 1, 721 (1968).

Nakayama, N.;
Jap. J. Appl. Phys. 8 , 450 (1969).

Okamoto, H.;
Jap. J. Appl. Phys. 4, 821 (1965); 5, 177 (1966); and 5, 251 (1966).

Prince, M.B.;
J. Appl. Phys. 26, 534 (1955).

Radler, K., Frey, H., Müller, W., Schuller, K.H. and Wienskowski, J.;
Thin Solid Films 59, 13 (1979).

Reynolds, D.C., Leies, G., Antes, L.L. and Marburger, R.E.;
Phys. Rev. 96, 533 (1954).

Rothwarf, A. and Böer, K.W.;
Progress in Solid State Chemistry 10 (2), 71 (1975).

Rothwarf, A.;
University of Delaware, Institute of Energy Conversion, USA, Technical Report (1976).

Rothwarf, A. and Barnett, A.M.;
IEEE Trans. (Devices), ED-24, 381 (1977).

Rothwarf, A., Phillips, J. and Wyeth, C.N.;
Proc. IEEE 13th Photovoltaic Spec. Conf., New York,
p. 399 (1978).

Runyan, W.R.;
"Semiconductor Measurement and Instrumentation",
McGraw-Hill Co., Kogakushe Ltd (1975).

Ryvkin, S.M.;
"Photoelectric Effects in Semiconductors", Consultants
Bureau, New York, p. 4o (1964).

Savelli, M. and Bougnot, J.;
Topics in Applied Physics, vol. 31, "Solar Cell Conversion",
Solid State P sics Aspects, Ed. Seraphin, B.O. (1979),
Publ. Springer Verlag, Berlin (1979).

Shay, J.L., Wagner, S., Bachmann, K.J., Bueler, E. and
Kasper, H.M.;
Proc..IEEE 11th Photovoltaic Spec. Conf., Ariz.,
p. 5o3 (1975).

Shay, J.L., Wagner, S., Bachmann, K.J. and Bueler, E.;
J. Appl. Phys. 47, 614 (1976).

Shay, J.L., Wagner, S., Bettini, M., Bachmann, K.J. and
Bueler, E.;
IEEE Trans. Elec. Dev., ED-24, 483 (1977).

Shirland, F.A. and Hietanen, J.R.;
Proc. 19th Ann. Power Sources Conf., Fort Monmouth,
p. 177 (1965).

Shirland, F.A.;
Advanced Energy Conversion 6, 201 (1966).

Sklyarevskii, I.N. and Korneeva, T.I.;
Optica and Spect. 24, 398 (1968).

Smith, R.W.;
Phys. Rev. 97, 1525 (1955).

Smith, A.;
J. Vac. Sci. Technol. 15, 2 (1978).

Te Velde, T.S ;
Solid State Electronics 16, 1305 (1973).

Tyagi, R.C. and Kumar, R.;
Thin Solid Films 25, S21 (1975).

University of Delaware, Institute of Energy Conversion,
USA, Report No. XS-9-83091-05, February (1981).

US Department of Energy, Division of Solar Technology,
Photovoltaic Programs Report (1978).

van der Pauw, L.J.;
Phillips Res. Repts. 13, 1 (1958).

van der Pauw, L.J.;
Phillips Technical Rev. 20, 8 (1958).

Wendland, P.H.;
J. Opt. Soc. Amer. 52/1, 581 (1962).

Wilson, J.I.B. and Woods, J.;
J. Phys. Chem. Solids 34, 171 (1973).

Wyeth, N.C.;
Solid State Electronics 20, 629 (1977).

Yamaguchi, K., Matsumoto, H., Nakayama, N. and Ikegami, S.;
Jap. J. Appl. Phys. 15, 1575 (1976).

oooOooo

O

APPENDIX A

REPORTS

Report 1&2 Environmental Pollution Control And Abatement Studies, Annual Report (Sept. 1979 to Aug. 1980). National Research Center, Cairo, and Environmental Protection Agency, USA.

Report 3 Multidisciplinary Environmental Studies, Report (Sept. 1980 to Feb. 1981). National Research Center, Cairo, and Environmental Protection Agency, USA.

Report 4 Multidisciplinary Environmental Studies, Report (March 1981 to Aug. 1981). National Research Center, Cairo, and Environmental Protection Agency, USA.